

## **FINAL REPORT**

### **Effects of Service Life of Aluminized Steel Corrugated Pipe with Visible and Not Visible Coating Deficiencies within the Lock System**

FDOT Contract Number: BDV25-977-62

USF Contract Number: 2104 1304 00

FDOT Project Manager: Ronald Simmons

PI: Christopher L. Alexander, University of South Florida, Tampa, FL.

#### **Report Prepared by:**

Mohammed Al Yaarubi

Mahmood Aliofkhazraei

Ishanka Roshen Indran

Christopher L. Alexander

**Department of Civil and Environmental Engineering**



**UNIVERSITY OF  
SOUTH FLORIDA**

**Tampa, FL 33620**

**July 2021**

## **DISCLAIMER**

The opinions, findings, and conclusions expressed in this publication are those of the authors and not necessarily those of the Florida Department of Transportation.

The contents of this report reflect the views of the authors, who are responsible for the facts and the accuracy of the information presented herein. This document is disseminated under the sponsorship of the Department of Transportation's University Transportation Centers Program, in the interest of information exchange. The U.S. Government assumes no liability of the contents or use thereof.

# UNIVERSAL CONVERSION TABLE

| SI* (MODERN METRIC) CONVERSION FACTORS                             |                               |                             |                                |                   |                                       |                                |             |                               |                     |
|--|-------------------------------|-----------------------------|--------------------------------|-------------------|---------------------------------------|--------------------------------|-------------|-------------------------------|---------------------|
| APPROXIMATE CONVERSIONS TO SI UNITS                                |                               |                             |                                |                   | APPROXIMATE CONVERSIONS FROM SI UNITS |                                |             |                               |                     |
| SYMBOL   | WHEN YOU KNOW                 | MULTIPLY BY                 | TO FIND                        | SYMBOL            | SYMBOL                                | WHEN YOU KNOW                  | MULTIPLY BY | TO FIND                       | SYMBOL              |
| <b>LENGTH</b>  |                               |                             |                                |                   | <b>LENGTH</b>                         |                                |             |                               |                     |
| in   | inches                        | 25.4                        | millimeters                    | mm                | mm                                    | millimeters                    | 0.039       | inches                        | in                  |
| ft   | feet                          | 0.305                       | meters                         | m                 | m                                     | meters                         | 3.28        | feet                          | ft                  |
| yd   | yards                         | 0.914                       | meters                         | m                 | m                                     | meters                         | 1.09        | yards                         | yd                  |
| mi   | miles                         | 1.61                        | kilometers                     | km                | km                                    | kilometers                     | 0.621       | miles                         | mi                  |
| <b>AREA</b>  |                               |                             |                                |                   | <b>AREA</b>                           |                                |             |                               |                     |
| in <sup>2</sup>  | square inches                 | 645.2                       | square millimeters             | mm <sup>2</sup>   | mm <sup>2</sup>                       | square millimeters             | 0.0016      | square inches                 | in <sup>2</sup>     |
| ft <sup>2</sup>  | square feet                   | 0.093                       | square meters                  | m <sup>2</sup>    | m <sup>2</sup>                        | square meters                  | 10.764      | square feet                   | ft <sup>2</sup>     |
| yd <sup>2</sup>  | square yard                   | 0.836                       | square meters                  | m <sup>2</sup>    | m <sup>2</sup>                        | square meters                  | 1.195       | square yards                  | yd <sup>2</sup>     |
| ac   | acres                         | 0.405                       | hectares                       | ha                | ha                                    | hectares                       | 2.47        | acres                         | ac                  |
| mi <sup>2</sup>  | square miles                  | 2.59                        | square kilometers              | km <sup>2</sup>   | km <sup>2</sup>                       | square kilometers              | 0.386       | square miles                  | mi <sup>2</sup>     |
| <b>VOLUME</b>  |                               |                             |                                |                   | <b>VOLUME</b>                         |                                |             |                               |                     |
| fl oz  | fluid ounces                  | 29.57                       | milliliters                    | mL                | mL                                    | milliliters                    | 0.034       | fluid ounces                  | fl oz               |
| gal  | gallons                       | 3.785                       | liters                         | L                 | L                                     | liters                         | 0.264       | gallons                       | gal                 |
| ft <sup>3</sup>  | cubic feet                    | 0.028                       | cubic meters                   | m <sup>3</sup>    | m <sup>3</sup>                        | cubic meters                   | 35.314      | cubic feet                    | ft <sup>3</sup>     |
| yd <sup>3</sup>  | cubic yards                   | 0.765                       | cubic meters                   | m <sup>3</sup>    | m <sup>3</sup>                        | cubic meters                   | 1.307       | cubic yards                   | yd <sup>3</sup>     |
| NOTE: volumes greater than 1000 L shall be shown in m <sup>3</sup> |                               |                             |                                |                   |                                       |                                |             |                               |                     |
| <b>MASS</b>  |                               |                             |                                |                   | <b>MASS</b>                           |                                |             |                               |                     |
| oz   | ounces                        | 28.35                       | grams                          | g                 | g                                     | grams                          | 0.035       | ounces                        | oz                  |
| lb   | pounds                        | 0.454                       | kilograms                      | kg                | kg                                    | kilograms                      | 2.202       | pounds                        | lb                  |
| T  | short tons<br>(2000 lb)       | 0.907                       | megagrams<br>(or "metric ton") | Mg<br>(or "t")    | Mg<br>(or "t")                        | megagrams<br>(or "metric ton") | 1.103       | short tons<br>(2000 lb)       | T                   |
| <b>TEMPERATURE (exact degrees)</b>                                 |                               |                             |                                |                   | <b>TEMPERATURE (exact degrees)</b>    |                                |             |                               |                     |
| °F   | Fahrenheit                    | 5 (F-32)/9<br>or (F-32)/1.8 | Celsius                        | °C                | °C                                    | Celsius                        | 1.8C+32     | Fahrenheit                    | °F                  |
| <b>ILLUMINATION</b>  |                               |                             |                                |                   | <b>ILLUMINATION</b>                   |                                |             |                               |                     |
| fc   | foot-candles                  | 10.76                       | lux                            | lx                | lx                                    | lux                            | 0.0929      | foot-candles                  | fc                  |
| fl   | foot-Lamberts                 | 3.426                       | candela/m <sup>2</sup>         | cd/m <sup>2</sup> | cd/m <sup>2</sup>                     | candela/m <sup>2</sup>         | 0.2919      | foot-Lamberts                 | fl                  |
| <b>FORCE and PRESSURE or STRESS</b>                                |                               |                             |                                |                   | <b>FORCE and PRESSURE or STRESS</b>   |                                |             |                               |                     |
| lbf  | poundforce                    | 4.45                        | newtons                        | N                 | N                                     | newtons                        | 0.225       | poundforce                    | lbf                 |
| lbf/in <sup>2</sup>  | poundforce per<br>square inch | 6.89                        | kilopascals                    | kPa               | kPa                                   | kilopascals                    | 0.145       | poundforce per<br>square inch | lbf/in <sup>2</sup> |

\*SI is the symbol for the International System of Units. Appropriate rounding should be made to comply with Section 4 of ASTM E380.

(Revised March 2003)

## TECHNICAL REPORT DOCUMENTATION PAGE

|   |   |   |       |
|---|---|---|-------|
| 1. Report No.   | 2. Government Accession No.                       | 3. Recipient's Catalog No.                                  |       |
| 4. Title and Subtitle:<br>Effects of Service Life of Aluminized Steel Corrugated Pipe with Visible and Not Visible Coating Deficiencies within the Lock System  |   | Report Date: 7/31/21  |       |
|   |   | Performing Organization Code                                |       |
| Author(s): Mohammed Al Yaarubi, Mahmood Aliofkhaezai, Ishanka Roshen Indran, Christopher L. Alexander   |   | Performing Organization Report No.                          |       |
| Performing Organization Name and Address:<br><br>Department of Civil and Environmental Engineering<br>University of South Florida (USF)<br>4202 E Fowler Avenue, ENC 3300<br>Tampa, FL 33620  |   | Work Unit No. (TRAI5)                                       |       |
|   |   | Contract or Grant No.<br>BDV25-977-62                       |       |
| Sponsoring Agency Name and Address<br><br>Florida Department of Transportation<br>605 Suwannee St. MS 30 Tallahassee, Florida 32399<br>(850)414-4615  |   | Type of Report and Period Covered<br><br>Draft Final Report |       |
|   |   | Sponsoring Agency Code                                      |       |
| Supplementary Notes   |   |   |       |
| <p>Abstract: The electrochemical behavior of aluminized and galvanized steel is investigated to determine the corrosion performance of coating deficiencies generated within the lock-seams during the fabrication of aluminized and galvanized steel corrugated pipe. Electrochemical techniques and visual and profilometric analysis are used to assess the ability of the aluminum and zinc coating to provide sufficient galvanic protection to the underlying steel in the presence of a crevice. Also, crevice coupons and lock-seam samples were used in this investigation in different environmental conditions simulating natural water conditions to relate the corrosion rate with the level of protection that the coating will provide. In addition, a model was developed to identify the influence of the confined geometry of the lock-seam on the corrosion rates at a defect location. The results have shown that defects in the aluminum coating can act as initiation sites for the corrosion of the steel. However, defects located external to the lock-seam may corrode at higher rates than those within the lock-seams due to the limited availability of oxygen.</p> |   |   |       |
| Key Words: bond strength; electrochemical testing; damage forecast  |   | Distribution Statement: No restrictions                     |       |
| Security Classif. (of this report)<br>Unclassified.   | Security Classif. (of this page)<br>Unclassified. | No. of Pages:<br>83   | Price |

## ACKNOWLEDGEMENTS

The authors acknowledge the pipe manufacturing plants that donated the pipe sections and materials for this research. For anonymity, their names are not identified.

## EXECUTIVE SUMMARY

In this work, the corrosion performance of defected aluminized and galvanized steel lock-seams was assessed when exposed to representative solutions of natural water. While the behavior of galvanized steel is well documented based on the studies performed on the cut edge in corrosive solutions comprising chlorides and sulfates, there was not much information on the performance of defects within confined geometries. Lock-seam immersion showed that the zinc corrosion of the coating outside of the lock-seam produces corrosion products that seem to plug the mouth of the crevice and prevent any corrosion from occurring within the lock-seam. Alternatively, the aluminum coating of aluminized steel did not readily corrode and was shown to only corrode after being immersed for a substantial amount of time, at which point, steel corrosion producing visual products occurred at defect locations outside and inside the lock-seam.

Crevice cells constructed to monitor corrosion of aluminized steel with defects within confined spaces showed that in the more aggressive solution, in two of the three samples, corrosion tubercles developed at the defect site and remained within the crevice while the corrosion products seemed to be able to escape the crevice of the samples exposed to mild conditions. The results suggested that there may be some influence of the crevice geometry on the ability of the aluminum to become activated. This was supported with finite element simulations that showed that cathodic activity which would produce a local alkaline condition promoting aluminum corrosion was limited in confined regions with limited oxygen availability. The simulations also revealed that corrosion may be limited within the lock-seam by producing tighter seams.

Based on the results, it cannot be concluded that deficiencies within the lock-seams produced because of the manufacturing process would reduce service life. However, models used in this work to help reach this conclusion do not consider local changes in pH due to hydrolysis of corrosion products or cathodic activity within confined regions. Future work is required to confirm long-term performance, potentially by continued field assessments coupled with long-term laboratory exposure testing and time-dependent corrosion damage simulations. The experimental results presented in this work, while more indicative of initial short-term exposure, do not suggest any influence of pH change within confined region, but the short-term results may not extrapolate well to long-term performance.

## TABLE OF CONTENTS

|   |     |
|---|-----|
| DISCLAIMER .....  | ii  |
| UNIVERSAL CONVERSION TABLE .....                              | iii |
| TECHNICAL REPORT DOCUMENTATION PAGE .....                     | iv  |
| ACKNOWLEDGEMENTS .....  | v   |
| EXECUTIVE SUMMARY .....                                       | vi  |
| LIST OF FIGURES .....   | ix  |
| LIST OF TABLES .....  | xii |
| CHAPTER 1. METALLIC COATED DRAINAGE PIPES.....                | 1   |
| 1.1. Manufacturing Process and Material Composition .....     | 1   |
| 1.2. Florida Natural Water and Soils.....                     | 2   |
| 1.3. Pipe Failures and Prior Evidence of Corrosion.....       | 3   |
| 1.4. Service Life Prediction Methods.....                     | 4   |
| 1.4.1. California Method.....                                 | 4   |
| 1.4.2. AISI Method .....                                      | 4   |
| 1.4.3. AK Steel Method .....                                  | 4   |
| 1.4.4. FDOT Method.....                                       | 5   |
| 1.5. Project Objectives and Report Organization.....          | 5   |
| CHAPTER 2. CORROSION OF ALUMINIZED AND GALVANIZED STEEL ..... | 7   |
| 2.1. Corrosion Mechanisms.....                                | 7   |
| 2.1.1. Zinc and Galvanized Steel .....                        | 7   |
| 2.1.2. Aluminized Steel.....                                  | 12  |
| 2.1.3. Influence of Impurities on Corrosion.....              | 15  |
| 2.2. Summary .....  | 16  |
| CHAPTER 3. PIPE LOCK-SEAM ASSESSMENT .....                    | 18  |
| 3.1. Pipes Obtained.....                                      | 18  |
| 3.2. Methods.....   | 19  |
| 3.3. Results .....  | 21  |
| 3.3.1. Control Tests.....                                     | 22  |
| 3.3.2. Lock-seam Looseness .....                              | 23  |
| 3.3.3. Plant A .....  | 25  |
| 3.3.4. Plant B.....   | 29  |
| 3.3.5. Plant C.....   | 30  |
| 3.3.6. Plant D .....  | 31  |

|  |    |
|--|----|
| 3.4. Discussion .....  | 33 |
| 3.5. Conclusion.....   | 34 |
| CHAPTER 4. EXPOSURE TESTING .....                                | 35 |
| 4.1. Testing Solutions.....                                      | 35 |
| 4.2. Lock-Seam Immersion Cells.....                              | 35 |
| 4.3. Crevice Cells with Defect .....                             | 40 |
| 4.4. Potentiodynamic Polarization Scans .....                    | 48 |
| 4.5. Scanning Vibrating Electrode Technique (SVET) Samples ..... | 50 |
| CHAPTER 5. FINITE ELEMENT SIMULATION .....                       | 53 |
| 5.1. Model Formulation.....                                      | 53 |
| 5.2. Simulation Results.....                                     | 58 |
| 5.3. Summary and Discussion.....                                 | 61 |
| CHAPTER 6. POTENTIAL IMPLICATIONS TO SERVICE LIFE.....           | 62 |
| 6.1. Description of Model .....                                  | 62 |
| 6.2. Summary .....   | 63 |
| CHAPTER 7. CONCLUSIONS .....                                     | 65 |
| REFERENCES .....   | 66 |



## LIST OF FIGURES

|  |    |
|--|----|
| Figure 1.1. Metallographic image of the cross-section of a lock-seam cut from a corrugated pipe.<br>9 .....  | 1  |
| Figure 2.1. Schematic diagrams for interpreting the corrosion mechanism of galvanized steel<br>under cyclic wet and dry conditions. <sup>23</sup> .....                    | 11 |
| Figure 3.1. Schematic showing the designations of depth and width of the defect. The top image<br>shows the cross-sectional view while the bottom shows the top view. .... | 19 |
| Figure 3.2. Surface analysis results of a coating scrape along the corrugation of an aluminized<br>pipe.....   | 20 |
| Figure 3.3. Loose lock-seam from Plant D galvanized steel pipe. ....   | 20 |
| Figure 3.4. Common three types of coating defects in the lock-seam.....  | 21 |
| Figure 3.5. Coating defects within the bends of a lock-seam. ....  | 22 |
| Figure 3.6. The coating of the controlled galvanized steel sample.....   | 23 |
| Figure 3.7. The coating of the controlled aluminized steel sample. ....  | 23 |
| Figure 3.8. Aluminized steel pipe lock-seams from four different manufacturers. ....   | 24 |
| Figure 3.9. Galvanized steel pipe lock-seams from four different manufacturers.....  | 24 |
| Figure 3.10. Average looseness of lock-Seam in millimeters from plants A, B, C, and D. ....  | 25 |
| Figure 3.11. Preexisting corrosion in the form of pits around the corrugations and the lock-seam<br>aluminized steel from Plant A.....                                     | 26 |
| Figure 3.12. Common scrapes in the lock-seam and the corrugations of galvanized steel from<br>Plant B.....   | 26 |
| Figure 3.13. Common dents that occur in the lock-seam in all pipe types in aluminized steel from<br>Plant A. ....  | 27 |
| Figure 3.14. Metallographic image of a common coating break in the lock-seam in Plant A-A1.27  |    |
| Figure 3.15. Metallographic images of coating break and shards in aluminized steel pipe from<br>Plant A. ....  | 28 |
| Figure 3.16. Metallographic images of coating break and shards in galvanized steel pipe from<br>Plant A. ....  | 28 |
| Figure 3.17. Metallographic image of coating break and shards in galvanized steel pipe from the<br>Plant B.....  | 29 |
| Figure 3.18. Metallographic image of coating break and shards in galvanized steel pipe from the<br>Plant B.....  | 31 |
| Figure 3.19. Metallographic image of coating break and shards in galvanized steel pipe from the<br>Plant B.....  | 31 |
| Figure 3.20. Additional spray-coated pipe in an aluminized steel pipe from Plant D. ....   | 32 |
| Figure 3.21. Metallographic image of coating break and shards in galvanized steel pipe from the<br>Plant B.....  | 33 |

|   |    |
|---|----|
| Figure 4.1. Prepared sample (6×6 inches) sealed inside Plexiglas container for long-duration immersion tests. ....  | 36 |
| Figure 4.2. Galvanized steel long-term immersion cell after 227 days inside and outside the lock-seam: (a) Lock-seam of galvanized steel in aggressive solution; (b) surface image of the galvanized steel long-term sample in aggressive solution; (c) Lock-seam of galvanized steel in mild solution; (d) surface image of the galvanized steel long-term sample in mild solution. .... | 37 |
| Figure 4.3. Aluminized steel long-term immersion samples at 51 days (left column) and after 227 days (right column) of immersion in aggressive and mild solutions for Plants A and B. ....  | 38 |
| Figure 4.4. Aluminized steel long-term immersion samples at 51 days (left column) and after 227 days (right column) of immersion in aggressive and mild solutions for Plants C and D. ....  | 39 |
| Figure 4.5. Lock-seam images after immersion in aggressive and mild solutions for 227 days for Plant A and B: (a) Plant-A long-term immersion cell lock-seam in mild solution; (b) Plant-A long-term immersion cell lock-seam in aggressive solution; (c) Plant B long-term .....   | 40 |
| Figure 4.6. Lock-seam images after immersion in aggressive and mild solutions for 227 days for Plant C and D: (a) Plant C long-term immersion cell lock-seam in mild solution; (b) Plant C long-term immersion cell lock-seam in aggressive solution; (c) Plant D long-term. ....   | 40 |
| Figure 4.7. Schematic figure of crevice sample with artificial defect. ....   | 41 |
| Figure 4.8. Aluminized steel etched crevice sample with a line scan using profilometric device with variations in depths in the etched defect before immersion, where the lowest depth is 33 $\mu\text{m}$ and the maximum is 95 $\mu\text{m}$ . The sample is called Sample (A) and immersed under the mild solution. ....   | 42 |
| Figure 4.9. Open circuit potential of the samples immersed during the 90-day period in aggressive and mild solutions. To convert the reference potential from titanium to SCE, 197 mV is added to the OCP in the aggressive solution and 166 mV for the mild solution. ....   | 43 |
| Figure 4.10. EIS results over time for the aluminized steel samples in the aggressive and the mild solution: sample immersed in the mild solution (top) and sample immersed in the aggressive solution (bottom).....  | 44 |
| Figure 4.11. Polarization resistance for aluminized steel crevice samples in aggressive solution (black) and mild solution (blue) for two replicates for 90 days of immersion. ....   | 45 |
| Figure 4.12. Crevice samples with no defect; a) in aggressive solution inside crevice; b) in aggressive solution outside crevice; c) in mild solution inside crevice; d) in mild solution outside crevice. ....   | 46 |
| Figure 4.13. Crevice coupons of aluminized steel in mild solution (A) after immersion of 90 days and the only sample with discoloration. a) inside crevice.; b) crevice entrance; c) defect.....  | 47 |
| Figure 4.14. Aluminum B aggressive only sample with CP accumulation and discoloration inside. Other sample with accumulation inside but no substantial discoloration. Other sample no accumulation but discoloration outside. ....  | 47 |
| Figure 4.15. Anodic potentiodynamic polarization scans of aluminized and galvanized coatings in mild and aggressive solutions (room temperature, scan rate 0.16 mV/s). ....   | 49 |
| Figure 4.16. Cathodic potentiodynamic polarization scans of aluminized and steel in aggressive solutions (room temperature, scan rate 0.16 mV/s). ....  | 49 |

|  |    |
|--|----|
| Figure 4.17. Schematic figure of sample made for SVET scanning.....  | 50 |
| Figure 4.18. SVET results of galvanized steel in 0.5 g/L sodium chloride and 0.03 g/L sodium sulfate; current density map (right); sample after 4 -hr scan (left). The blue color indicates the most cathodic locations, and the red color indicates the most anodic locations.....                          | 51 |
| Figure 4.19. Galvanized steel SVET line scans under aggressive solution (0.5 g/L NaCl + 0.03 g/L Na <sub>2</sub> SO <sub>4</sub> ) for the first 4 hours (yellow line) and after 24 hours (orange line). .....   | 51 |
| Figure 4.20. SVET results of aluminized steel in 0.5 g/L sodium chloride and 0.03 g/L sodium sulfate; a) sample after 4 hours scan; b) sample after 24 hours scan; a) current density map. The blue color indicates the most cathodic locations, and the red color indicates the most anodic locations. .... | 52 |
| Figure 5.1. The 2D-mesh geometry of the confined location entrance (right) and the defected aluminum coating that exposes the steel (orange). ....   | 54 |
| Figure 5.2. Polarization diagram of the reactions considered in the model according to the parameters listed in Table 5.1. ....  | 58 |
| Figure 5.3. Steel corrosion current density as a function of position along defect surface with crevice gap width as a parameter for the passive condition: a) conductivity 0.01 S/m; b) conductivity = 0.1 S/m.....   | 59 |
| Figure 5.4. Oxygen reduction current density on aluminized surface as a function of position with crevice gap width as a parameter for the passive condition: a) conductivity 0.01 S/m; b) conductivity = 0.1 S/m.....   | 59 |
| Figure 5.5. Anodic current density as a function of position with crevice gap width as a parameter for the active 1 condition with aggressive conductivity: a) steel; b) aluminum. ....  | 60 |
| Figure 5.6. Current density as a function of position with crevice gap width as a parameter for the active 2 condition with aggressive solution: a) anodic; b) cathodic. ....  | 61 |
| Figure 6.1. Corrosion damage propagation model schematic for defected aluminized steel. ....   | 62 |

## LIST OF TABLES

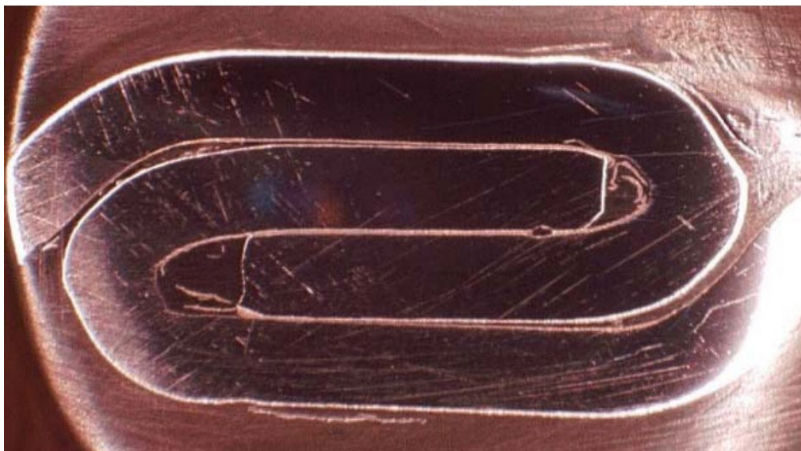
|  |    |
|--|----|
| Table 1.1. Maximum Impurities in Aluminum Type 2 Coating.....  | 2  |
| Table 1.2. Typical Environmental Parameters of Florida Natural Waters and Soils. <sup>13</sup> ..... | 2  |
| Table 1.3. Chemical Compositions and Resistivity of Florida Simulated Natural Waters.....            | 3  |
| Table 1.4. Florida Field Failures of Aluminized Pipe. <sup>16</sup> .....                            | 3  |
| Table 3.1. Pipes Received from Each Plant.....   | 18 |
| Table 3.2. Type, Size, and Location of Visible Defects in Plant A Pipes. ....                        | 26 |
| Table 3.3. Type, Size, and Possible Cause of Defects in Plant B Pipes. ....                          | 29 |
| Table 3.4. Type, Size, and Possible Cause of Defects in Plant C Pipes. ....                          | 30 |
| Table 3.5. Type, Size, and Possible Cause of Defects in Plant D Pipes. ....                          | 32 |
| Table 4.1. Average Defect Depth with the Estimated Corrosion Rate in $\mu\text{m}/\text{year}$ ..... | 48 |
| Table 5.1. Parameters Used in the Finite Element Model. ....   | 56 |

## CHAPTER 1. METALLIC COATED DRAINAGE PIPES

Metallic coated corrugated steel pipes are used in great numbers for FDOT applications, notably drainage culverts. A wide variety of wall thicknesses (gauges), corrugation geometries, diameters and pipe section lengths permit a choice of materials to meet specific job site requirements.<sup>1,2</sup> Corrugated steel drainage pipes must meet AASHTO M36 “Standard Specification for Corrugated Steel Pipe, Metallic-Coated, for Sewers and Drains”.<sup>1</sup> Two types of metallic coated pipe most often used are galvanized (zinc-coated) or aluminized (aluminum-coated), selected based on the environment and service life required.

### 1.1. Manufacturing Process and Material Composition

Metal-coated drainage pipes are manufactured by a hot-dip method according to ASTM A929 and AASHTO M274.<sup>2,3</sup> Prior to dipping, the steel sheets are degreased by alkali cleaning or by heating to temperatures between 450°C and 600°C.<sup>4</sup> The sheets are then rinsed by water and put through a pickling process using strong acids to remove impurities by exposing them to hydrogen gas, which cleans the metal in a non-oxidizing atmosphere.<sup>4</sup> After cleaning and activating, the steel sheets are dipped into a hot molten aluminum bath of an approximate temperature of 700°C, and/or a zinc bath for galvanized steel at an approximate temperature of 460°C which causes a formation of an intermetallic layer between the steel and the aluminum or the zinc during the interdiffusion process between the two metals.<sup>4,5</sup> The resulting coating thickness should be 40 μm.<sup>4</sup> After dipping the sheets into the coating, the sheets are rolled into a pressing machine that creates ribs or corrugations while being lubricated with a soapy solution to reduce friction.<sup>4,6,7</sup> These corrugations add strength to the pipe, which were also found to be critical in the premature corrosion process due to defects resulting from the forming process.<sup>4,7,8</sup> The sheets are connected by folding the sheets and connecting one side of the fold to the other side of the sheet in the rib section.<sup>4</sup> The two sides are connected in a way that the segments of the corrugations are well connected in interlocks that are called lock-seams, as shown in Figure 1.1.<sup>4</sup>



The purity of the steel and the coating has a significant influence on the level of protection of the intermetallic layer, which can either prevent corrosion or induce it.<sup>10,11</sup> While the galvanized steel

pipes are made with at least 99% zinc, the aluminum Type 2 coating has a maximum limit of impurities according to ASTM A 929, which are shown in Table 1.1.<sup>12</sup>

*Table 1.1. Maximum Impurities in Aluminum Type 2 Coating*

| Composition    | Maximum Content |
|----------------|-----------------|
| Iron           | 3%              |
| Silicon        | 0.35%           |
| Magnesium      | 0.5%            |
| Other each     | 0.05%           |
| Total of other | 0.2%            |
| Aluminum       | Balance         |

## 1.2. Florida Natural Water and Soils

The composition of Florida natural waters and soils has a great impact on the corrosion performance of metallic coated pipes. Chlorides, sulfates, resistivity and pH are considered to be the primary influencing factors.<sup>4,13</sup> While these parameters are site-specific, some overall generalities can be made to allow researchers to effectively simulate them in terms of corrosion aggressiveness. Table 1.2 presents values of environmental parameters established as either low moderate or high according to the FDOT Drainage Manual. Values of pH greater than 9 or less than 5 are known to be corrosive.<sup>13</sup> Sulfate concentrations rarely exceed 1,500 ppm but values greater than 5,000 ppm are known to cause accelerated deterioration for concrete especially.<sup>13</sup> The chloride concentration can vary greatly but the higher concentrations (>2000 ppm) are usually observed near the coast.

*Table 1.2. Typical Environmental Parameters of Florida Natural Waters and Soils.<sup>13</sup>*

| Variable      | Low    | Moderate | High    |
|---------------|--------|----------|---------|
| pH            | ≤5     | 5-9      | ≥ 9.0   |
| Cl (ppm)      | <2,000 | 2,000    | >2,000  |
| Sulfate (ppm) | <5,000 | 5,000    | > 5,000 |

Table 1.3 shows formulations of simulated natural waters based on these primary parameters. The sulfate and chloride concentrations tested were approximately between 15 and 35 ppm. The pH and resistivity ranged from 5.5 - 9 and 1 - 11 kΩcm, respectively. In addition, the Southwest Florida Water Management District evaluated water samples from different lakes in Florida.<sup>14</sup> Based on their samples they calculated average concentrations of chlorides and sulfates of 19.87 ± 10.55 ppm and 21 ± 18.88 ppm, respectively.<sup>14</sup> Also, they found that the average pH was 7.29 ± 0.86 with a conductivity of 198.6 ± 128 μS/cm (or an average resistivity of 5,035 Ωcm).<sup>14</sup> This shows that the simulated solutions used in the prior studies exemplified average natural water conditions but did not consider more aggressive solutions.

Table 1.3. Chemical compositions and resistivity of Florida simulated natural waters.

| Study  | Sulfate Concentration (ppm) | Chloride Concentration (ppm) | pH   | Resistivity ( $\Omega$ -cm) |
|--|-----------------------------|------------------------------|------|-----------------------------|
| Akhoondan (2012) <sup>4</sup>  | 30                          | 34                           | 7    | 5000                        |
|  | 30                          | 230                          | 7    | 1000                        |
| Sagues, A. A., Poor, N. D., Caseres, L., & Akhoondan, M. (2009) <sup>7</sup> | 62.9                        | 34.7                         | 5.56 | 5,200                       |
|  | 28.8                        | 14.5                         | 6.50 | 8,200                       |
|  | 17.2                        | 15.0                         | 6.93 | 11,100                      |
| Caseres, L., & Sagüés, A. (2005) <sup>15</sup>                               | -                           | 370                          | 7-9  | 1,140                       |

### 1.3. Pipe Failures and Prior Evidence of Corrosion

Corrosion of the internal wall of drainage pipes usually occurs on the lower half or quadrant of the pipe where there is water flow. However, in some cases premature corrosion at mechanically formed ribs has drastically reduced the service life of aluminized steel drainage pipes.<sup>13</sup> A list of recently reported corrosion failures of aluminized steel is presented in Table 1.4. The failures occurred between 2 and 10 years after installation, well short of the intended 75 to 100-year design life. The failures at the St. Cloud and Largo sites were externally manifested by roadway depression only 2 years after installation. Other failures became evident upon inspection of the pipe interior, as for example visual leaks into the pipe at the Jacksonville site after only 3 years of service.

Table 1.4. Florida Field Failures of Aluminized Pipe.<sup>16</sup>

| Identifier            | Location                      | Year Reported | Date Installed | Full Penetration |
|-----------------------|-------------------------------|---------------|----------------|------------------|
| St. Cloud, Fl.        | Indiana Ave.                  | 2005          | ~2003          | Yes              |
| Largo, Fl.            | West Bay/ 6 <sup>th</sup> St. | 2005          | ~2003          | Yes              |
| Pasco County          | SR-54 & US-19                 | 2006          | 2001           | No               |
| Curlew Rd. Clearwater | SR-586                        | 2007          | 1997           | Yes              |
| Jacksonville          | SR-212                        | 2009          | 2006           | Yes              |

In addition to the failures reported in Florida, there were other incidents of corrosion of metal corrugated pipes observed within the lock-seams in the state of Maine and was reported by Maine Department of Transportations in 2000. Two pipes were reported to have corrosion in the lock-seam and both were Aluminized steel pipes type 2.<sup>17</sup> The first one was a 16-gauge pipe and was 10 years old, where a severe corrosion was observed visually in the re-rolled sections (lock-seams).<sup>17</sup> The second pipe was reported in Ripley and it was a 16 year old 12 gauge pipe. In this particular case, severe corrosion damage of the lock-seams was observed not just at the pipe invert but around the entire circumference of the pipe.<sup>17</sup>

Premature corrosion failures sparked an immediate damage evaluation and laboratory investigation to identify the mechanisms of corrosion involved. In work reported in 2009,<sup>7</sup> the USF Corrosion Engineering Laboratory, examined field samples of culvert pipes as well as the soil and water at sites where corrosion failure occurred. Significant parameters that were identified to influence corrosion were temperature, oxygen concentration, resistivity, pH, and scaling tendency, as well as microbial activity. Further work performed by the same laboratory reported in 2012, sought to establish whether corrosion at coating breaks could be mitigated by appropriate galvanic protection afforded by the aluminum coating.

In their work two modes of deterioration were identified. For the mode of deterioration in the first 4 failures, analysis of as received pipes from several manufacturers showed instances where helical cuts in the pipe were present. The cuts may have been the result of obstacles to rotation of the dies used to form the ribs and the seams, perhaps from debris. Also, in cases where large cuts were not present, the stress induced on the materials to plastically deform into the desired shapes resulted in brittle fractures of the intermetallic layer and even ductile fractures of the aluminum coating leaving bare steel exposed.

#### 1.4. Service Life Prediction Methods

The existing service life prediction models are based on the environmental conditions of the contact solution and soil as well as the gauge thickness of the pipes. While pipe thickness is a strong influencer of service life, there is currently no consideration of possible coating defects that may cause premature corrosion. Therefore, coating defects could be a possible parameter to be introduced to the service life prediction models of corrugated pipes.

##### *1.4.1. California Method*

The California method to estimate the service life of galvanized drainage pipes was developed based on observational data of over 7,000 galvanized pipes. Their method considers the resistivity and pH of both the soil and water, as well as gauge thickness.<sup>18</sup> It established the end of the service life as full perforation of the pipe wall regardless of remaining structural durability. The method was initially intended for galvanized steel pipes and while it includes multiplication factors for high pH environments does not include specific modifications for aluminized steel. The California method also does not consider specific influences of aggressive ions or scale forming conditions and therefore greatly under predicts service life in hard waters.<sup>18</sup>

##### *1.4.2. AISI Method*

The American Institute of Steel and Iron (AISI) developed another service life prediction method by modifying the factor associated with pH values greater than 7.3 used by the California method.<sup>7</sup> In addition, the end of the service life is reached when there is a total metal loss of 25% as opposed to pipe wall perforation. The resulting estimated service life can be up to twice as much as those predicted by the California method.<sup>6,7,18</sup>

##### *1.4.3. AK Steel Method*

The AK steel method was developed to incorporate scale forming solutions as a result of calcium carbonate concentration.<sup>6</sup> The method is a service life method for both galvanized and type II



aluminized steel, where it uses the scaling tendency, which equals the total hardness plus the total alkalinity minus the free CO<sub>2</sub> versus the conductivity of the solution.<sup>19</sup> However, there is a possibility of overestimating the service life of the aluminized steel if the scale forming conditions created alkaline conditions, where the aluminum oxide film is not stable.<sup>6</sup>

#### *1.4.4. FDOT Method*

The selection of the drainage pipe material in Florida relies on the FDOT Culvert Service Life Estimator (CSLE) which considers pH, chloride concentration, sulfate concentration, minimum resistivity and pipe diameter as input parameters.<sup>13,20</sup> The service life is defined as the amount of time required until full penetration of the pipe wall occurs. Site specific environmental parameters are obtained of the soil and water at the structure site, on substructure materials, and on any backfill materials used. Based on the design service life, a list of suitable pipes is provided for a particular service environment.

The CSLE relies on empirical curves of service life as a function of minimum resistivity with pH as a parameter. Thus, while the chloride and sulfate concentrations are listed as input parameters in the CSLE software, they are not used in the calculation of service life for aluminized or galvanized pipes. Instead, the resistivity is the sole measure of ionic aggressiveness. Examples of the empirical curves are presented in Appendix M of the FDOT Drainage Design Guide.<sup>13</sup> For aluminized steel, values of pH between 5 and 9 are considered mild while a pH of less than 4 is considered highly aggressive. Most Florida soils and waters have a pH less than 10. In application to corrosion, ionically conductive media promotes ionic movement between anodic and cathodic sites on a metal surface and therefore promotes corrosion. A high resistivity is considered to be greater than 3,000 Ohm-cm and a low resistivity is considered to be anything below 1,000 Ohm-cm. Low (< 5) and high (>9) pH coupled with low resistivity provides a corrosive environment for aluminum.

Generally aluminized steel is expected to perform better than galvanized steel except in high pH and low resistivity environments. As an example, for a 16-gauge aluminized steel pipe in a service environment with a pH of 9 and a minimum resistivity of 1000 Ohm-cm, the estimated service life is only 19 years while for galvanized steel it is 34 years. For a neutral pH environment with a minimum resistivity of 3000 Ohm-cm, the estimated service life for 16-gauge aluminized steel is 87 years while the galvanized steel is only 30 years. However, premature corrosion of aluminized steel pipes due to pre-existing coating deficiencies has occurred resulting in pipe failures and reduction in service life to only 2 years in some cases. At this time, the CSLE does not include pre-existing coating defects in its estimate of service life.

#### 1.5. Project Objectives and Report Organization

The objective of this work is to determine the corrosion performance of coating deficiencies generated within the lock-seams during the fabrication of AASHTO M36 aluminized and galvanized steel corrugated pipe. A plan was proposed to address this concern by securing production pipe samples from FDOT suppliers and conducting a detailed electrochemical analysis of the influence of coating defects on corrosion initiation and propagation within and outside of the lock-seams. Additionally, finite element models are used to simulate the influence of the lock-seam geometry on the corrosion rates. The results of these experiments and simulations will be

used to determine whether pre-existing coating deficiencies within lock-seams reduces the service life of aluminized steel pipes

## CHAPTER 2. CORROSION OF ALUMINIZED AND GALVANIZED STEEL

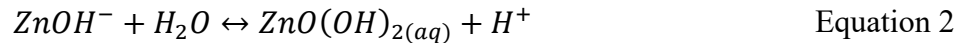
A literature review was conducted to identify existing evidence of the effect of coating defects within the lock-seams on the service life of galvanized and aluminized drainage pipes in Florida natural waters. Included in the review is corrosion mechanisms of aluminized and galvanized steel, as well as a discussion of the findings used to determine the knowledge gaps in the factors affecting corrosion within the lock-seams of drainage pipes. The review, while meant to be exhaustive, may not include all prior research related to this topic.

### 2.1. Corrosion Mechanisms

From internal images of the pipe walls and documented observations, the most severe corrosion occurs at the pipe invert or the bottom surface where water flows and in some cases propagates upward along the corrugations above the water line.<sup>4,19</sup> Since corrosion occurs at the corrugations due to coating defects, the same may be true for defects within the lock-seams. The purpose of this portion of the review is to discuss the various forms of corrosion and to determine the most severe form that would need to be considered in the estimation of service life. Galvanized steel corrosion mechanisms are presented followed by aluminized steel. Also, since the presence of impurities in the metal materials also influences corrosion, the forms of impurities and their specific influence on corrosion is also presented.

#### 2.1.1. *Zinc and Galvanized Steel*

As zinc corrodes, zinc hydroxide complexes are formed as zinc cations are hydrolyzed by water as



Reactions (Equation 1) and (Equation 2) are known to buffer the pH of the solution and the final product of reaction (Equation 2) is the white precipitate, which has a low solubility and acts like a barrier against further corrosion<sup>22</sup>. This mechanism of protecting the galvanized steel from further corrosion also occurs even when there is a defect, where El-Mahdy developed a corrosion mechanism for galvanized steel under wet and dry cycles, which consists of three stages.<sup>23</sup>

The first stage, dissolution of the zinc layer at defects within the coating occurred, where in this stage, the corrosion rate of the zinc and the size of the defects increases, and the steel was cathodically protected.<sup>23</sup> In the second stage, the zinc corrosion products accumulated on the surface of both the zinc and the steel, and the corrosion rate decreased. At the end of stage two, red rust began to appear on the surface indicating that steel corrosion initiated beneath the zinc corrosion products.<sup>23</sup> In stage three, the steel corrosion product continued to develop but the corrosion rate remained constant. Interestingly, the corrosion potential shifted to a value close to that of carbon steel despite the remaining zinc layer.<sup>23</sup>

Zinc-coated (galvanized) pipes provide corrosion protection in both a barrier and a sacrificial fashion in which the zinc, that corrodes moderately in neutral and acidic pH (pH < 8.5) environments, provides a barrier to the underlying steel. If there are coating breaks in the zinc coating, galvanic coupling occurs between the zinc and the underlying steel, which is passive in alkaline pH as long as aggressive ions such as chlorides are not present. During galvanic protection, the zinc acts as the corroding anode and the steel as the cathode.<sup>11,14,15,17,19,24</sup> Since the steel acts as the cathode, the local pH on the surface can become highly alkaline due to oxygen reduction. In alkaline solutions, zinc corrosion products precipitate or become solid and can deposit onto the steel surface and act as a cathodic inhibitor. By preventing oxygen reduction on the steel surface, further corrosion of the zinc is prevented. The ability of the corrosion products to accumulate on the bare steel depends on the solution pH, ionic concentration, and the ratio of the surface area of bare steel and zinc.<sup>15,17</sup> Also, whether the coating defect is located in a fully immersed location of the pipe where water flow is likely, or on the pipe wall above the water line where it may be easier for aggressive and or inhibiting species to deposit, or within the lock-seams where aggressive solutions may form will also influence that rate of corrosion. The following sections present information on the corrosion mechanisms in each of these scenarios.

#### 2.1.1.1. Influence of water composition

In immersed conditions, the galvanized steel is affected by the solution chemistry, which includes pH, total dissolved ions, dissolved oxygen, hardness and alkalinity as well as microbial content.<sup>7,24</sup><sup>19</sup> Generally for Florida natural waters, the chloride and sulfate concentrations will be low to moderate and the pH will be near neutral. Since water in the pipe flows at a certain velocity, the oxygen concentration is constantly renewed and therefore cannot be consumed by cathodic reactions. The total concentration of dissolved ions is usually presented as the resistivity or the conductivity of the solution.<sup>19</sup> Ions that are important to study are the aggressive ions, such as chloride and sulfate, that react with the zinc layer to produce soluble corrosion products.<sup>22,25-29</sup> Additionally, the ions that may act as corrosion inhibitors should be considered.

Using the scanning vibrating electrode technique (SVET) and pH microscopy, Ogle et al. characterized the behavior of the galvanized steel in chloride solutions.<sup>30</sup> On the cut-edge of galvanized steel, which comprises a steel section with two layers of zinc on both sides, the authors observed that in a 0.03 M (1740 ppm) chloride solution, corrosion of the zinc surface was in the form of localized pits.<sup>30</sup> The zinc corrosion products precipitated at locations surrounding the pits and the cathodic current on the exposed steel was nonuniform meaning that the level of galvanic protection varied with position on the steel surface. It was also shown that the nonuniformity was a function of the steel to zinc surface area ratio. As the area of steel increased, the galvanic current distribution became more uniform. The corrosion products in chloride solutions were identified to be zinc hydroxy chloride and zinc hydroxide. Their results after 18 hours of exposure showed that the entire zinc surface acted as an anode, however, they noticed red iron corrosion products, where they assumed the SVET's poor resolution didn't show the entire local current behavior on the zinc surface.<sup>30</sup> Ogle et al. didn't comment on the behavior, but this could be due to the uneven distribution of the chloride ions on the surface.<sup>29,31</sup>

For the sulfate solution, Ogle et al. observed uniform corrosion of the zinc unlike the behavior in the chlorides solution.<sup>30</sup> However, two of the seven samples didn't show the same behavior, where they assumed that it was due to the difference in sample preparations.<sup>30</sup> Sulfate ions react with the hydroxides to form zinc hydroxysulfate.<sup>32</sup> These products are soluble and with the increase of their

concentration they tend to precipitate within the cathode region, where they can act as a barrier to prevent further corrosion.<sup>33,26</sup> Also, another corrosion product that is formed by the reaction of sulfate ions with the zinc layer is zinc sulfate ( $ZnSO_4$ ), which is similar to  $ZnCl_2$  and can be dissolved easily in neutral water flow.<sup>28</sup> It was also shown that the corrosion of the zinc layer is worse in the sulfate environment than the chloride environment.<sup>23</sup>

Additionally, a solution with a high concentration of sulfate can be a suitable environment for bacteria that are called sulfate reducing bacteria (SRB) which are the major bacteria that contribute to microbiologically induced corrosion (MIC).<sup>24</sup> SRB can be found in many systems that are exposed to sulfate like sewage and drainage systems, where they form a film on the surface of the system<sup>24</sup>. These bacteria transform inorganic sulfate to hydrogen sulfide for its metabolism, where hydrogen sulfide is considered to be the main factor in MIC.<sup>24</sup> Even though zinc is considered to be toxic to SRB, it was found that SRB induced corrosion of galvanized steel by dissolving the zinc layer and diffusing through the biofilm created by the SRB.<sup>24</sup> However, Sungar et al. found no correlation between the corrosion rate and the number of SRB cells indicating that the corrosion could have been the result of a different mechanism.<sup>24</sup> While SRB can induce corrosion, the biofilms that are created by some bacteria can inhibit corrosion by consuming the oxygen and reducing the diffusion of other corrosive gases.<sup>7</sup> Other bacteria that were found to induce corrosion are iron oxidizing bacteria (IOB), and sulfate oxidizing bacteria (SOB).<sup>7</sup> While there have been cases where MIC could have contributed to corrosion of galvanized steel, in non-stagnant water the bacteria are less likely to develop and act as a corrosion promoter.<sup>7</sup> For the state of Florida, Sagues et al. concluded that there is a possibility that MIC can have a role of MIC for premature corrosion of culvert pipes but it's still not definite, and requires further investigation.<sup>7</sup>

Another influencing factor on the rate of galvanized steel corrosion is the tendency for the waters to form insoluble scales. Scales are precipitants of soluble salts such as calcium carbonate, these salts precipitate in a supersaturated conditions to bring the solution to an equilibrium state.<sup>34,35</sup> The scales that form from Florida waters are calcium carbonates, the formation of which can be predicted using the Langelier saturation index (LSI), which is the most widely used index for water scale potential.<sup>34</sup> LSI can be calculated by taking the difference between the measured pH of water and the pH of water after mixing with a saturated calcium carbonate, where a positive value means a favoring environment of scale formation and a negative value means a favoring of scale dissolution.<sup>7</sup> The formation of scales on the surface of galvanized steel can be a protective layer that reduces the possibility of corrosion.<sup>34</sup>

While the composition of Florida natural waters may only be mildly corrosive, variations in the water level in the pipes, as well as the relative humidity and temperature can result in droplets or thin layers of highly concentrated solutions. Corrosion under such conditions is referred to as atmospheric corrosion. Tomashov developed the theory that shows that the corrosion rate of a metal under thin layers of an electrolyte increases as the layer thickness decreases and reaches a maximum value at thicknesses of only a few microns.<sup>36</sup> The maximum corrosion rate value is often much greater than the corrosion rate in less concentrated immersed conditions but will vary as a function of surface moisture. The reason for this, is the increased availability of oxygen for thinner layers and the increased concentration of aggressive ions. The corrosion rate of an anodic region under a thin film is dependent on the rate of oxygen reduction by the surrounding cathode region. Under increasingly thin layers, the rate of oxygen reduction is determined by the diffusion rate of oxygen across the electrolyte layer which increases as the layer thickness decreases up until the

While atmospheric corrosion will likely not occur within the lock-seams of the pipes, coating defects on the internal walls of the pipes may be susceptible locations where the potential for premature corrosion may be likely.

Dubuisson et al.<sup>29</sup> studied the corrosion of galvanized steel under an electrolyte droplet containing chlorides and sulphates. In electrolytes with high concentrations of chlorides, the corrosion rate increased linearly with temperature; whereas the corrosion rate under electrolytes with low levels of both sulphate and chloride was less and did not change with temperature. Results showed that the anodic region initiates at the center of the droplet and results in deep pitting of the zinc layer that reaches the steel. This initial corrosion results in the formation of a porous insoluble product called simonkolleite. The porous structure of the simonkolleite allows diffusion of species such as zinc cations outward and into the cathodic region where the pH is much more alkaline and promotes the formation of  $\text{ZnO}$  and  $\text{Zn}(\text{OH})_2$  which can more effectively inhibit oxygen reduction by acting as a barrier.

More applicable to the atmospheric corrosion mechanism in drainage pipes than a static drop of electrolyte, is the simulation of wetting and drying cycles that may result from variations in flow conditions. The corrosion of galvanized steel was studied by El-Mahdy et al. with wet and dry cycles of 0.05 M (2900 ppm) NaCl or  $\text{Na}_2\text{SO}_4$  where they used zinc electroplated steel sheets with a coating thickness of 3 microns.<sup>23</sup> They observed a red rust when the corrosion of the steel initiated, where 70% of the zinc layer did not corrode, which indicates that the zinc layer corroded nonuniformly.<sup>23</sup> Thus, an un expected premature corrosion would occur in the galvanized steel. From their results, they developed a 3 stage corrosion mechanism, a schematic of which is shown in Figure 2.1.<sup>23</sup> In the first stage, dissolution of the zinc layer at defects within the coating occurred. During this stage, the corrosion rate of the zinc and the size of the defects increased and the steel was cathodically protected.<sup>23</sup> In the second stage, the zinc corrosion products accumulated on the surface of both the zinc and the steel and the corrosion rate decreased. At the end of stage two, red rust began to appear on the surface indicating that steel corrosion initiated beneath the zinc corrosion products. In stage three, the steel corrosion product continued to develop but the corrosion rate remained constant. Interestingly, the corrosion potential shifted to a value close to that of carbon steel despite the remaining zinc layer.

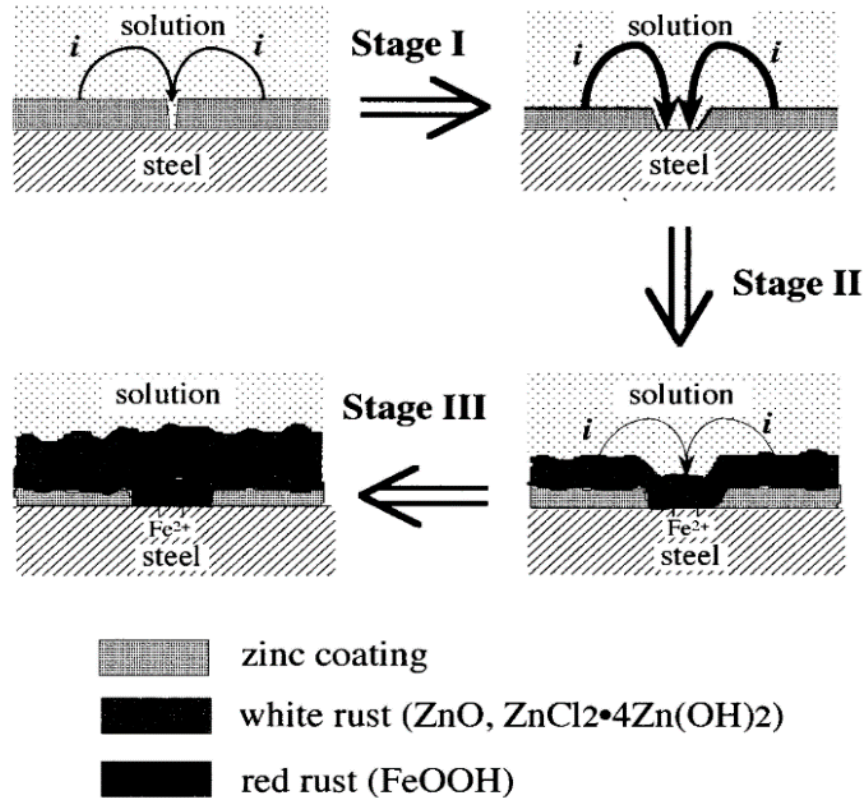


Figure 2.1. Schematic diagrams for interpreting the corrosion mechanism of galvanized steel under cyclic wet and dry conditions.<sup>23</sup>

#### 2.1.1.2. Influence of Defects

When preexisting coating defects are present, exposure to a corrosive environment results in galvanic activity in which the zinc uses its sacrificial property by initiating the corrosion on itself to protect the steel.<sup>37</sup> This forces the steel to become a cathode and the zinc layer to become an anode.<sup>38</sup> This process continues as long as the defect in the coating is not so large that the current required to protect the available current produced by the zinc corrosion. If this does occur, corrosion on the steel surface will initiate and will have selective corrosion, which is the corrosion of a base metal alloy that is less noble due to a leaching of a less noble metal in the alloy.<sup>39,40</sup> This shows that even if the thickness of the coating was large, the existence of coating defects will still reduce the service life of the galvanized steel as it was confirmed by multiple authors.<sup>37,41</sup>

#### 2.1.1.3. Crevice Corrosion

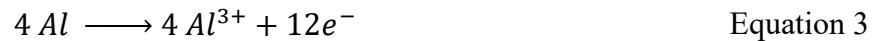
Since the metal corrugated pipes contain lock-seams, which might have limited access to the solution, crevice corrosion might need to be considered when evaluating the service life of the drainage pipe. Crevice corrosion is defined as a form of localized corrosion that occurs in narrow regions such as gaps and cracks called crevices due to oxygen depletion and dirt deposits.<sup>39</sup> Crevice corrosion of galvanized steel was studied and presented in multiple papers.<sup>42,43</sup> According to Stewart, when the entrance gap of the crevice gets wider, the corrosion rate decreases as it makes the electrical or chemical conditions unstable.<sup>44</sup> The three main corrosion products that are found in galvanized steel crevice corrosion are zinc oxide, hydrozincite and simonkolleite.<sup>43</sup> The

electrolyte in the crevice is a thin layer that ions or other molecules such as carbon dioxide can easily diffuse through.<sup>43</sup> If carbon dioxide diffuses into the crevice, it will dissolve in the electrolyte and reduce the pH, of the electrolyte in the crevice and induce corrosion.<sup>43</sup> In addition, the hydrolysis reactions of metal salts reduce the pH which creates a positively charged area, which also attracts negatively charged ions such as chloride.<sup>44</sup>

Fujita and Mizuno investigated the corrosion of galvanized steel in the crevice of lapped sheets.<sup>42</sup> They performed accelerated corrosion tests by wet and dry cycles and found that the perforation corrosion was mainly influenced by the weight of the coating.<sup>42</sup> They showed that initially the zinc layer corrodes, and the corrosion products accumulate on the surface until regions of steel are exposed. Once there are locations of steel exposure, the zinc corrodes more quickly to sacrifice itself. At this point, the steel begins to corrode under the zinc corrosion products at a rate similar to bare steel exposed to the same environment and eventually leads to perforation of the metal.

### 2.1.2. Aluminized Steel

Aluminized steel is protected against corrosion by an aluminum oxide film that forms on the surface and is thermodynamically stable for a pH range, of 5-8.5. Outside of this range the aluminum oxide will dissolve, leaving the bare aluminum to readily corrode. The oxide film primarily consists of  $Al_2O_3$  and  $Al(OH)_3$ , where  $Al_2O_3$  is more stable and less soluble in water and provides more protection to the metal surface than the zinc oxide layer in a neutral pH solution.<sup>4,6,31</sup> The aluminum oxide layer forms according to reactions Equation 3, Equation 4, and Equation 5.<sup>45</sup>



The aluminum layer and its oxide act as a barrier that protects the underlying steel.<sup>4</sup> The oxide however is not uniform in thickness and contains defects.<sup>45</sup>

#### 2.1.2.1. Influence of Water Composition

Chloride ions are able to adsorb and absorb within the outer layer of the oxide at localized sites and initiate corrosion pitting.<sup>39</sup> The formation of corrosion pits results in a localized drop in pH and the formation of a salt film that regulates the transport of ions into and out of the pit resulting in a diffusion-limited corrosion rate. Also, sulfate ions can initiate corrosion of the aluminum layer.<sup>31</sup> However, the sulfate-aluminum corrosion products do not dissolve in neutral solutions, unlike chloride-aluminum products, and can protect the aluminum from further corrosion. Therefore, sulfate ions are considered to be less aggressive than chloride ions to aluminized steel.<sup>45,46</sup>

As mentioned earlier, atmospheric corrosion occurs under thin layers of highly concentrated electrolyte, the thickness of which depends on the relative humidity and temperature. While there are not many studies on atmospheric corrosion of aluminized steel, some information can be gained from work performed on atmospheric corrosion on pure aluminum. In general, the air-formed oxide film of aluminum provides excellent protection against atmospheric corrosion at relative humidities below 70%. At greater relative humidity, sulfur dioxide if present can eventually form



into sulfuric acid which can breakdown the oxide film. The resulting corrosion product in such an environment is  $\text{Al}_2(\text{SO}_4)_3 \cdot 18\text{H}_2\text{O}$ . Over time however, the formation of corrosion products will help protect the aluminum.<sup>7</sup> While this information is useful, aluminized steel has slightly different surface features and includes iron precipitates and coating defects that are referred to in the literature as fissures that may extend to the base steel layer. The iron precipitates in the aluminum layer are cathodic to aluminum and corrosion will preferentially occur around the precipitates leaving pits.<sup>7</sup> In one study, atmospheric corrosion of aluminized steel was studied in two different mediums, one with high concentrations of chlorides and another one in a chloride-free medium.<sup>47</sup> After 3.5 years, the aluminized steel sample in the high chloride concentration medium was protected by the aluminum layer.<sup>47</sup> However, the sample with no chloride ions formed a passive layer on the aluminum and was not able to provide galvanic protection to the exposed steel.<sup>47</sup>

#### 2.1.2.2. Influence of Defects

While aluminized steel is more corrosion resistant than galvanized steel, breaks or severe cuts in the coating formed during manufacturing could be more likely to cause premature corrosion if the aluminum is not able to provide galvanic protection to the bare steel. In prior FDOT-sponsored work at USF, it was shown that large coating defects formed during manufacturing caused premature corrosion in ribbed locations of aluminized steel. Smaller coating breaks due to plastic deformation, while not as severe or consistent, were also identified as potential causes for premature corrosion.<sup>7</sup>

For aluminized steel with coating defects, the corrosion behavior changes mostly with the number of corrosive ions in the medium and the size of defects on the surface. The implications on service life of both large helical cuts and small plastically formed cuts in the coating were assessed through laboratory experiments in solutions that ranged from mildly to moderately aggressive, as well as waters likely to form precipitates resulting in surface scales.<sup>6</sup> It was concluded that helical cuts formed during the manufacturing process were the major source of premature corrosion in the field failures.

Mechanically formed aluminized steel sheets without large cuts but with a smaller bending radius, meant to represent the forming of lock-seams, resulted in enhanced corrosion within the formed region. The galvanic protection afforded by the aluminum coating was minimal. Despite this and due to variability of results, there was not enough evidence to conclude that cracks in the aluminum coating due to strain forming of the ribs and seams would consistently account for the observed unexpected corrosion failures.

Severe manufacturing deficiencies were later simulated by studying the corrosion of the aluminized steel cut edge. It was shown that the cut edge readily corroded in both mild and aggressive solutions indicated insufficient galvanic protection by the aluminized layer.<sup>16</sup> Finite element simulations formulated under the assumption of pure cathodic activity of the defect and anodic activity of the coating showed high corrosion rates of the coating near the defect resulting in increasing the exposed area of steel.<sup>4,16</sup>

Lemmens et al. (2014) used SVET to study the galvanic activity of aluminized steel in the presence of defects of different depths in a 0.05 M (2900 ppm) NaCl solution.<sup>48</sup> Their work showed that the aluminum layer was cathodic to both the intermetallic layers as well as the underlying steel suggesting an ability to provide galvanic protection to both. However, the potentials were

measured separately, and they did not present any direct evidence of sufficient galvanic protection to protect defect. Also, they only performed measurement for 30 minutes of immersion and did not present any long-term exposure results.

In a later study, Lemmens et al.(2018) studied the influence of the intermetallic layer thickness on the mechanical properties of aluminized steel with varying contents of silicon.<sup>49</sup> A part of their work included salt spray experiments on mechanically stressed specimens. Their results showed that even though tensile stresses resulted in small coating breaks, corrosion only resulted after 300 hours of exposure on the most strained samples. They suggested that the coating defects were small enough to be cathodically protected by the aluminum layer at least for a period. Their work also showed that a dipping process resulting in thinner intermetallic layer improved the corrosion performance of stressed samples. Straining of aluminized steel with thicker intermetallic layer can result in flaking of the aluminized coating.

#### 2.1.2.3. Crevice Corrosion

Aluminized steel pipes with lock-seams may also be vulnerable to crevice corrosion because of the narrow gap in the lock-seam. There are two models that explains crevice corrosion, the critical crevice solution (CCS), and the IR drop model (IR).<sup>44</sup> The CCS model is stating that initially the corrosion occurs in the same rate in both outside and inside the crevice, and due to the limited access to oxygen in the crevice, the oxygen is depleted by the oxygen reduction reaction inside the crevice.<sup>44</sup> The depletion of oxygen and the further hydrolysis of the metal cations causes a pH drop, which will also cause diffusion of chloride ions to the crevice to balance the metal cations, which results in a more aggressive solution than the initial solution, which causes the metal to corrode more.<sup>44</sup> On the other hand, the IR crevice model, which explains the crevice corrosion that is caused due to the IR drop between inside and outside the crevice, where once the oxygen inside the crevice gets depleted, the charge of the metal inside the crevice acts as an anode and the outside metal acts as a cathode, which causes a current flow from inside the crevice to the outside metal.<sup>44</sup>

A study was conducted to investigate the mechanism of breakdown of the passive layer of the aluminum in 0.05M NaCl solution and iron in several dilute mixtures in a crevice with different heights.<sup>50</sup> They built a crevice corrosion cell that they used to monitor pH, electrode potential and net current distribution and their results were compared to different crevice corrosion models. Their results showed that after minutes from the crevice formation, an anodic current reached a maximum point and then decreased gradually, to a constant value and after a few hours, the anodic current increased, which they referred to as breakdown process, where the passive layer lost its protective ability and an increase in the anodic dissolution occurred.<sup>50</sup> They observed bubble formation right before the breakdown process, which the bubbles filled 4% of the crevice in 3 hours of immersion.<sup>50</sup> They also observed three color distinct areas, where inside the crevice showed blue tint, the edge/opening of the crevice with similar color to the original sample, and outside the crevice, which had a gold tint and non-uniform regions with light hue.<sup>50</sup> Their results showed an initial increase of the pH inside the crevice that they attribute to the consumption of hydrogen ions by the oxygen reduction reaction and then a decrease to values near pH of 4.1 due to mostly by the metal ion hydrolysis.<sup>50</sup> With different gap width of the crevice, only current distributions of aluminum were obtained in which they found that the smaller the gap the faster the breakdown process occurs.<sup>50</sup>

Another study performed experiments on a hot stamped aluminized steel.<sup>51</sup> They connected two plates with an adhesive tape and exposed them to an aggressive environment in an atmospheric condition, where they found that corrosion attack reached a maximum depth of 200  $\mu\text{m}$ .<sup>51</sup> This study, with some modifications, may be replicated using lock-seams to assess the potential for crevice corrosion to occur. However, experimental methods are difficult to be performed under the crevice due to the limited space and inserting any other materials such as electrodes might influence the natural corrosion process inside the crevice.<sup>44</sup> Therefore, a number of mathematical and finite element models were developed to simulate the crevice corrosion.<sup>44,52-57</sup>

### *2.1.3. Influence of Impurities on Corrosion*

As the melted coating is in contact with the steel, an interdiffusion process occurs at the interface between the steel and the coating that creates a new layer of different phases of elements from both the coating and the steel.<sup>4,10,11</sup> The composition and thickness of the intermetallic layer is mostly dependent on the purity of the steel and the coating metal. Depending on their composition and amount, the impurities can either contribute to protecting the steel or promote corrosion.<sup>10,11,58</sup>

Impurities in the coating can be beneficial, when it can act as sacrificial elements to protect the steel, like manganese in the zinc coating as it is more reactive than zinc.<sup>59</sup> However, some impurities negatively affect the steel, where they create layers that induce corrosion such as silicon in the aluminum coating.<sup>10,11</sup> For the silicon content in the aluminum used, it was found that as the silicon content increases, the shape of the interlayer changes and gets smoother.<sup>11</sup> Also, the increase in silicon results in two separate layers comprising  $\text{Fe}_2\text{Al}_5$  and  $\text{Fe}_3\text{Al}$ .<sup>11</sup> The  $\text{Fe}_2\text{Al}_5$  layer resides next to the steel and is reduced when more silicon is added and the  $\text{Fe}_3\text{Al}$  layer next to the aluminum gets thicker as the silicon content increases.<sup>11</sup> Several researchers have found that while aluminizing steel with pure aluminum, the intermetallic layer that is created between the steel and the aluminum consists of orthorhombic  $\text{Fe}_2\text{Al}_5$  phase, which has a lattice orientation that is expected to be found in aluminized steel pipes used in the current project.<sup>10,11,60</sup> The microstructure of the intermetallic layer can also affect the corrosion behavior of the coated steel, as this layer is known to be brittle and could allow further corrosion.<sup>11</sup> As a result, minimizing the thickness of the intermetallic layer is beneficial.<sup>11</sup>

For galvanized steel, the intermetallic layer between the zinc coating and the steel consists mostly of different crystalline phases of Fe-Zn.<sup>61</sup> The reactions that occur in the intermetallic layer are affected by the temperature and duration of dipping.<sup>62,63</sup> Bico et al. studied the effect of dipping temperature on the thickness of the intermetallic layer by increasing the melt temperature by 10°C increments starting at 450°C. They found that the maximum thickness of the coating was in the temperature of 480°C.<sup>62</sup> While Giorgi et al. studied the diffusion of iron in the zinc coating in the hot dipping process by developing a rotating desk device.<sup>63</sup> According to the phase diagram developed by Kubachewski<sup>61</sup>, since the temperature used in the dipping of the galvanized steel is between 415 to 600°C, the phases most likely to be present are delta and  $\text{FeZn}_{13}$ . The impurities in the steel also have an effect on the microstructure of the intermetallic layer between the steel and the coating.<sup>58</sup> It was found that the silicon in the steel can react in the galvanizing process, where it creates non-uniformity in the zinc coating.<sup>58</sup> As a result, the intermetallic layers are controlled mostly by the coating and iron or impurities.

## 2.2. Summary

Corrugated galvanized and aluminized steel pipes have experienced premature corrosion in many cases, the cause of which has been linked to coating deficiencies generated during manufacturing and perhaps handling stages prior to or during placement. The mechanical forming of the lock-seams generates coating defects not only in the form of cracks but also in the form of pile-ups and delamination. The influence of these coating defects on service life of drainage pipes has not been studied and it is the primary objective of this project to determine the susceptibility of the lock-seams to prematurely corrode. To do this, a comprehensive understanding of the corrosion mechanisms of galvanized and aluminized steel must be established for conditions relevant to Florida natural waters.

This review presented information on the corrosion mechanism of galvanized and aluminized steel under different exposure conditions including full immersion, atmospheric, and crevice conditions. The primary influencers of corrosion were presented, and their level of influence was assessed. From the literature it was confirmed that the zinc layer on galvanized steel with coating defects in most relevant conditions can provide galvanic protection to the exposed steel. However, the limits of this protection depend on the exposed area of steel as well as on the conductivity and composition of electrolyte. Missing from the literature is the quantification of the limits of the protection afforded by the zinc layer in terms of maximum defect size or quantifiable modifications of service life estimates to account for defects. However, based on the expected sizes of the manufacturing induced coating defects (< 1 mm) and the results of Ogle et al. on the corrosion at a cut edge, the zinc should be able to provide protection to the expected defect sizes for a time frame that is dependent on the nature of the contacting electrolyte.

For aluminized steel, the ability of the aluminum coating to provide full galvanic protection to the steel is minimal and only achievable in highly concentrated solutions of chloride which serves to activate aluminum corrosion.

Based on the information obtained from the literature review and the geometry of the lock-seams shown in Figure 1.1, we can begin to formulate possible scenarios that may bound the corrosion susceptibility within the lock-seams for both aluminized and galvanized steel. If flowing waters can fill the space within the lock-seams and reside there without appreciable flow, and are aggressive enough to initiate corrosion, the corrosion may proceed according to the mechanisms described for immersed conditions. Alternatively, there could be a scenario in which oxygen within the lock-seams, or a crevice formed by a coating defect, is depleted resulting in the formation of a crevice corrosion condition.

Under these circumstances, several possible scenarios are plausible. If a coating defect forms a crevice within the lock-seams of galvanized steel, the zinc that encapsulates the crevice would corrode as opposed to the underlying steel thereby eliminating the crevice. Depending on the solution conditions, the zinc corrosion products could deposit within the lock-seam and potentially block any further ingress of solution. Alternatively, if the solution can flow freely through the lock-seams at rates fast enough to prevent the deposition of corrosion products, corrosion may continue.

In the case of aluminized steel, the corrosion at defect locations within the lock-seams may be more complicated. In this case, the underlying steel would corrode preferentially, and oxygen

reduction would occur on the aluminum surface until a critical concentration of chlorides is reached within the crevice. Within the lock-seam, it is likely that the surface area of aluminum is far greater than that of the exposed steel, making any cathodic limitation to the corrosion only dependent on the access of oxygen to regions within the lock-seam. The access of oxygen would depend on the geometry of the crevice, whether this portion of the lock-seams is fully immersed or not, and whether the water within the pipe is flowing.

In addition to corrosion mechanisms of galvanized and aluminized steel, a short review of service life prediction models was presented. In most cases, the service life predictions models are based on empirical, or field data collected over the years at various locations. The models therefore rely on prior experience rather than mechanistic knowledge and therefore cannot account for variations in conditions and cannot be used to explain situations such as the influence of coating defects. Any modification or added factor to current service life prediction models to account for coating deficiencies would require the assumption that the existing models reliably and accurately estimate service life based on exposure conditions. However, it has been confirmed by many studies that in some cases the service life models can be either over or under conservative.<sup>7,17</sup> The clear limitations in the service life models include lack of consideration for the influence of chloride or sulfate concentrations, and the lack of scaling tendencies in all models except the AK steel model. A more reliable alternative would be models based on the mechanisms of galvanized and aluminized steel corrosion in conditions relevant to Florida natural waters.

The question that will need to be addressed by our experimental work is whether coating deficiencies within the lock-seams influence the service life. To determine the possible conditions required for this to occur, it will first need to be determined under what conditions galvanic activity at defects within the lock-seams is expected. If it turns out that the defects within in the lock-seams are susceptible to premature corrosion, the corrosion rate as a function of exposure conditions will need to be quantified to predict the duration of the serviceability period. An assumption may be made that establishes the serviceability limit state as full penetration of a single pipe wall within the lock-seam. The duration of the corrosion propagation period within the lock-seams will be compared to that of a coating defect on the pipe wall to establish the worst-case scenario.

The following chapter includes an assessment of pipe sections obtained from different plants approved by FDOT. The purpose of the assessment is to quantify the typical defect sizes that may be present on the pipe and within the lock-seams prior to placement in the service environment. Additionally, the variation in lock-seam geometry will be quantified to inform performance observations and corrosion simulations.

## CHAPTER 3. PIPE LOCK-SEAM ASSESSMENT

In this chapter, the results of a detailed inspection of as-received pipes from 4 different plants and 3 manufacturers is presented. The pipe samples were assessed for visible defects that may result in premature corrosion including deep scratches and pre-existing corrosion pits. Sections of the pipe including flat, corrugated, and lock-seams were cut out for further analysis of the shape and size of the defects. For each region of coating deficiency, the likely cause was inferred based on the form of the deficiency. The coating breaks were quantified based on surface topography measurements and metallographic images of cross-sections where coating breaks were found. The analysis provided specific size and shape characteristics of the coating breaks to be used in future electrochemical experiments. Additionally, the analysis helped identify the typical range of quality for the lock-seams amongst the manufacturers and plants assessed.

### 3.1. Pipes Obtained

Manufacturers of aluminized and galvanized steel pipe were contacted and sent a list of requested samples to be studied for this project. Three, 2-ft sections of 18 and 36-inch diameters were requested for both aluminized and galvanized metals. Additionally, sheet sections were also requested for future electrochemical studies. The quantities received of each material and the dates they were received are documented in Table 3.1.

*Table 3.1. Pipes Received from Each Plant.*

| Plant   | Date Received | Material   | Form       | Dimension     |             | Quantity Requested | Quantity Received |
|---------|---------------|------------|------------|---------------|-------------|--------------------|-------------------|
|         |               |            |            | Diameter (in) | Length (ft) |                    |                   |
| Plant A | 06/20/19      | Aluminized | Pipe       | 36            | 2           | 3                  | 3                 |
|         |               |            |            | 18            | 2           | 3                  | 3                 |
|         |               |            | Flat Sheet | -             | 2           | 3                  | 6                 |
|         |               | Galvanized | Pipe       | 36            | 2           | 3                  | 3                 |
|         |               |            |            | 18            | 2           | 3                  | 3                 |
|         |               |            | Flat Sheet | -             | 2           | 3                  | 6                 |
| Plant B | 06/19/19      | Aluminized | Pipe       | 36            | 2           | 3                  | 3                 |
|         |               |            |            | 18            | 2           | 3                  | 3                 |
|         |               |            | Flat Sheet | -             | 2           | 3                  | -                 |
|         |               | Galvanized | Pipe       | 36            | 2           | 3                  | 3                 |
|         |               |            |            | 18            | 2           | 3                  | 3                 |
|         |               |            | Flat Sheet | -             | 2           | 3                  | -                 |
| Plant C | 07/08/19      | Aluminized | Pipe       | 36            | 2           | 3                  | 6                 |
|         |               |            |            | 18            | 2           | 3                  | 3                 |
|         |               |            | Flat Sheet | -             | 2           | 3                  | 1                 |
|         |               | Galvanized | Pipe       | 36            | 2           | 3                  | 3                 |
|         |               |            |            | 18            | 2           | 3                  | 6                 |
|         |               |            | Flat Sheet | -             | 2           | 3                  | 1                 |
| Plant D | 08/15/19      | Aluminized | Pipe       | 36            | 2           | 3                  | 3                 |
|         |               |            |            | 18            | 2           | 3                  | 3                 |
|         |               |            | Flat Sheet | -             | 2           | 3                  | 4                 |

Table 3.1(Continued). Pipes Received from Each Plant.

| Plant   | Date Received | Material   | Form       | Dimension     |             | Quantity Requested | Quantity Received |
|---------|---------------|------------|------------|---------------|-------------|--------------------|-------------------|
|         |               |            |            | Diameter (in) | Length (ft) |                    |                   |
| Plant D | 08/15/19      | Galvanized | Pipe       | 36            | 2           | 3                  | 3                 |
|         |               |            |            | 18            | 2           | 3                  | 3                 |
|         |               |            | Flat Sheet | -             | 2           | 3                  | 4                 |

### 3.2. Methods

The as-received condition of the pipes was assessed according to the presence of visible defects identified by optical images, the amount of coating deficiencies outside of the lock-seams determined by surface topography, and the amount of coating deficiencies within the lock-seams determined by metallographic images. To ensure the cutting procedure did not influence the presence of coating defects, unbent samples from galvanized and aluminized pipes were cut, mounted in an epoxy and polished to analyze the coating deficiencies using an optical microscope.

The defects found on the as received pipes were categorized as coating breaks, scrapes/scratches, dents and preexisting corrosion. For each type of defect, the width and the depth of the defect was measured to determine the maximum and minimum sizes of defects in each pipe and each plant. Figure 3.1 shows the depth and the width of the defect that is measured on the surface of the metal. The depth and the width of the defects was measured with a 3D profilometer capable of quantifying the shape and size of surface topography features. An example of the analysis of a scrape along a corrugation is presented in Figure 3.2. The surface and lock-seam defect sizes were compared between the different plants. The sizes of defects found will be used for further investigation on their effect on the service life of the metal drainage pipe.

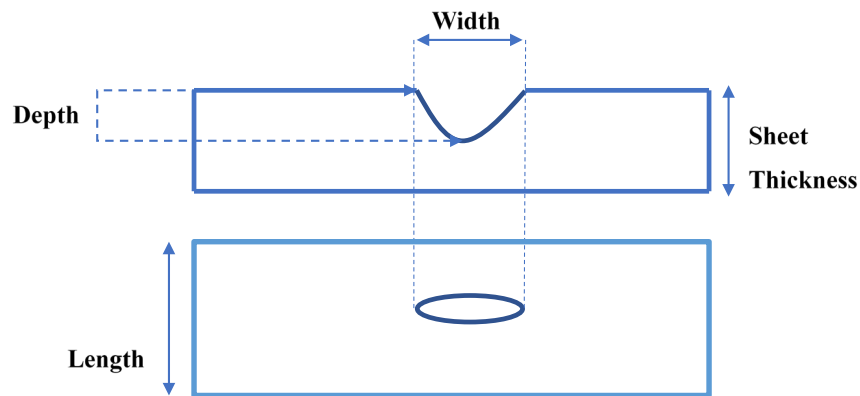


Figure 3.1. Schematic showing the designations of depth and width of the defect. The top image shows the cross-sectional view while the bottom shows the top view.

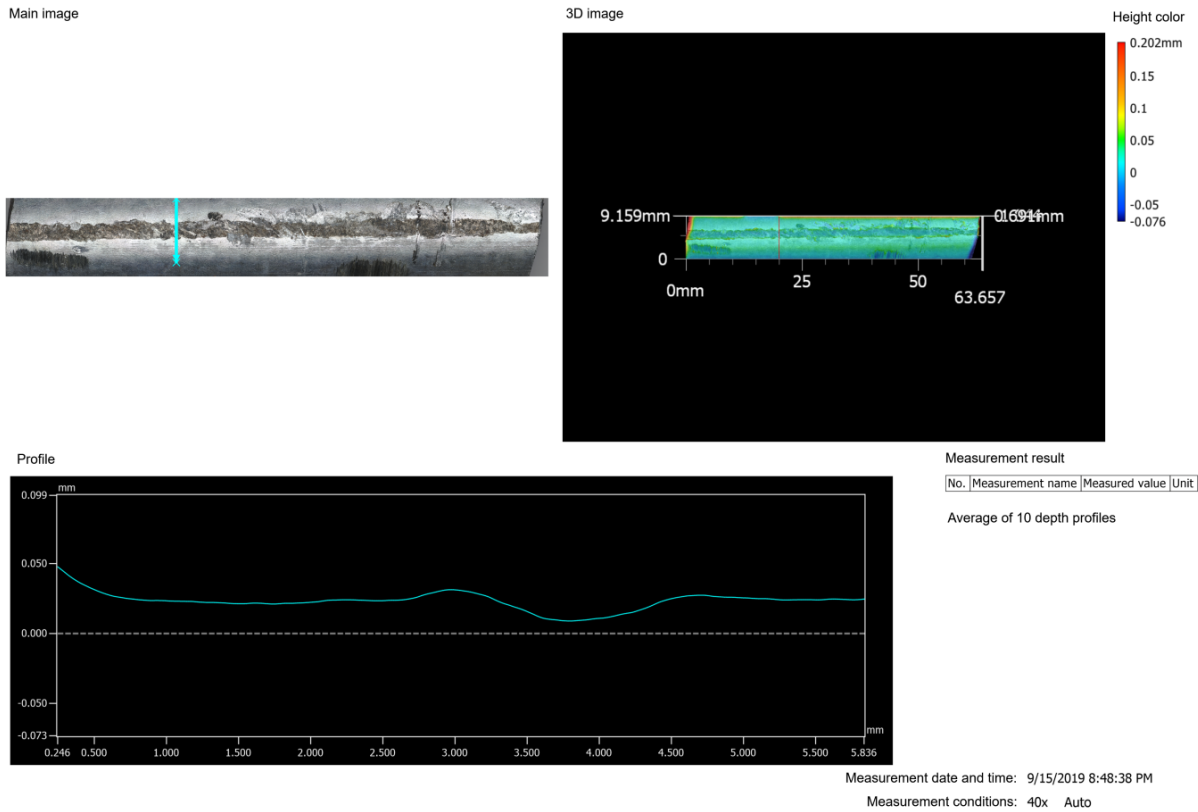


Figure 3.2. Surface analysis results of a coating scrape along the corrugation of an aluminized pipe.

Additionally, the coating thickness was assessed for compliance with the standard requirements. According to ASTM A 929, the minimum coating weight for aluminum and zinc coating should be 1 oz/ft<sup>2</sup> [305 g/m<sup>2</sup>] and 2 oz/ft<sup>2</sup> [610 g/m<sup>2</sup>] respectively.<sup>64</sup> Therefore, the minimum allowable coating thickness is approximately 3.7 mils (95 μm) for aluminum and 3.4 mils (86 μm) for zinc. According to AASHTO M36, the pipes should be rejected if a one of the conditions in the list of specifications were violated.<sup>1</sup> One of the rejection conditions is loose lock-seams, however the specific definition of a “loose” lock-seam is not provided. In our analysis, it was noticed that some of the lock-seams were not as tightly locked as others and an example of which is shown in Figure 3.3.<sup>1</sup>

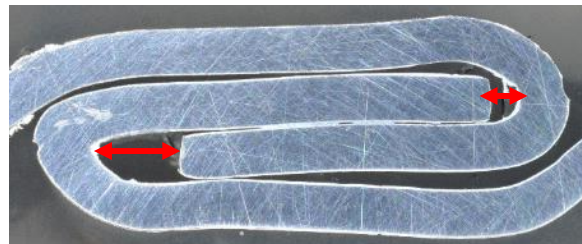


Figure 3.3. Loose lock-seam from Plant D galvanized steel pipe.



The looseness of the lock-seam was quantified in terms of the distance between the end of the sheet to the bend of the seam. The average and standard deviation of the maximum distance is reported in the results sections for each group of pipe samples analyzed.

### 3.3. Results

The pipe condition results are now presented for each plant and material analyzed. The results of the control test were ensured that the cutting method did not produce coating defects. Tables are provided for each manufacturer as a summary of the defects present. Defects within the lock-seams are characterized as breaks, delamination, and shards. The metallographic images of lock-seam sections are shown in Figure 3.4. The defect types were identified as cracks, delamination, and coating shards. Image 1 obtained in the bend of the lock-seam (location D) shows piled-up shards of coating, likely the result of mechanical forming. Image 2 shows coating breaks without delamination in the flat portion of the lock-seam (location A), again likely the result of mechanical forming resulting in tensile stress in the material at this location. Image 3 shows coating delamination in which the coating seemed to have flaked off. This could be a result of mechanical forming or also poor application of the coating materials resulting in little adhesion. Because the coating is applied via a hot-dipping process, the second scenario is unlikely. However, this behavior was observed in many of the lock-seams, examples of which are presented in Figure 3.5. In the first image, a picture of the inside wall at the fold of the lock-seams shows coating flakes formed when the coating had delaminated from the base metal. In the second image, a similar phenomenon is observed except the coating had uniformly delaminated and not produced flaking pieces of the coating but instead a single unadhered piece of metal. Electrochemical experiments provided information about the corrosion susceptibility of these regions.

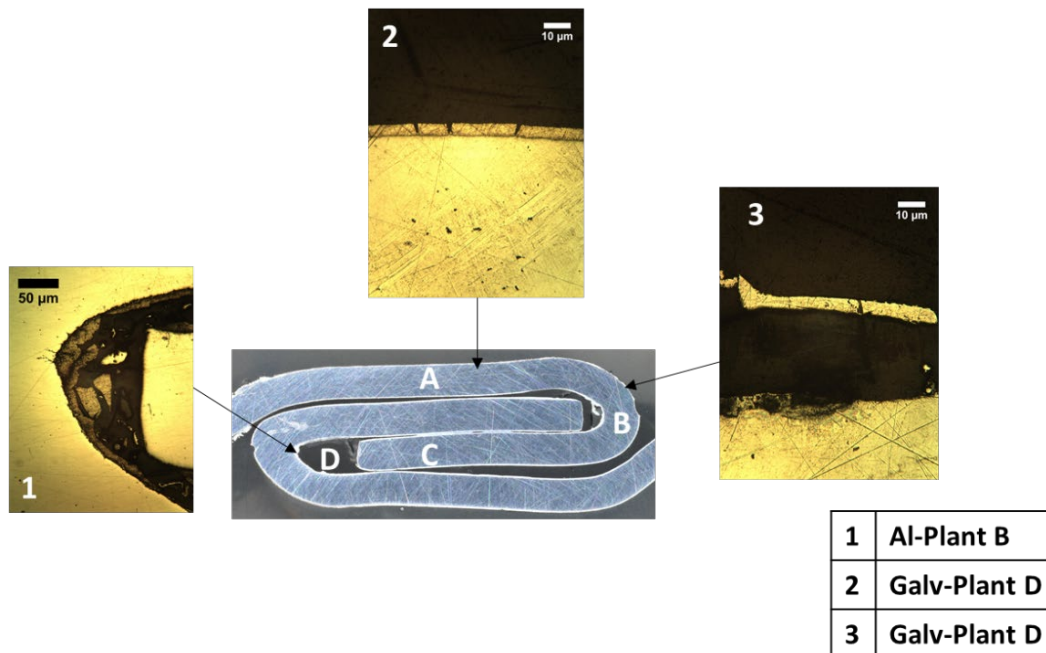


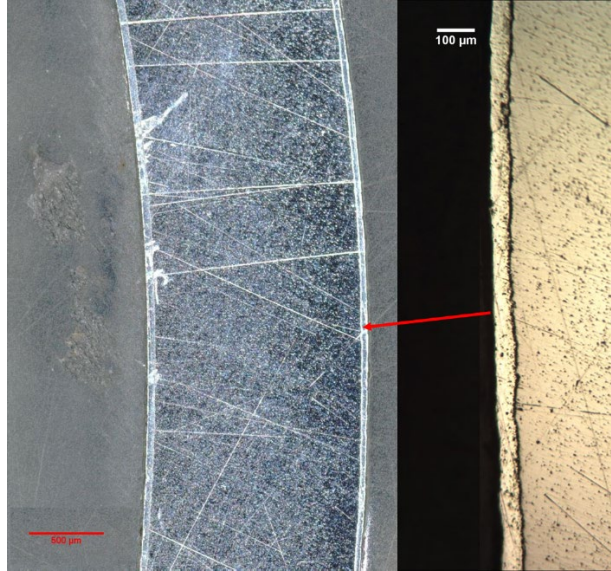
Figure 3.4. Common three types of coating defects in the lock-seam.



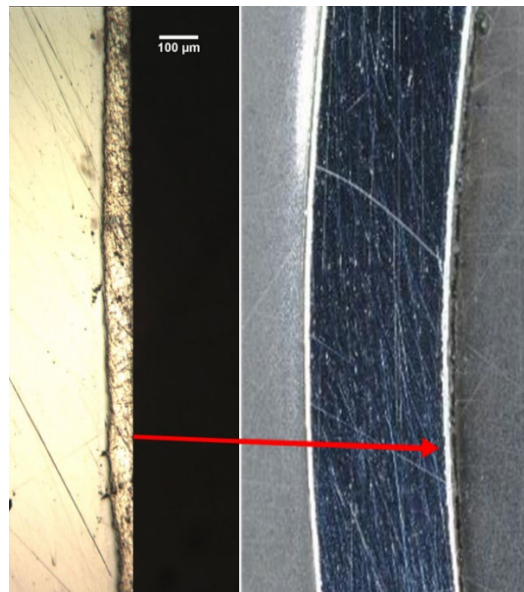
*Figure 3.5. Coating defects within the bends of a lock-seam.*

### *3.3.1. Control Tests*

To verify that the method used for analyzing the lock-seams did not introduce defects, a control sample was cut from the flat region of a pipe. The coating quality was determined by metallographic analysis. The results of the coating assessment for the controlled samples are presented in Figure 3.6 and Figure 3.7 for both galvanized and aluminized steel, respectively. No coating defects were observed, confirming that the cutting procedure could be used to analyze defects within the lock-seams.



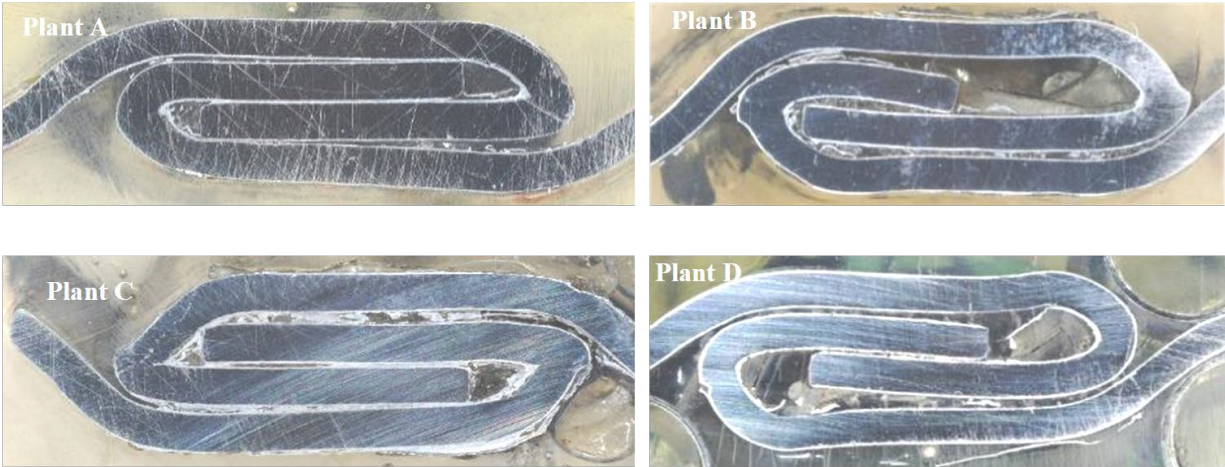
*Figure 3.6. The coating of the controlled galvanized steel sample.*



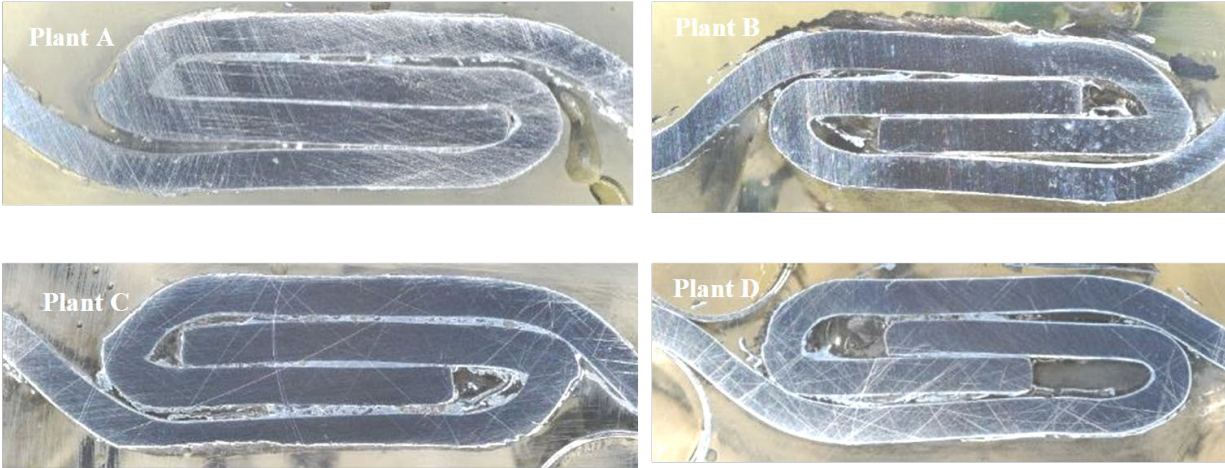
*Figure 3.7. The coating of the controlled aluminized steel sample.*

### 3.3.2. Lock-seam Looseness

Even though each plant followed the same standard to form drainage pipes, the lock-seams from each plant differed in terms of the way that the two sheets locked together. For some plants the lock-seam was looser than others. Figure 3.8 and Figure 3.9 show the different shapes and looseness of the lock-seams from each plant for both the aluminized and galvanized steel pipes, respectively.



*Figure 3.8. Aluminized steel pipe lock-seams from four different manufacturers.*



*Figure 3.9. Galvanized steel pipe lock-seams from four different manufacturers.*

Figure 3.10 shows the average looseness of the lock-seams quantified according to the method provided in Figure 3.3, for each metal type and manufacturer analyzed. The maximum average looseness was found in aluminized steel pipes from Plant B, which was 7.2 mm with a standard deviation of 0.7 mm. Loose lock-seams may result in leaks in the pipes and will have a role on the durability of the lock-seams. The looseness of the lock-seams will be used to select best and worst cases for further electrochemical testing by immersion experiments.

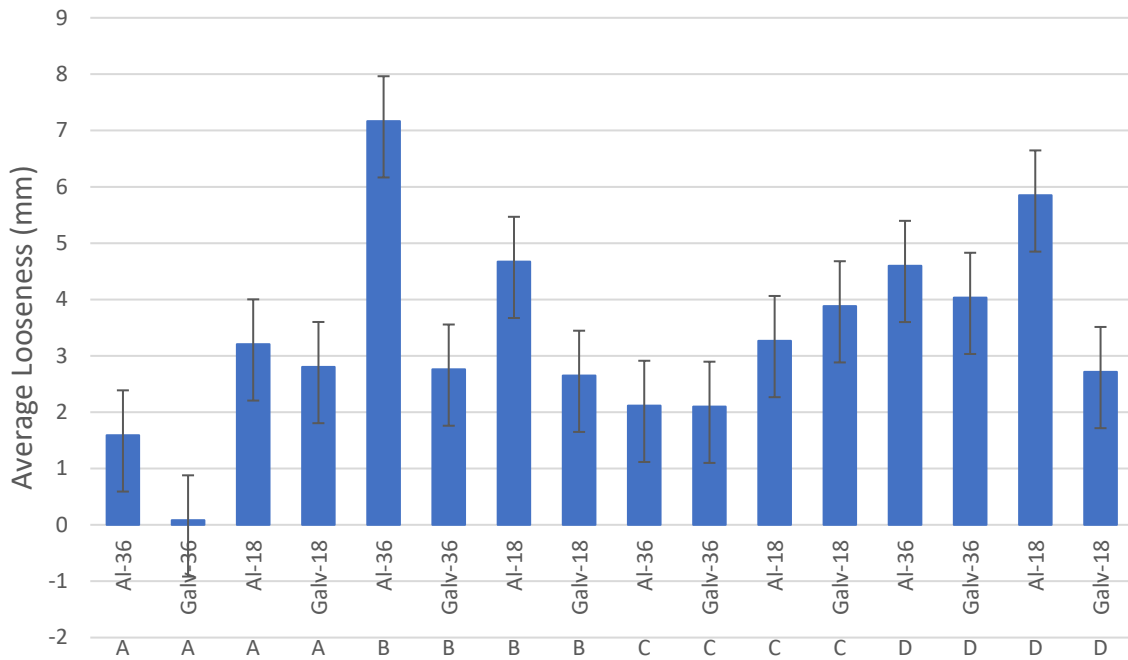


Figure 3.10. Average Looseness of Lock-Seam in millimeters from plants A, B, C and D.

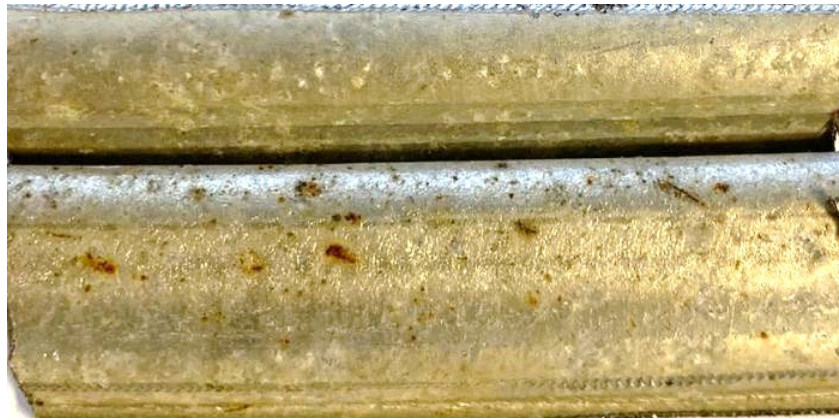
The following sections provide quantitative results of the defects observed on the pipes obtained from each plant. All the pipes obtained contained defects within the lock-seams.

### 3.3.3. Plant A

Table 3.3 shows the sizes, location, and the possible cause of visible and non-visible defects in both aluminized and galvanized steel pipes obtained from Plant A. Pre-existing corrosion pits sized between 1.3 to 2.6 mm were observed on the aluminized steel surface in the region of the lock-seams as well as elsewhere on the pipe surface as is shown in Figure 3.11. With a maximum pit depth of 0.26 mm, a good portion of the metal thickness is already lost and would likely result in significant decreases in the expected service life of the pipe assuming further corrosion occurs on the external wall of the pipe after placement in soil. Pre-existing pits were not observed on galvanized steel pipes likely due to the ability of the zinc coating to galvanically protect the underlying steel.

*Table 3.2. Type, Size, and Location of Visible Defects in Plant A Pipes.*

| Material   | Type of Defects              | Location                    | Width (mm) | Depth (mm)  |
|------------|------------------------------|-----------------------------|------------|-------------|
| Aluminized | Preexisting Corrosion (Pits) | Corrugations and Lock-seams | 1.3-2.6    | 0.13-0.26   |
|            | Scratches/Scrapes            | Corrugations                | 0.05-2     | 0.015-0.045 |
|            | Dents                        | Lock-seams and Corrugations | 0.54-7     | 0.15-0.34   |
|            | Coating Breaks               | Lock-seam                   | 0.03-0.1   | -           |
| Galvanized | Preexisting Corrosion (Pits) | -                           | -          | -           |
|            | Scratches/Scrapes            | Corrugations                | 0.05-2     | 0.015-0.045 |
|            | Dents                        | Lock-seams and Corrugations | 7-8        | 0.15        |
|            | Coating Breaks               | Lock-seam                   | 0.04-0.1   | -           |

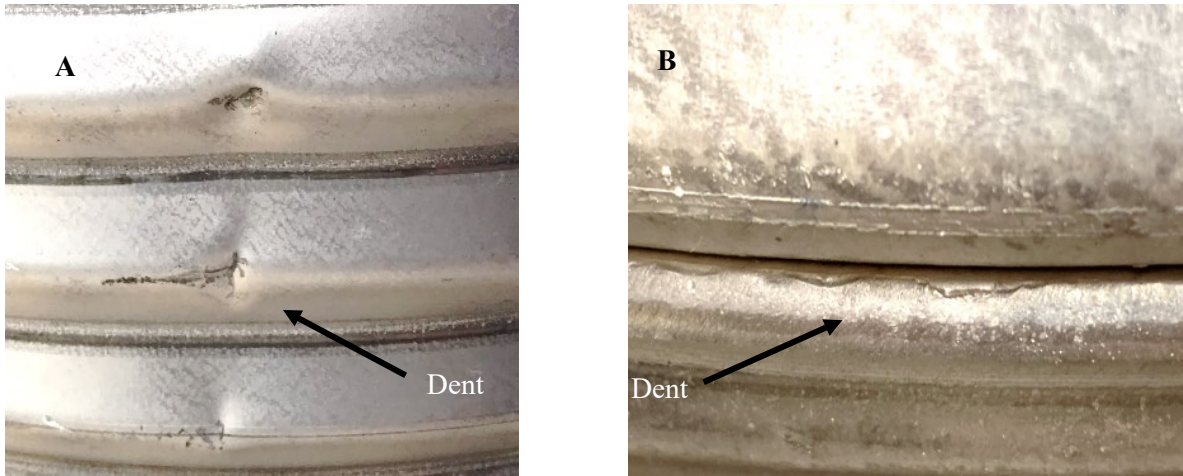


*Figure 3.11. Preexisting corrosion in the form of pits around the corrugations and the lock-seam aluminized steel from Plant A.*

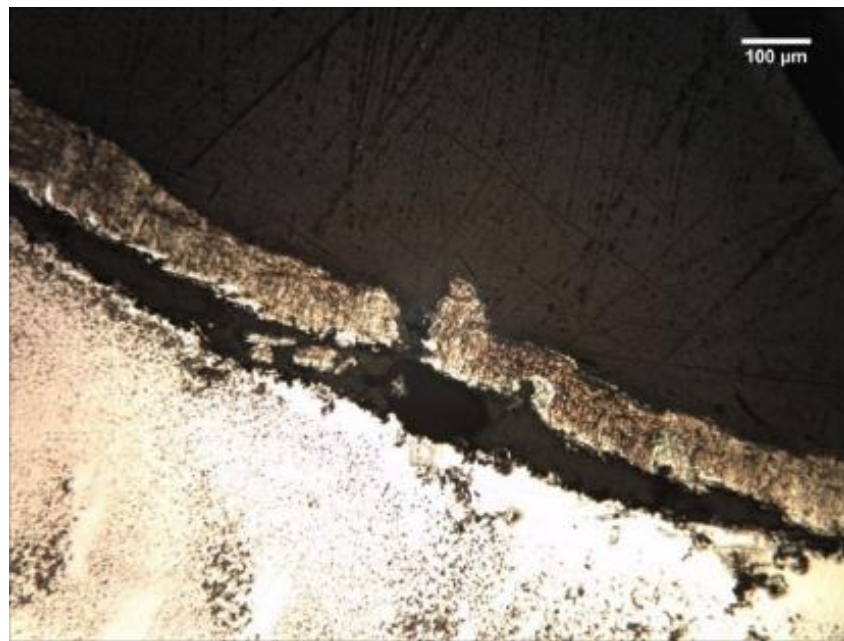


*Figure 3.12. Common scrapes in the lock-seam and the corrugations of galvanized steel from Plant B.*

Both of the aluminized and galvanized steel pipes had coating scrapes along the corrugations likely a result of transportation and handling as shown above in Figure 3.12. The scrapes did not seem to penetrate the full thickness of the coatings but did result in coating losses of as much as half the coating thickness. Figure 3.13 shows the two types of dents that are common in the metal corrugated pipes. Subfigure A shows an example of a bigger dent that is commonly located in the corrugations, while image B shows the smaller dents that are mostly located in the lock-seams. Figure 3.14 shows a metallographic image of a common coating break in the lock-seam. Not only is there a break in the coating but also delamination from the base metal around the break.

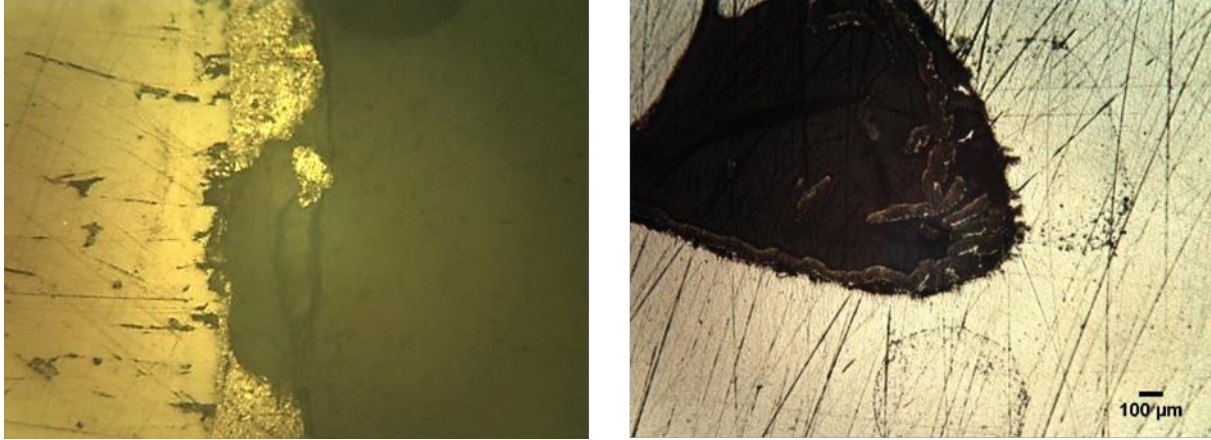


*Figure 3.13. Common dents that occur in the lock-seam in all pipe types in aluminized steel from Plant A.*

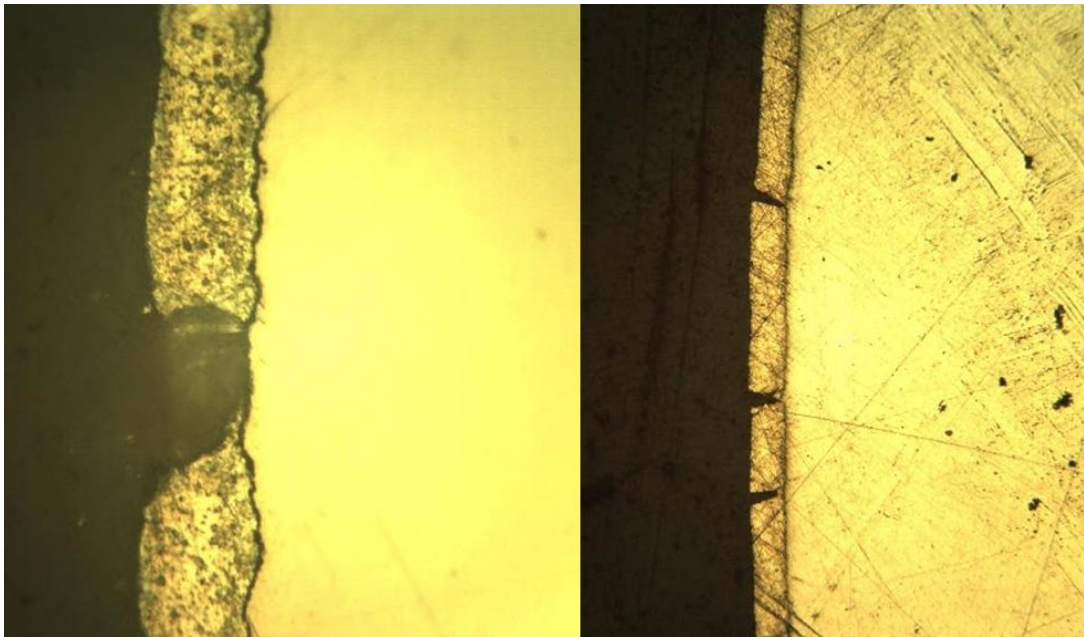


*Figure 3.14. Metallographic image of a common coating break in the lock-seam in PLANT A-Al.*

Figure 3.15 and Figure 3.16 show two types of defects in the lock-seam in the aluminized and galvanized steel pipes from Plant A. In both aluminized and galvanized steel, coating breaks and breaks in the intermetallic portions of the coating were observed in all lock-seams. Similar images were obtained from samples of lock-seams from the other plants as well. Since defects within the lock-seams were visible in all of the pipes analyzed, the remainder of the report presents only the size of the defects with only a single photo example from each plant.



*Figure 3.15. Metallographic images of coating break and shreds in aluminized steel pipe from Plant A.*



*Figure 3.16. Metallographic images of coating break and shreds in galvanized steel pipe from Plant A.*

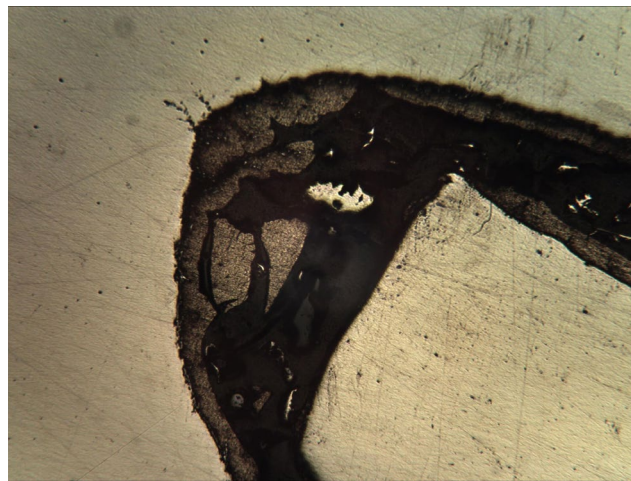


### 3.3.4. Plant B

The defects in Plant B metal drainage pipes were investigated, and the location, size and possible cause of defects are presented in Table 3.4. Similar to the results of the analysis of the pipes from Plant A, only the aluminized pipes showed visible signs of pre-existing corrosion but with much shallower pits. The coating breaks in both aluminized and galvanized pipes were similar in size ranging from 0.05 – 0.08 mm. Delamination of the coating with shards of coating were also present in the folds of the lock-seam as shown in Figure 3.17.

*Table 3.3. Type, Size and Possible Cause of Defects in Plant B Pipes.*

| Material   | Type of Defects              | Location                    | Width (mm) | Depth (mm)  |
|------------|------------------------------|-----------------------------|------------|-------------|
| Aluminized | Preexisting Corrosion (Pits) | Corrugations and Lock-seams | 1 -2.5     | 0.09-0.02   |
|            | Scratches/Scrapes            | Corrugations                | 0.05-2     | 0.015-0.045 |
|            | Dents                        | Lock-seams and Corrugations | 5-7        | 0.15-0.25   |
|            | Coating Breaks               | Lock-seam                   | 0.07-0.11  | -           |
| Galvanized | Preexisting (Pits)           | -                           | -          | -           |
|            | Scratches/Scrapes            | Corrugations                | 0.05-2     | 0.015-0.045 |
|            | Dents                        | Lock-seams and Corrugations | 7-20       | 0.15-0.21   |
|            | Coating Breaks               | Lock-seam                   | 0.05-0.078 | -           |



*Figure 3.17. Metallographic image of coating break and shreds in galvanized steel pipe from the Plant B.*

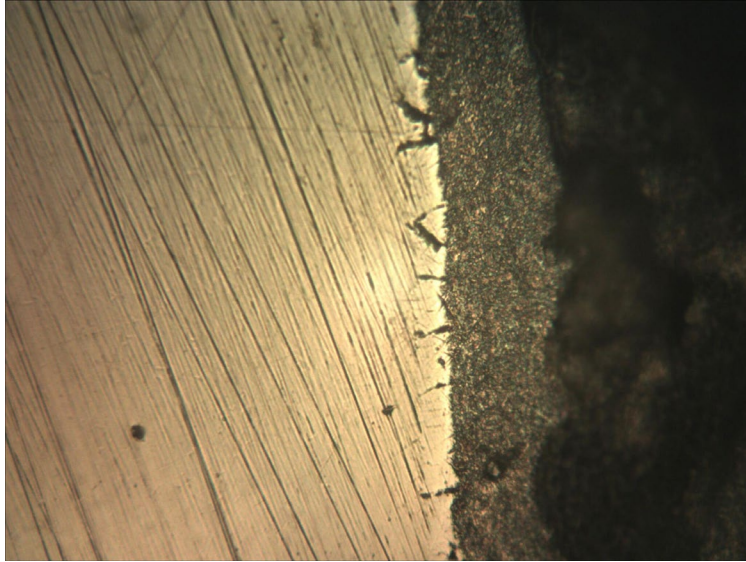
### 3.3.5. Plant C

The defect analysis of Plant C pipes is shown in Table 3.6. Similar to the pipes from Plant B and Plant A, the galvanized pipes from Plant C showed less defects than aluminized steel pipes. In this case the galvanized pipes also had some pre-existing pits and the coating breaks for both pipe materials were similar in size compared to the previously presented sizes from other plants.

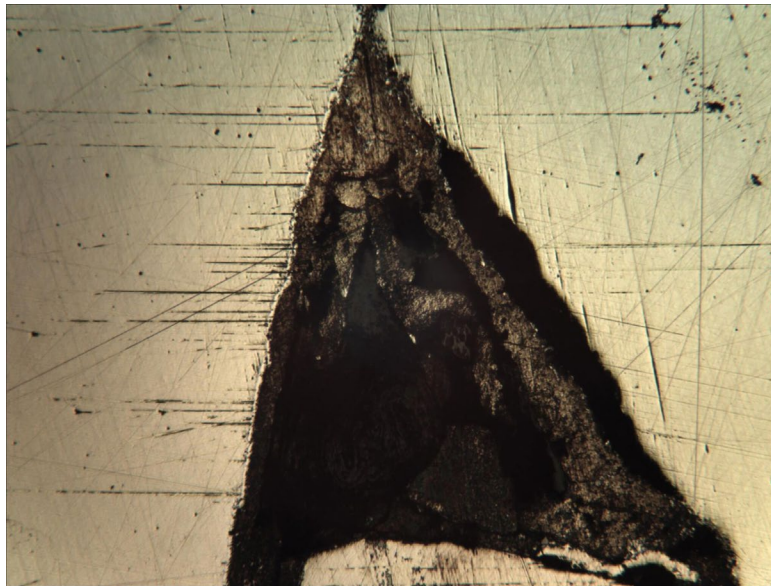
*Table 3.4. Type, Size and Possible Cause of Defects in Plant C Pipes.*

| Material   | Type of Defects              | Location                    | Width (mm) | Depth (mm)  |
|------------|------------------------------|-----------------------------|------------|-------------|
| Aluminized | Preexisting Corrosion (Pits) | Corrugations and Lock-seams | 1-3.5      | 0.13-1.1    |
|            | Scratches/Scrapes            | Corrugations                | 0.05-2     | 0.015-0.045 |
|            | Dents                        | Lock-seams and Corrugations | 3-5        | 0.1-0.4     |
|            | Coating Breaks               | Lock-seam                   | 0.06-0.18  | -           |
| Galvanized | Preexisting (Pits)           | Corrugations and Lock-seams | 0.16-0.8   | -           |
|            | Scratches/Scrapes            | Corrugations                | 1-1.5      | 0.2-0.28    |
|            | Dents                        | Lock-seams and Corrugations | 0.7-0.75   | 0.19-0.4    |
|            | Coating Breaks               | Lock-seam                   | 0.05-0.15  | -           |

Figure 3.18 and Figure 3.19 show examples of coating defects within the lock-seams. In Figure 3.19 a metallographic image is shown of an intact coating but with breaks in the intermetallic layer. This would be the ideal result of formed lock-seams in which the forming only results in some damage to the brittle intermetallic layer but no damage to the metallic coating. Figure 3.19 shows again, coating shards within the fold of the lock-seams. This form of coating damage may be unavoidable due to the compressive action of the region.



*Figure 3.18. Metallographic image of coating break and shards in galvanized steel pipe from the Plant B.*



*Figure 3.19. Metallographic image of coating break and shards in galvanized steel pipe from the Plant B.*

### 3.3.6. Plant D

Both the lock-seam and the corrugation locations were analyzed for defects and Table 3.8 presents the results for the aluminized and galvanized steel pipes from Plant D.

Table 3.5. Type, Size and Possible Cause of Defects in Plant D Pipes.

| Material   | Type of Defects              | Location                    | Width (mm) | Depth (mm)  |
|------------|------------------------------|-----------------------------|------------|-------------|
| Aluminized | Preexisting Corrosion (Pits) | Corrugations/ Scratches     | 1.0-1.4    | 0.04-0.095  |
|            | Scratches/Scrapes            | Corrugations                | 1-3.8      | 0.043-0.065 |
|            | Dents                        | Lock-seams and Corrugations | 0.4-0.45   | 0.1-0.36    |
|            | Coating Breaks               | Lock-seam                   | 0.07-0.21  | -           |
| Galvanized | Preexisting (Pits)           | Lock-seams and Corrugations | 2.8-3      | -           |
|            | Scratches/Scrapes            | Corrugations                | 1-7        | 0.06-0.6    |
|            | Dents                        | Lock-seams and Corrugations | 1.5-3      | 0.15-0.21   |
|            | Coating Breaks               | Lock-seam                   | 0.01-0.08  | -           |

The pipes from Plant D were additionally sprayed to protect the coating from further damage as shown in Figure 3.20 which shows the spray-coated metal pipes.



Figure 3.20. Additional spray-coated pipe in an aluminized steel pipe from Plant D.

The additional coating of the sides of the pipe affected the quantification and detection of visible coating defects in the pipe. Despite this metallographic samples obtained still showed coating defects within the lock-seam of the pipes and pre-existing corrosion pits were observed on both aluminized and galvanized steel pipes. Figure 3.21 shows an example of a coating defect observed within the lock-seam of one of the pipes. In this particular case, there is a break in the outer coating layer but little visible damage to the intermetallic layer.



*Figure 3.21. Metallographic image of coating break and shards in galvanized steel pipe from the Plant B.*

#### 3.4. Discussion

From complete analysis of the pipes, the galvanized steel pipes have the least number of visible defects compared to the aluminized steel pipe. This could be a result of the higher ductility of zinc compared to that of aluminum. Also, the ultimate tensile strength for zinc and aluminum is found to be approximately 328 MPa<sup>64</sup> and 150 MPa<sup>65</sup>, respectively. As a result, the aluminum coating can break more easily due to stresses during the forming process than the zinc coating in the galvanized steel.

For pre-existing corrosion, most of the pits were observed in the aluminized steel pipes in all manufacturers. Additionally, the loosest lock-seams were observed on aluminized steel pipes of Plant B and Plant D. These lock-seams might have been rejected according to AASHTO M36. However, AASHTO M36 does not quantify the amount of looseness in each lock-seam that consider as a rejection criterion .

Breaks in the coating are likely to be the result of manufacturing because they were observed in all pipe types of all manufacturers. However, scratches and scrapes along corrugations and lock-seams could be due to manufacturing or handling and transport. Previous work showed that debris in the rollers of the forming equipment can yield such forms of defects. It was also clear from the conditions of the pipes during the delivery, the handling was not very controlled, and pipes were placed on top of each other possibly resulting in scrapes of the pipes. Dents along corrugations are likely due to handling and transport, while the dents within the lock-seam could have been due to the forming process.

At this point, it is not known how the looseness of the lock-seams influences corrosion durability. A loose lock-seam would allow water to move freely within the lock-seams while tighter lock-seams would restrict flow. If defects are present within a loose lock-seam, they may cause a decrease in the service life. On the other hand, tight lock-seams may promote crevice corrosion.

The looseness and presence of defects within the lock-seams will be the focus of the preliminary experiments to be reported in the next report. Immersion experiments are currently set up focused on the loosest and tightest lock-seams of each material according to the results shown in Figure 3.10.

### 3.5. Conclusion

It can be concluded based on the results of the conditions of the pipes presented in this report that:

- All the lock-seams analyzed from the different plants contained defects likely due to the manufacturing process.
- The coating defects were in the form of breaks, delaminations, and shards of coating material.
- The galvanized pipes showed less defects within the lock-seams than aluminized steel pipes however all the pipes despite the material had at least some defects within the lock-seams.
- The aluminized steel showed more signs of pre-existing corrosion pits.
- The most distinguishable variable found between the lock-seams of different plants is the looseness of the lock-seams.
- The maximum looseness found was 8 mm in aluminized steel size 36 in from Plant B.
- The typical defect width inside the long seam and along corrugations is approximately 1 mm. This size will be used in formulating the influence of the defects on service life.

## CHAPTER 4. EXPOSURE TESTING

The experimental methods presented in this section of the report were formulated to address the question of whether defects within the lock-seams reduce service life. A description of simulated natural water solutions is provided. A description of short- and long-term immersion testing is presented as well.

### 4.1. Testing Solutions

Two types of solutions were formulated to simulate mild and aggressive conditions of Florida natural waters not considering water hardness. The mild solution comprised 30 ppm of sodium sulfate and 50 ppm of chloride yielding a resistivity of ~5800 Ohm-cm. The aggressive solution contained 500 ppm of chloride and 30 ppm of sulfates yielding a resistivity of ~850 Ohm-cm. The mild solution is similar to solution S previously used in project BDK84 977-11 with a slightly higher chloride concentration corresponding to an expected service life for aluminized steel pipes of approximately 100 years and ~59 years for galvanized steel. The values were obtained based on the empirical formula presented in the FDOT Drainage Design Guide for aluminized steel 16 ga. pipe expressed as

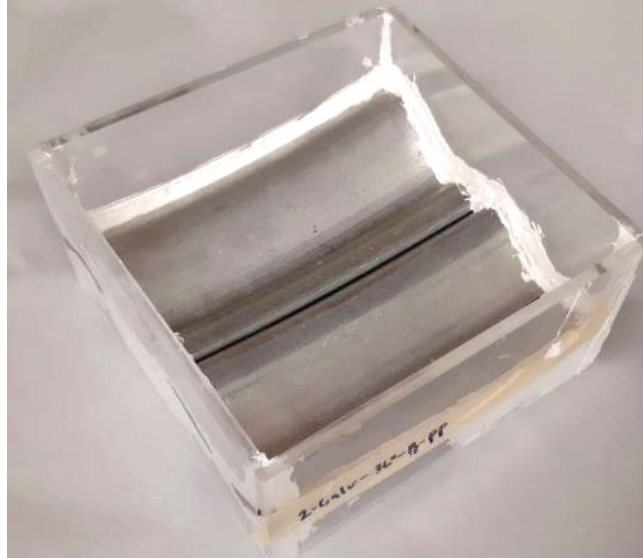
$$\text{Service Life} = 50(\log_{10} \rho - 1.746) \quad \text{Equation 6}$$

for the pH range of 7 to 8.5. The aggressive solution, while slightly more aggressive than natural water conditions, was used to promote activation of the aluminized coating to observe the full capability of the galvanic protection afforded by the aluminum coating. The expected service life for the aggressive solution is ~59 years for aluminized steel and 25 years for galvanized steel. In addition to these solutions, for some of the experiments, where necessary, more concentrated solutions with chloride such as 3 g/l, 5 g/l and 35 g/l were used. Inhibitive ions such as the ones that may result in protective scale formation were not considered but based on prior work on blemished aluminized steel, precipitating solutions would yield a service life slightly less than non-precipitating solutions.

### 4.2. Lock-Seam Immersion Cells

Lock-seam samples were cut out of the pipes with dimensions of 6×6 inches to study the long-term corrosion propagation. The samples were placed in a Plexiglas box and sealed with epoxy adhesive at the edges of the samples to contain ~300 mL of simulated solution. One of the important questions regarding corrosion within the lock-seam is whether the solution can reach and fill the space within the lock-seam. If solution is not able to fill the space, then a possibly more benign condition may result within the lock-seam in which a thin moisture layer may reside on the internal surfaces. Upon placement of the simulated solution, it was observed that the solution easily leaked through the lock-seams indicating that complete filling of the lock-seam space was possible. To prevent solution leaking, the bottom opening of the lock-seam was sealed with epoxy on what would normally be the soil side of the pipe. These samples were designed to simulate fully immersed conditions normally present at the bottom of drainage pipes. The electrolyte was replaced biweekly to ensure chemical consistency of the solutions. The specimens were housed in

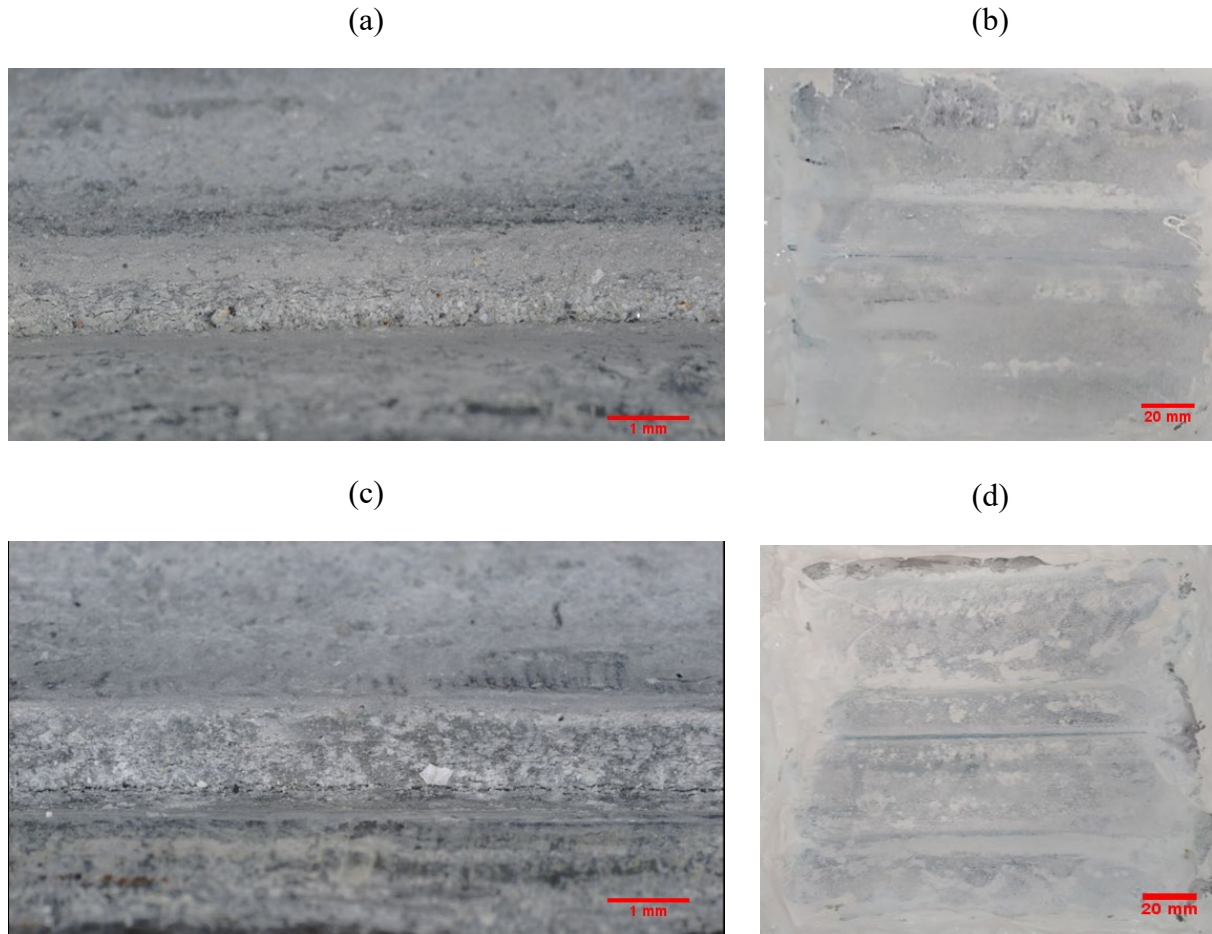
plastic containers to prevent evaporation of solution. A typical sample is as shown in Figure 4.1. Images of the samples are taken regularly for visual observation of corrosion damage evolution.



*Figure 4.1. Prepared sample (6×6 inches) sealed inside Plexiglas container for long-duration immersion tests.*





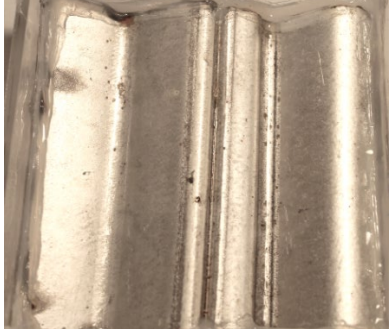
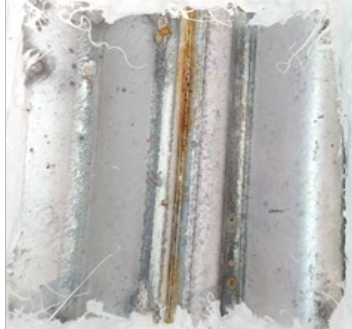

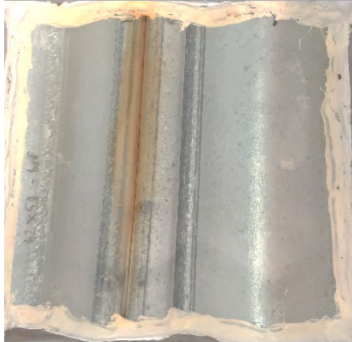
After 227 days of immersion, the samples were removed from the Plexiglas cells and visually assessed for corrosion damage. Figure 4.2 shows images of the exposed surfaces of the galvanized steel pipe sections in aggressive (Figure 4.2 b) and mild (Figure 4.2 d) solutions. In both cases, there is a substantial amount of zinc corrosion products with no signs of steel corrosion products, likely indicating that the zinc was able to provide sufficient sacrificial protection to any exposed steel. Within the lock-seam of the samples exposed to aggressive (Figure 4.2 a) and mild (Figure 4.2 c) solutions, there is not as much visible zinc corrosion products and again no signs of steel corrosion products. The fact that the zinc coating corroded more outside of the lock-seam provides verification that crevice corrosion does not seem to be of concern, at least within the time frame of the experiments. Therefore, the focus of the analysis will be on the aluminized steel samples.



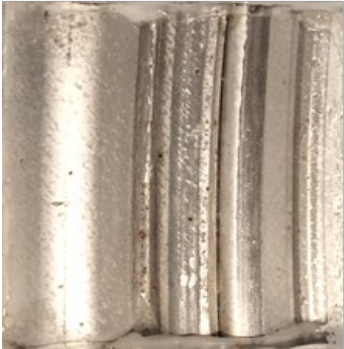

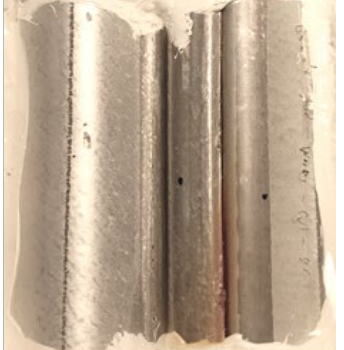



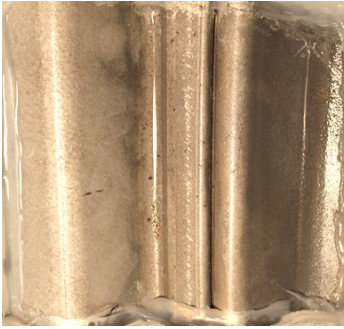



*Figure 4.2. Galvanized steel long-term immersion cell after 227 days inside and outside the lock-seam: (a) Lock-seam of galvanized steel in aggressive solution; (b) surface image of the galvanized steel long-term sample in aggressive solution; (c) Lock-seam of galvanized steel in mild solution; (d) surface image of the galvanized steel long-term sample in mild solution.*

Aluminized steel samples cut from plant A and B pipes are presented in Figure 4.3 and those of plant C and D are presented in Figure 4.4. After 51 days of immersion, the plant A specimens show clear signs of steel corrosion products at the mouth of the lock-seams, and this occurs more in the mild case. There are no signs of aluminum corrosion products at this stage of exposure indicating that the aluminum does not seem to provide any protection to exposed steel defects as was the case with the galvanized steel specimens. However, at the end of the exposure period (227 days), there is clear presence of general aluminum corrosion and in some cases aluminum corrosion around defects suggesting some protection ability after a certain exposure period. Similar results were observed for plants B, C, and D. This agrees with prior work which showed that initially the aluminum remains passive in natural waters until there is either a brief period where the bulk solution pH or local cathodic activity at the coating surface results in alkalinization. Additionally, there were also some cases in which the aluminum corrosion products were localized and surrounded small defects.

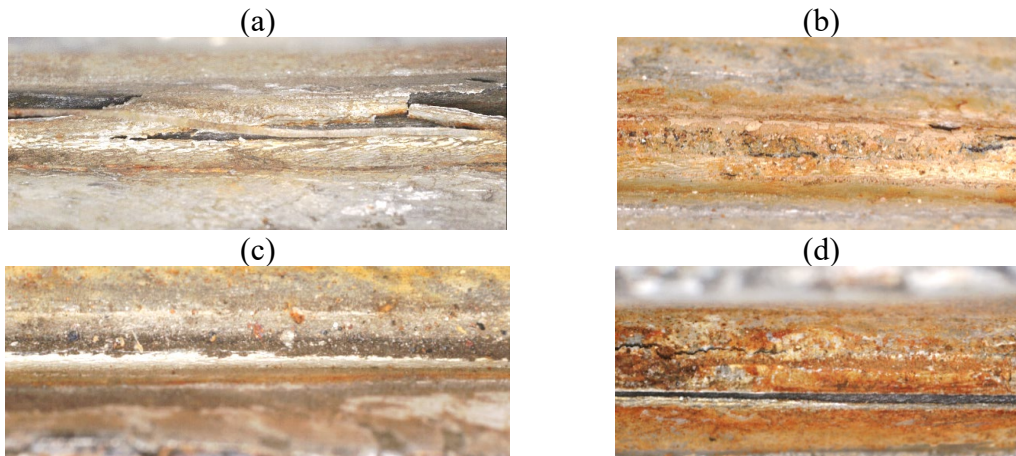
| Sample Name        | After 51 days of Immersion  | After 227 days of Immersion  |
|--------------------|---|--|
| Plant A Aggressive |    |    |
| Plant A Mild       |   |   |
| Plant B Aggressive |  |  |
| Plant B Mild       |  |  |

*Figure 4.3. Aluminized steel long-term immersion samples at 51 days (left column) and after 227 days (right column) of immersion in aggressive and mild solutions for Plants A and B.*

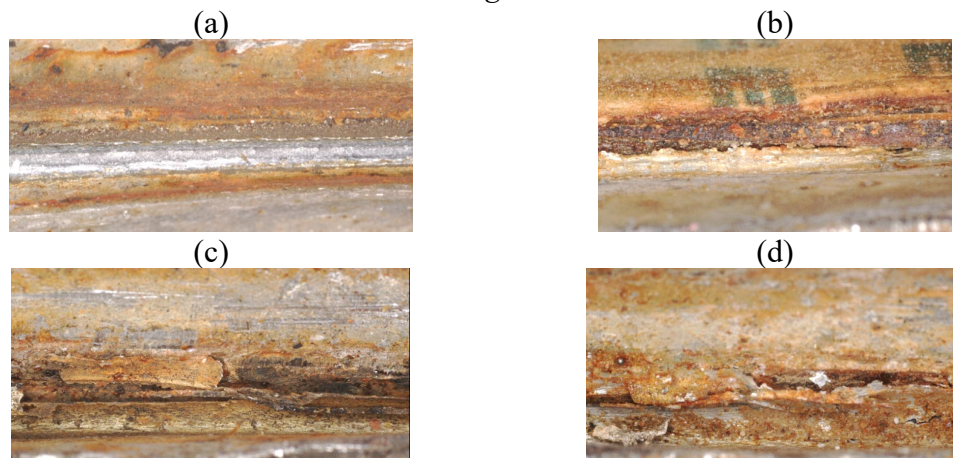
| Sample Name        | After 51 days of Immersion  | After 227 days of Immersion  |
|--------------------|---|--|
| Plant C Aggressive |    |    |
| Plant C Mild       |   |   |
| Plant D Aggressive |  |  |
| Plant D Mild       |  |  |

*Figure 4.4. Aluminized steel long-term immersion samples at 51 days (left column) and after 227 days (right column) of immersion in aggressive and mild solutions for Plants C and D.*

After visual inspection of the exposed surface of the lock-seam sections was completed, the seams were disengaged to determine the level of corrosion damage present within the confined regions of the lock-seams. Figure 4.5 and Figure 4.6 show images of the cut end and internal bends of the seams after unlocking. Generally, there were more corrosion products observed in the lock-seams for the samples exposed to the aggressive solution than the mild solution.



*Figure 4.5. Lock-seam images after immersion in aggressive and mild solutions for 227 days for Plant A and B: (a) Plant-A long-term immersion cell lock-seam in mild solution; (b) Plant-A long-term immersion cell lock-seam in aggressive solution; (c) Plant B long-term.*

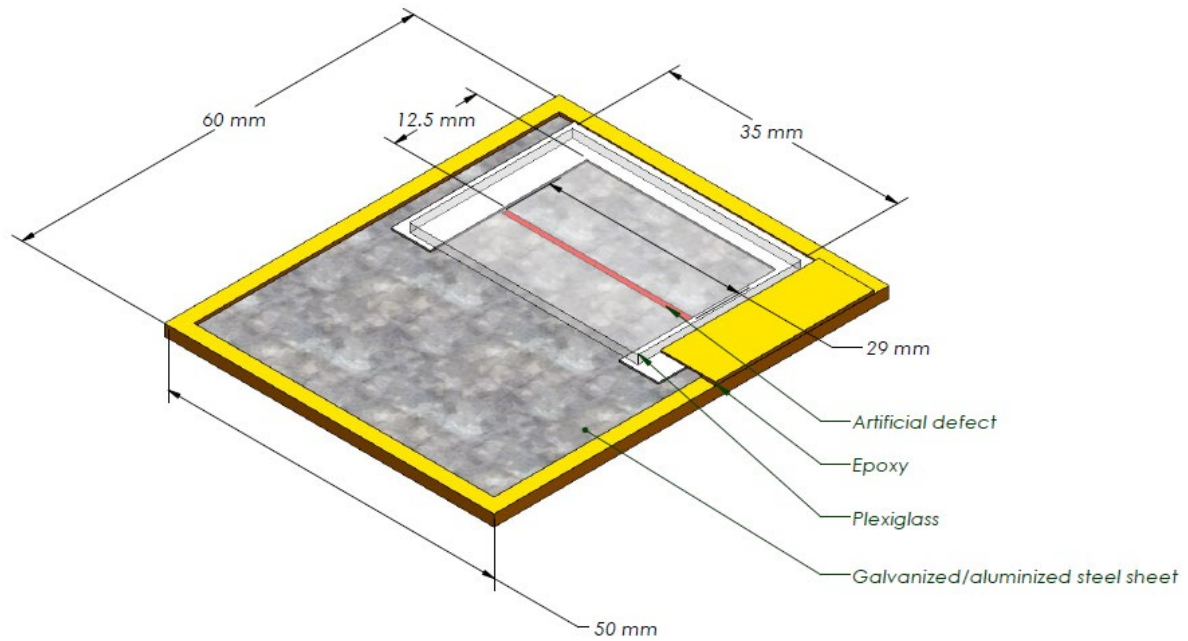


*Figure 4.6. Lock-seam images after immersion in aggressive and mild solutions for 227 days for Plant C and D: (a) Plant C long-term immersion cell lock-seam in mild solution; (b) Plant C long-term immersion cell lock-seam in aggressive solution; (c) Plant D long-term.*

#### 4.3. Crevice Cells with Defect

To determine the level of galvanic protection afforded by each coating material at defect locations, artificial defects were formed using acid etching. Since longitudinal defects were the most

prevalent form found within the lock-seams, defects in the form of small grooves were made on the surface of coatings. In order to achieve this, a 3d printed part with an opening was used in which concentrated HCl was inserted as droplets and left for 50-55 seconds. The part was secured to the specimen via zip ties and a PTFE gasket was used to mitigate leaking of acid outside the channel compartment. Once the etching process was complete, the steel sample was epoxied at the cut edge surfaces using Sikadur SLV 55. A 52-micrometer thick PTFE film was used to maintain a consistent gap space between a Plexiglas crevice former and the defected surface. The PTFE film was kept in place using the epoxy itself while the Plexiglas was fastened using zip ties. The setup is depicted below as Figure 4.7. The samples were immersed in simulating solutions of natural water to observe the protection capabilities of the coating materials.



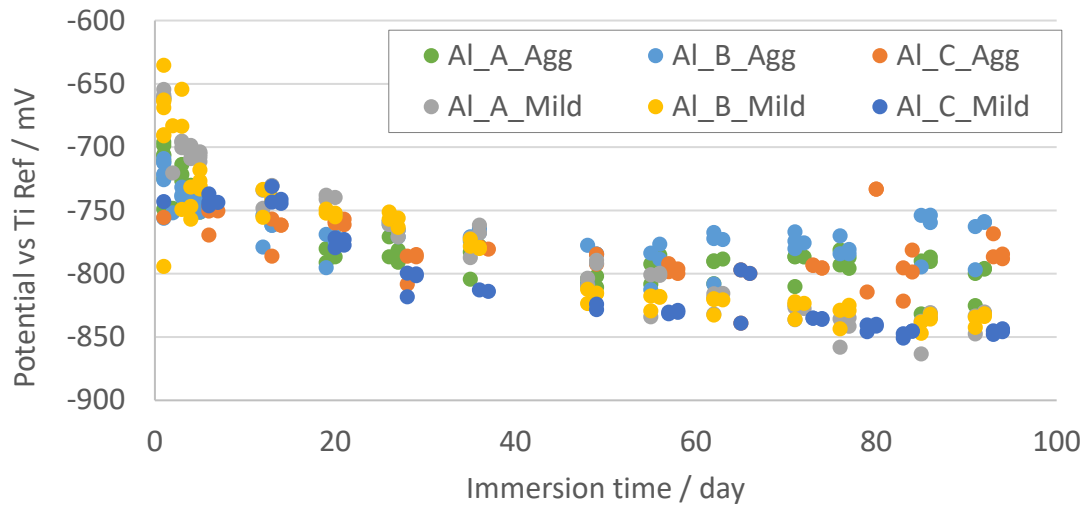
*Figure 4.7. Schematic figure of crevice sample with artificial defect.*

Prior to immersion, samples were scanned using a profilometric device to measure the depth of the defects. An example of the depth profile is shown in Figure 4.8. While originally it was thought that the defect consistently reached the steel substrate, it was later determined that in some cases, the defect only reached the intermetallic layer with distinct regions where the bare steel was exposed. In all samples, there was at least a part of the defect that exposed the bare steel. However, corrosion of the defect was observed in all samples. For the samples that were immersed later in the aggressive solution, the defect depth varied from 29 to 79  $\mu\text{m}$ , 14 to 71  $\mu\text{m}$  and 7 to 65  $\mu\text{m}$ , for samples A, B, and C, respectively. For the mild samples, the variations for samples B, and C were 10 to 65  $\mu\text{m}$ , and 47 to 101  $\mu\text{m}$ , respectively.



*Figure 4.8. Aluminized steel etched crevice sample with a line scan using profilometric device with variations in depths in the etched defect before immersion, where the lowest depth is 33  $\mu\text{m}$  and the maximum is 95  $\mu\text{m}$ . The sample is called Sample (A) and immersed under the mild solution.*

Open circuit potential and electrochemical impedance spectroscopy (EIS) measurements were performed on both types of coatings in both mild and aggressive solutions. The tests were performed in a three-electrode system with the coated sample as working electrode, a titanium mesh as the counter electrode and a saturated calomel electrode as the reference electrode. A frequency range of 100 kHz to 10 MHz was used with a 10 mV polarization amplitude for galvanized samples and 40 mV of polarization amplitude for aluminized samples. The open circuit potentials of the samples are shown in Figure 4.9. The OCP data over time for both samples immersed in mild and aggressive solutions showed a similar trend, where the OCP decreased slightly over time. The results do not provide any indication of surface modification or corrosion.



*Figure 4.9. Open circuit potential of the samples immersed during the 90-day period in aggressive and mild solutions. To convert the reference potential from titanium to SCE, 197 mV is added to the OCP in the aggressive solution and 166 mV for the mild solution..*

The EIS data is shown in Figure 4.10 in Nyquist format with time as a parameter for aggressive and mild solutions. A finite element simulation was performed to assess the sensitivity of the measurements to the corrosion rate of the defect within the crevice. It was determined that the impedance measurements were not sensitive to defect corrosion rate but are almost equally sensitive to changes in the corrosion rate of the aluminum coating within and external to the crevice. Therefore, the presented impedance data is used to assess any changes in the aluminum coating. Generally, the impedance of the samples immersed in mild solutions was greater than that of the aggressive solution indicating that the aggressive solution is more corrosive.

The impedance of aluminized steel shows at least two-time constants and while many models to interpret the data have been proposed, there is still uncertainty in what each time constant physically represents. Additionally, the presence of the crevice former induces frequency dispersion that makes a detailed analysis of the data difficult. Since such a study to address this is outside the scope of this work, the impedance was analyzed according to the overall polarization resistance,  $R_p$ , of the measurements, which is the difference between the high and low frequency limits of the real part of the impedance and is often used as a general measure of corrosion state.

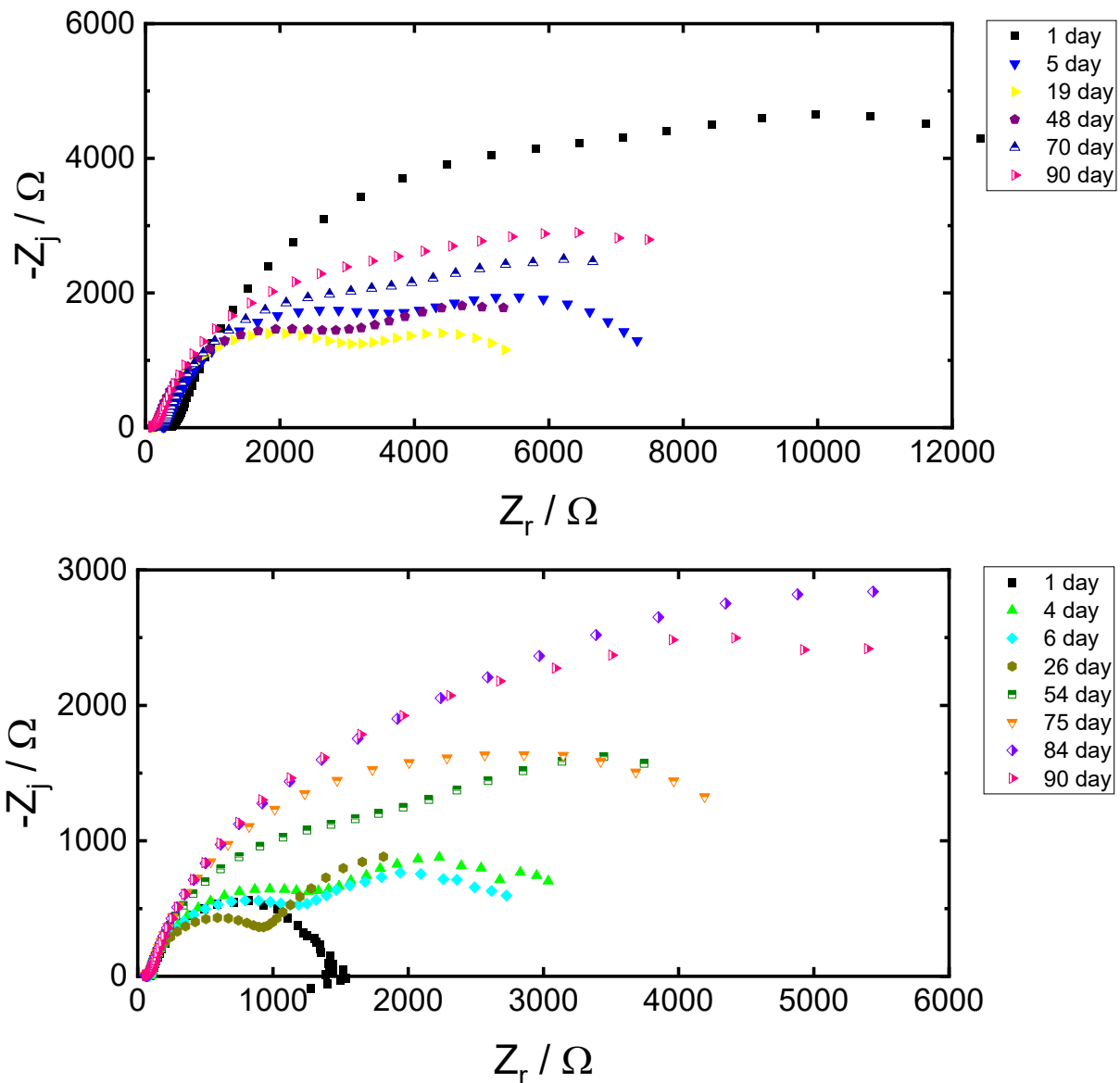


Figure 4.10. EIS results over time for the aluminized steel samples in the aggressive and the mild solution: sample immersed in the mild solution (top) and sample immersed in the aggressive solution (bottom).

From the Nyquist plot, the polarization resistance can be extracted using a measurement model that fits the data with a series of Voight elements data using a nonlinear regression method.<sup>66</sup> With the appropriate fit, the simulated data can be extrapolated to the high and low frequency limits of the real impedance to obtain estimates of the solution resistance and the zero-frequency limit of the real part of the impedance. The polarization resistance for both aluminized steel samples in the mild and aggressive solutions are shown in Figure 4.11. As the magnitude of the impedance data suggest, the polarization resistances for the mild solution are greater than those of the aggressive solution. Interestingly, the values of  $R_p$  for the mild solution decrease substantially over the first



couple of weeks. Following this, the  $R_p$  values of the mild solution show a continuous increase while the  $R_p$  values are low for the samples in the aggressive solution, and it stays mostly constant.

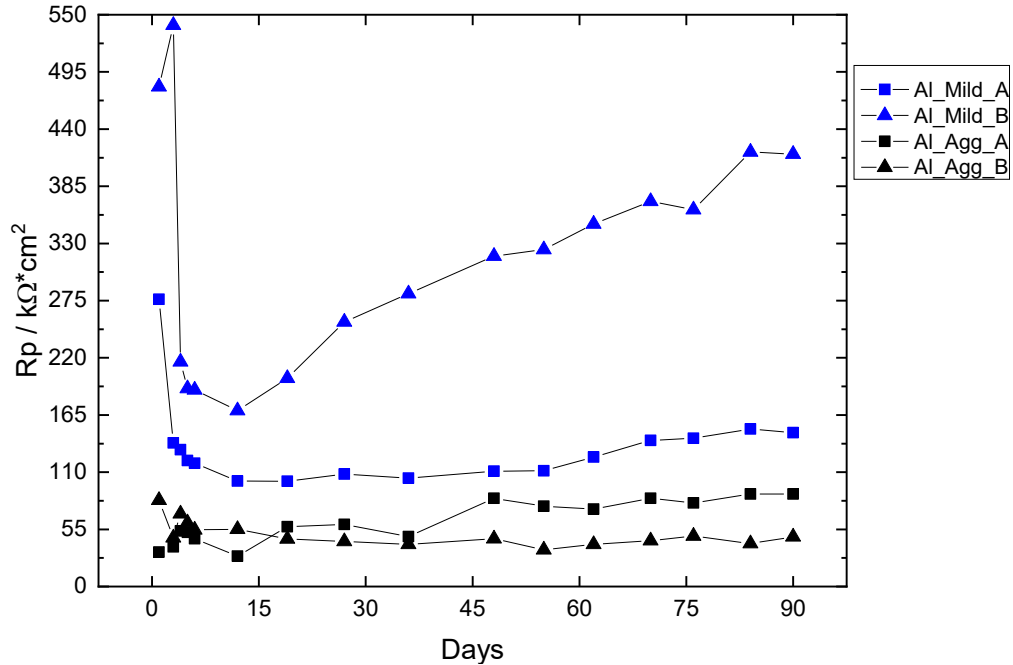
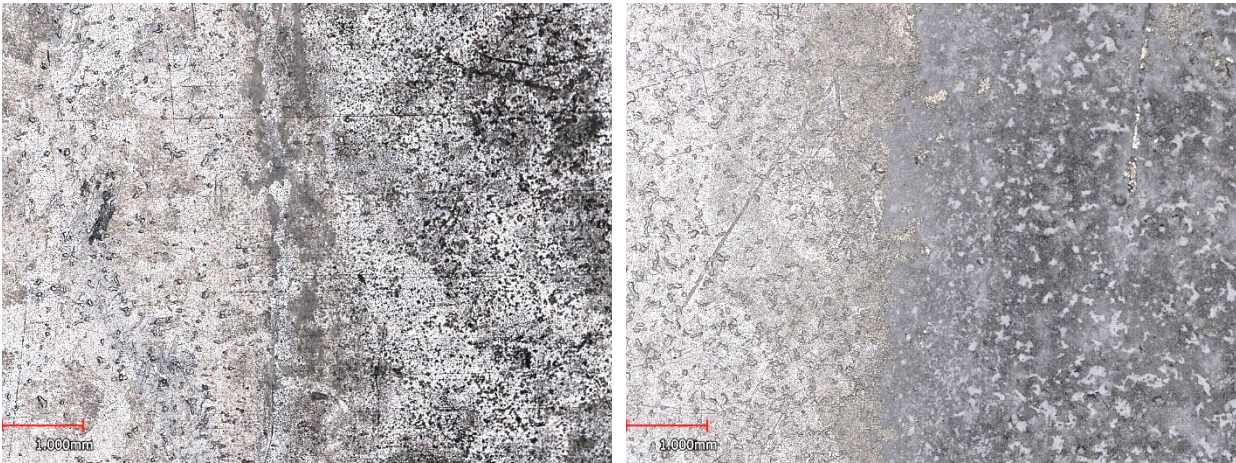


Figure 4.11. Polarization resistance for aluminized steel crevice samples in aggressive solution (black) and mild solution (blue) for two replicates for 90 days of immersion.

After 90 days of immersion, the samples were removed, cleaned, and analyzed. The aluminized steel samples with no defect in the aggressive solution showed a clear discoloration outside the crevice as Figure 4.12 shows, where the left side is inside the crevice, and the right side of the image is outside the crevice. In addition, the corrosion of the non-defected samples immersed in aggressive solution started at around 8 days, while the sample immersed in the mild solution started to show discoloration in the aluminum coating around 16 days.



*Figure 4.12. Crevice samples with no defect; a) in aggressive solution inside crevice; b) in aggressive solution outside crevice; c) in mild solution inside crevice; d) in mild solution outside crevice.*

Figure 4.13 shows one of the defected aluminized steel samples immersed in the mild solution. In this instance, aluminum discoloration, as shown in Figure 4.13 (b), occurred only on the unconfined region of the coating surface. In the other samples exposed to the mild condition, no coating discoloration was observed. Additionally, the sample shows rust diffusing outside the crevice location, which agrees with the results of the lock-seam immersion cells. Also, the presence of rust started to appear in samples immersed in the mild solution around 2 to 4 days, suggesting limited protection afforded by the aluminum coating.

For the defected samples immersed in the aggressive solution, the aluminized steel coupons showed corrosion of the exposed steel under the crevice as shown in Figure 4.14, where the appearance of rust was initially spotted between 4 to 8 days of immersion. The sample also shows a noticeable discoloration in the aluminum coating between inside and outside the crevice. Also, most of the samples showed accumulation of iron corrosion products in a specific location of the defect, as seen in Figure 4.14 (c). This accumulation was not present in the lock-seam samples suggesting that this may be a result of the defect forming process and not an indication of actual exposure performance. However, it does show that the aluminum was not able to provide adequate protection to exposed steel even in the aggressive solution.

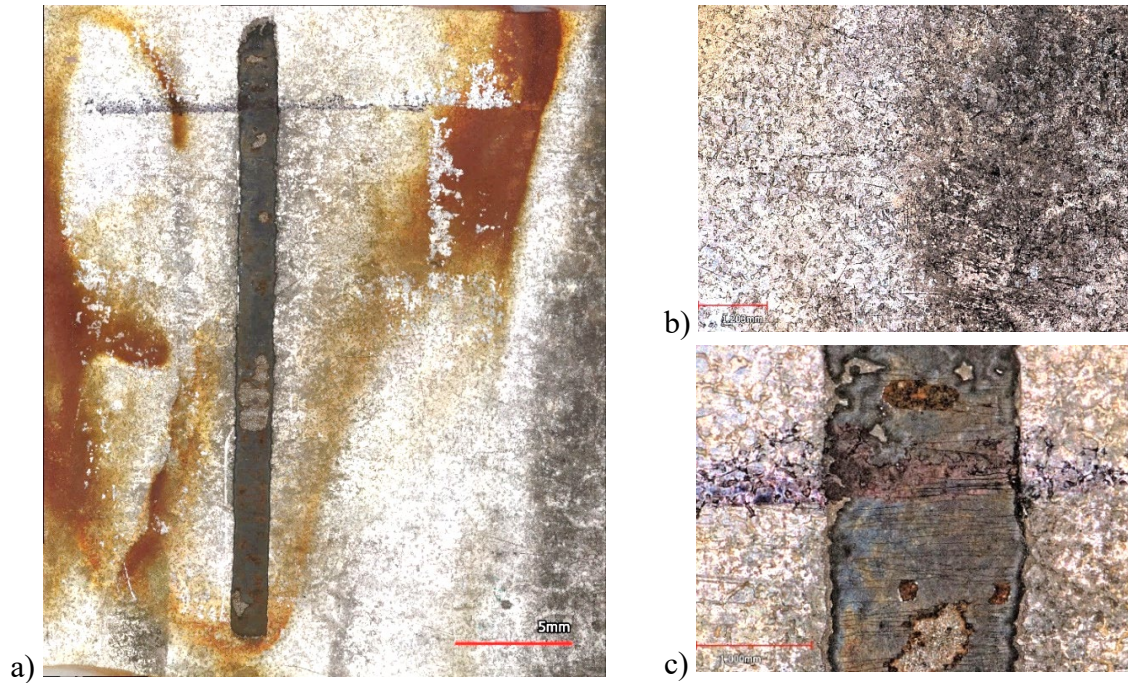


Figure 4.13. Crevice coupons of aluminized steel in a mild solution (A) after immersion of 90 days and the only sample with discoloration. a) inside crevice.; b) crevice entrance; c) defect.

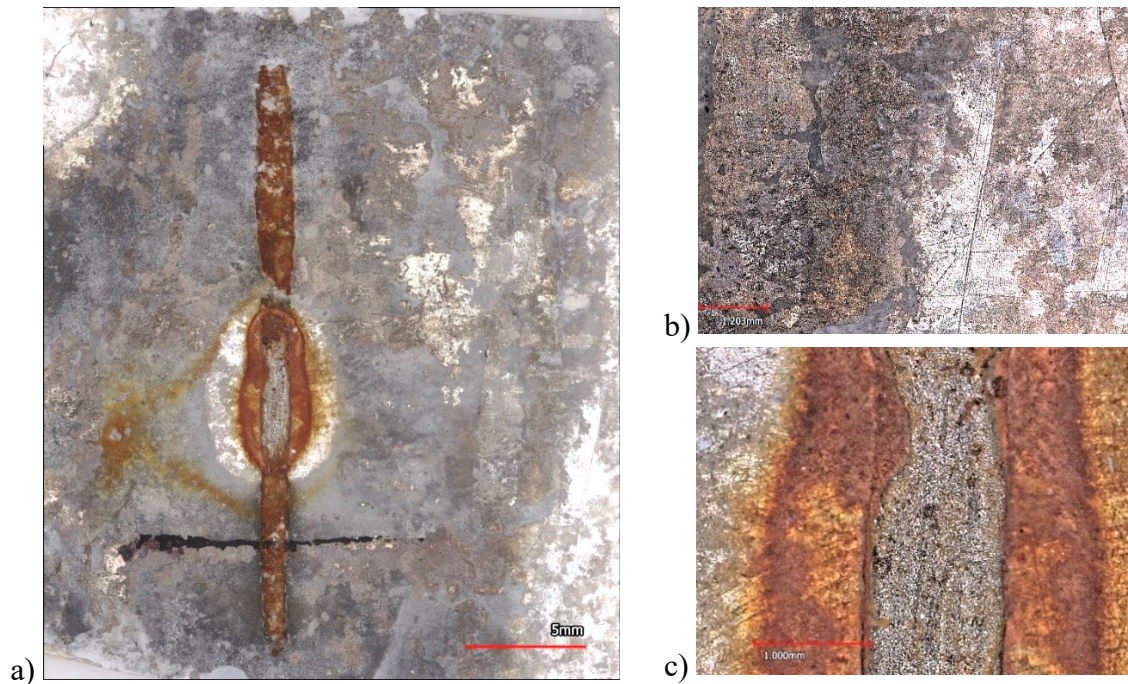


Figure 4.14. Crevice coupons of aluminized steel in an aggressive solution (A) after immersion of 90 days and the only sample with discoloration. a) inside crevice.; b) crevice entrance; c) defect..

Table 4.1. Average defect depth with the Estimated Corrosion Rate in  $\mu\text{m}/\text{year}$ .

|           | Avg Depth before | Max depth Before | Avg Depth After | Max depth After | Est. Steel Corrosion Rate $\mu\text{m}/\text{yr}$ |
|-----------|------------------|------------------|-----------------|-----------------|---|
| Al_Agg_C  | 27               | 32               | 150             | 266             | 580   |
| Al_Agg_B  | 47               | 71               | 152             | 258             | 490   |
| Al_Agg_A  | 45               | 86               | 43              | 119             | --  |
| Al_Mild_A | 42               | 69               | 33              | 157             | --  |
| Al_Mild_B | 46               | 66               | 33              | 102             | --  |
| Al_Mild_C | 65               | 101              | 48              | 118             | --  |

Table 4.1 shows the average and maximum defect depth prior to and following exposure. The depth values were obtained using the Keyence analyzer software of 3D profilometry data of the surface. Despite the visual appearance of steel corrosion products, in most of the samples, any corrosion damage at the defect was too small to be detected. The two samples that did show appreciable damage may have been influenced by the etching process. Since such damage was not observed on any of the lock-seam immersion samples, it may not necessarily reflect typical performance.

#### 4.4. Potentiodynamic Polarization Scans

Potentiodynamic polarization curves were obtained for steel, galvanized steel, and aluminized steel in the aggressive and mild solutions, which are shown in Figure 4.15 and Figure 4.16. The scan rate was  $0.16 \text{ mV/s}$ . The polarization curves exhibit a strong influence of solution resistance due to the low conductivities of the solutions used in the experiment. As a result, future work is needed to correct the polarization curves by compensating for the ohmic resistance. However, the obtained polarization curves are used to inform the finite elements model. The results in Figure 4.15 showed that the aluminized steel is slightly cathodic to the bare steel, while the galvanized steel is more cathodic. Also, the anodic kinetics were somewhat enhanced by chloride concentration. In Figure 4.16, the cathodic kinetics showed that the rate of oxygen reduction on steel may be greater than those of the aluminized steel surface, which shows some indication of mixed activation diffusion control.

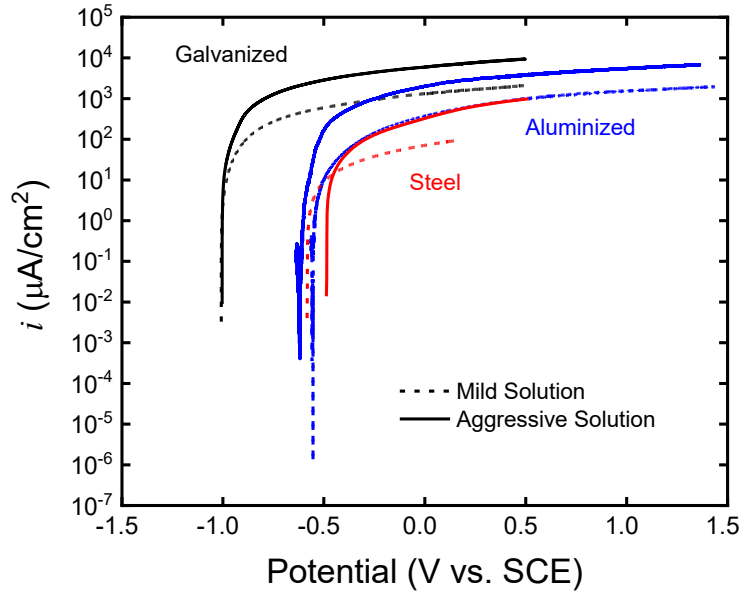


Figure 4.15. Anodic potentiodynamic polarization scans of aluminized and galvanized coatings in mild and aggressive solutions (room temperature, scan rate 0.16 mV/s).

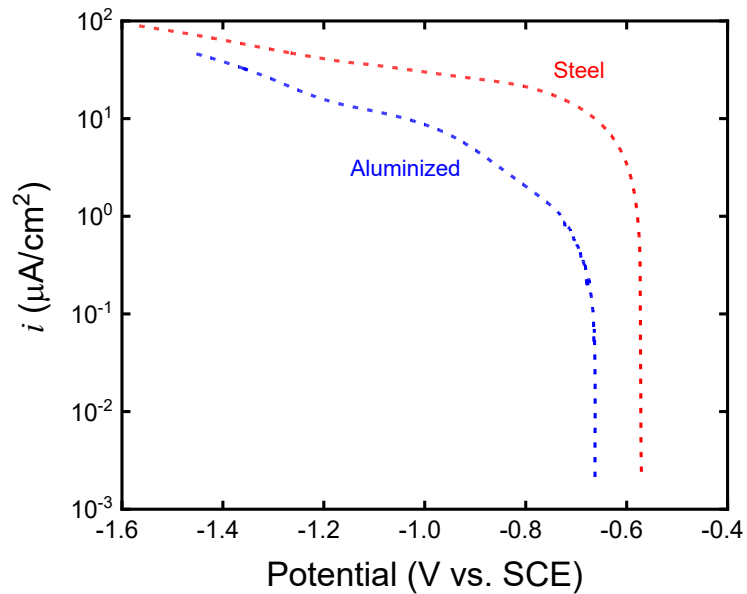


Figure 4.16. Cathodic potentiodynamic polarization scans of aluminized and steel in aggressive solutions (room temperature, scan rate 0.16 mV/s).

#### 4.5. Scanning Vibrating Electrode Technique (SVET) Samples

To simulate a defect for SVET scanning, two blocks of aluminum were placed on both sides of an aluminized carbon steel sheet as depicted in Figure 4.17. Aluminum blocks were adhered to the steel sheet by a conductive epoxy. After curing of epoxy for 12 hours, samples were cold mounted and the other side of samples were drilled and connected to a wire.

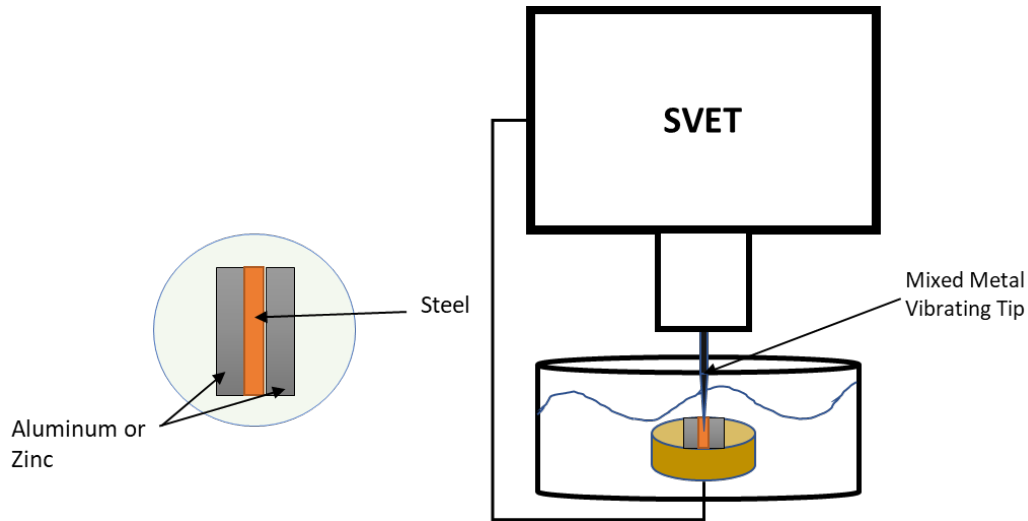


Figure 4.17. Schematic figure of sample made for SVET scanning.

Surface potential and current density mapping of the defected metals were obtained as a function of time and solution aggressiveness using a scanning vibrating electrode technique (SVET). This in situ, local technique consists of a vibrating conductive probe which measures the potential difference in an electrolyte above the surface of a substrate. The potential measured by the probe is instantaneous and therefore the vibration results in an ac potential signal which may be used to obtain potential maps across a corroding surface to identify regions of cathodic and anodic activity. The potential difference originates from a small electric field within the electrolyte solution due to corrosion activity. The potentials obtained from the SVET are converted to current densities using Ohm's law with the conductivities of the solutions and the amplitude that was used in the scan. Since it would be difficult or nearly impossible to obtain mapped surface corrosion information within corroding lock-seams, the results will be used to develop and evaluate finite element models designed to simulate the corrosion propagation within lock-seams.

A galvanized steel electrode with an artificial circular defect with a diameter of 3.6 mm was studied to measure the potential drop between the coating and the bare steel. The potential map across a quarter section of the surface is shown in Figure 4.18. The corresponding potential line scans are provided in Figure 4.19. It is important to note that the values of potential represent differentials within the electrolyte. The regions of red or positive values indicate anodic regions while the blue regions or negative values indicate cathodic regions. This shows that the galvanized steel is able to provide protection to the exposed steel even with a relatively large defect. Further experiments will be performed over time to determine the limit of this protection for both aluminized and galvanized steel.

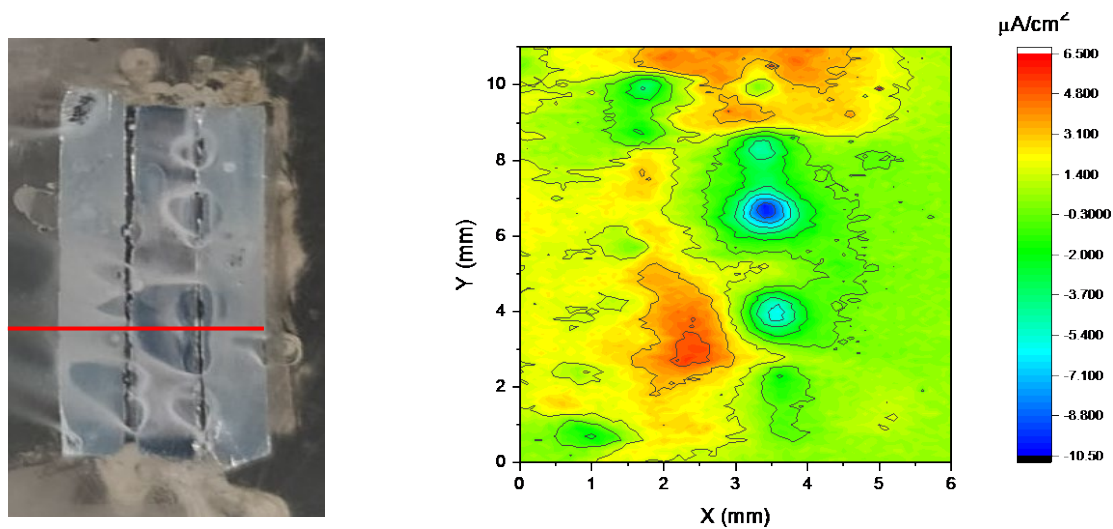


Figure 4.18. SVET results of galvanized steel in 0.5 g/L sodium chloride and 0.03 g/L sodium sulfate; current density map (right); sample after 4-hr scan (left). The blue color indicates the most cathodic locations, and the red color indicates the most anodic locations.

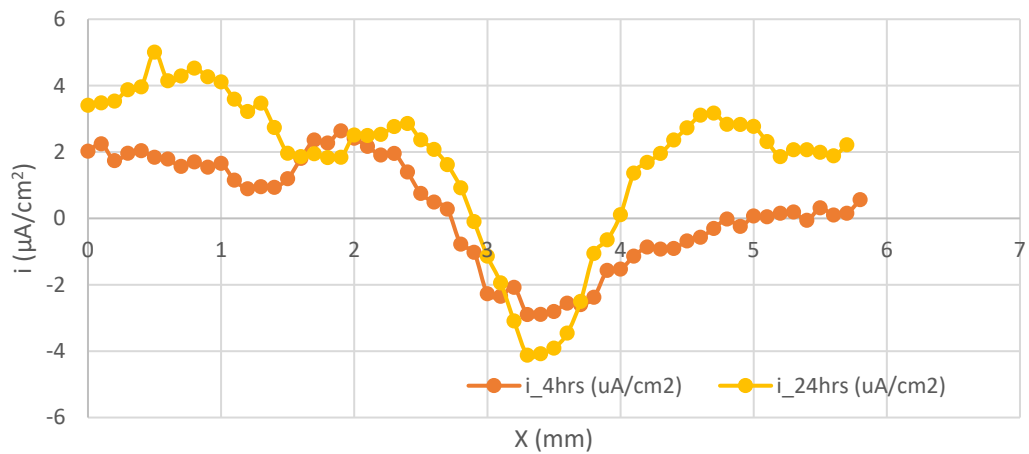


Figure 4.19. Galvanized steel SVET line scans under aggressive solution (0.5 g/L NaCl + 0.03 g/L Na<sub>2</sub>SO<sub>4</sub>) for the first 4 hours (yellow line) and after 24 hours (orange line).

For the aluminized steel in the aggressive solution, the steel sample showed both anodic and cathodic areas, as shown in Figure 4.20. Unlike the steel that was connected to zinc, aluminum did not provide enough coupling for the entire steel substrate, as it can be seen by the formation of steel corrosion products after 24 hours in the optical image shown in Figure 4.20. To further explain the corrosion behavior of defects in the aluminized steel under a confined region such as the lock-seam, a finite element model will be developed incorporating the main observations from the immersion results and the electrochemical characterization.

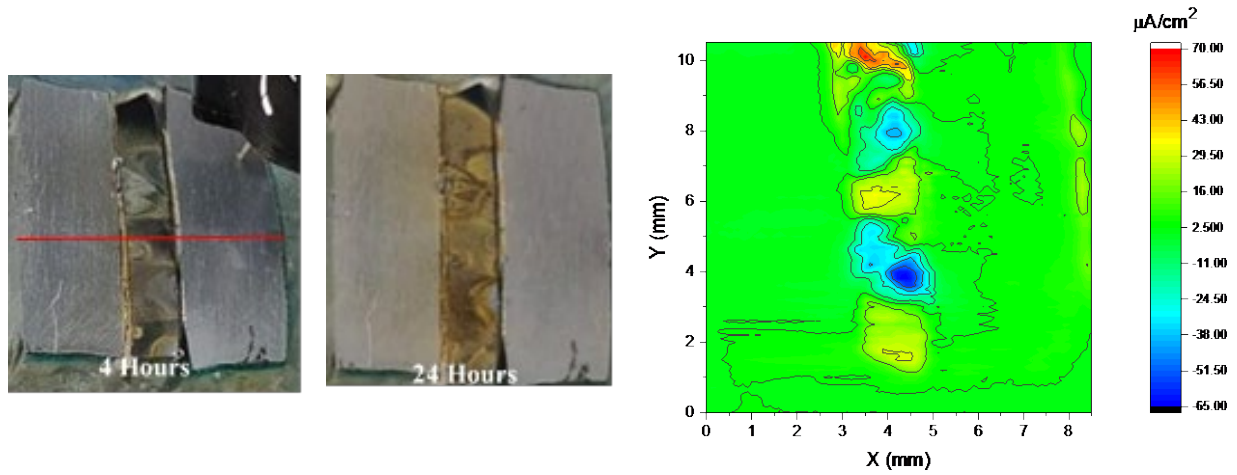


Figure 4.20. SVET results of aluminized steel in 0.5 g/L sodium chloride and 0.03 g/L sodium sulfate; a) sample after 4 hours scan; b) sample after 24 hours scan; a) current density map. The blue color indicates the most cathodic locations, and the red color indicates the most anodic locations.



## CHAPTER 5. FINITE ELEMENT SIMULATION

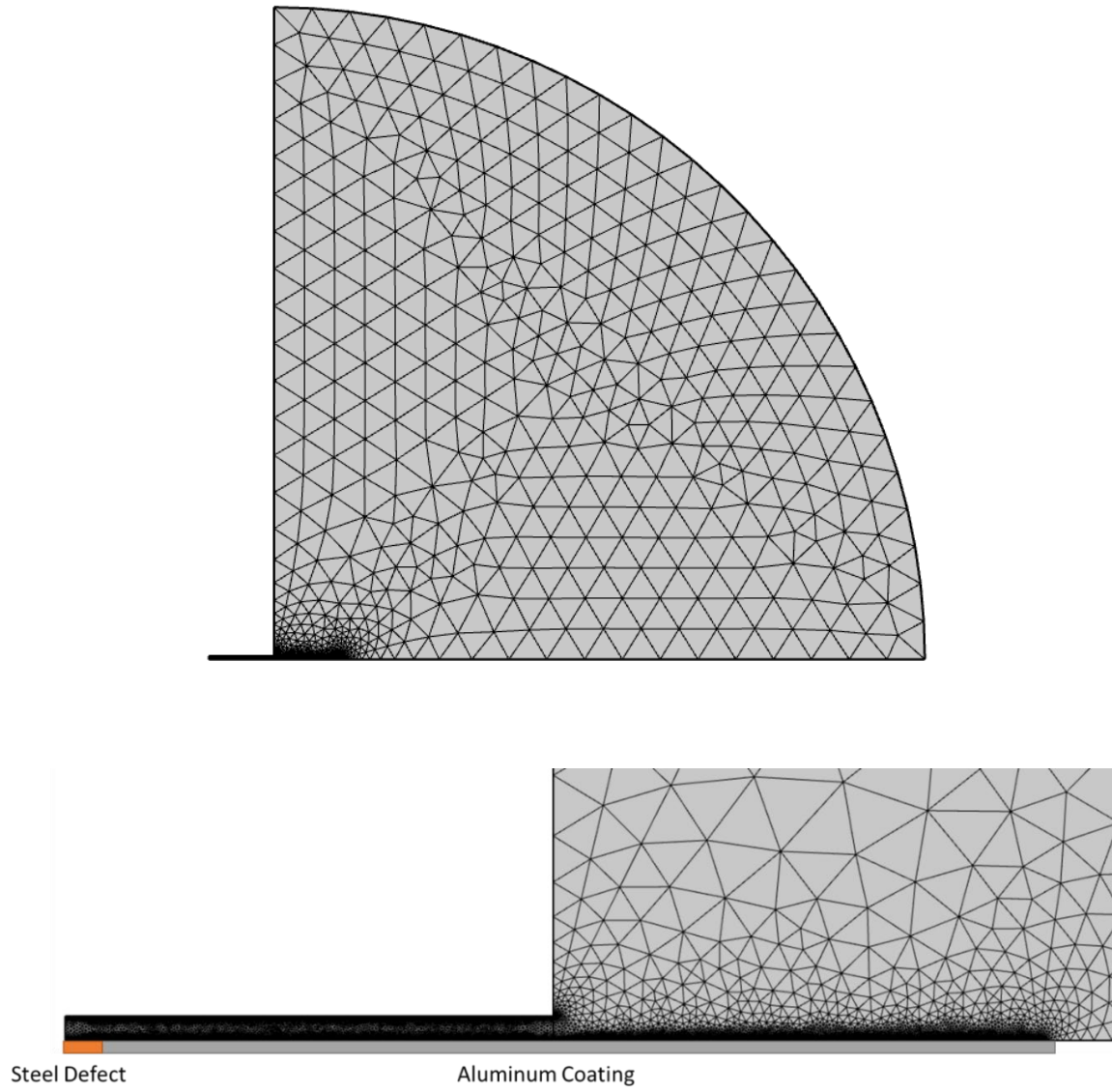
According to the exposure results and prior research, there is an initial period in which the aluminum coating remains passive and provides minimal protection to any steel defects. This period is followed by a seemingly uniformly active corroding aluminum of which the amount of protection afforded to defects would depend on the kinetic limitations of the corrosion reactions and solution composition and confinement.

One of the potential concern for corrosion in confined regions is the potential for crevice corrosion. In confined regions, oxygen depletion within the lock-seam may possibly initiate crevice corrosion resulting in corrosion of the aluminum coating. Literature focused on crevice corrosion of aluminum however shows that the result is pitting of the aluminum whereby surfaces surrounding the pits evolve hydrogen, resulting in the buildup of bubbles that replace the solution within the crevice<sup>50</sup>. While some bubbles were observed near the lock-seam of one of the aluminized steel samples, possibly indicating hydrogen evolution, there was no indication of corrosion damage typical of crevice conditions in the long-term immersion cells. Crevice corrosion within the lock-seam may therefore not be of any immediate significance.

Therefore, to simulate corrosion of a defect within the lock-seam, the primary stages that need to be considered are the initial period of aluminum passivity and the period following corrosion initiation of the aluminum. The objective is then to assess how the space within the lock-seam may either promote or arrest corrosion of defects and whether the corrosion rate would be more or less than those at defects located outside of the lock-seam.

### 5.1. Model Formulation

A finite element model was developed to identify the influence of the confined geometry of the lock-seam on the corrosion rates at a defect location. The simulated corrosion rates may not necessarily reflect actual conditions but can be used to determine whether corrosion at a defect may occur at a faster rate than a defect located outside of the lock-seam. The model geometry comprises a large quarter circle domain representative of the natural water that may reside within the pipe but outside of the lock-seam as shown in Figure 5.1. The lock-seam geometry is idealized as a small rectangle with variable height to reflect the looseness of the lock-seam.



*Figure 5.1. The 2D-mesh geometry of the confined location entrance (right) and the defected aluminum coating that exposes the steel (orange).*

The governing equations used to solve for the potential distribution and oxygen concentration throughout the model domain are

$$\nabla^2 \varphi = 0, \quad \text{Equation 7}$$

and

$$\nabla^2 c_{O_2} = 0, \quad \text{Equation 8}$$

where  $\varphi$  represents the potential within the electrolyte domain and  $c_{O_2}$  represents the concentration of oxygen. At the defect boundary, it is assumed that steel corrodes according to the reaction



under activation control with a current density expressed as

$$i_{Fe} = n_{Fe} k_{Fe} F \times \exp \left( (Vm - \varphi - E_{Fe}) \times \frac{2.303}{B_{Fe}} \right) \quad \text{Equation 10}$$

Oxygen reduction occurs at the coating and defect boundary according to the reaction



under mixed activation-mass transfer control considering the expression

$$i_{O_2,x} = (i_{act,x} \times i_{mt,x}) / (i_{act,x} + i_{mt,x}) \quad \text{Equation 12}$$

where  $i_{act,x}$  is expressed as

$$i_{act,x} = n_{O_2} F k_{O_2,x} c_{O_2} \exp \left( (Vm - \varphi - E_{O_2}) \times \frac{2.303}{B_{O_2,x}} \right) \quad \text{Equation 13}$$

and the mass transfer limited current density  $i_{mt,x}$  was set to a value for each boundary based on the measured cathodic kinetics in quiescent solution. Since oxygen is consumed at the metal boundaries, there must be a flux boundary condition based on the rate of the oxygen reduction reaction which can be expressed as

$$N_{O_{2,x}} = \frac{i_{O_{2,x}}}{4F} \quad \text{Equation 14}$$

For the passive condition, the anodic current density was set to a value indicative of passive dissolution. For the active condition the aluminum was assumed to corrode according to the reaction



Under activation control with a current density expressed as

$$i = nFk \times \exp\left((Vm - \varphi - Eal) \times \frac{2.303}{Bal}\right) \quad \text{Equation 16}$$

The curved boundary of the quarter circle domain was assumed to reflect bulk solution conditions where the oxygen concentration was set to the solubility of oxygen in the solution assumed to be 0.26 mol/m<sup>3</sup>.

The following input parameters were used. The kinetic parameters were abstracted from measured potentiodynamic polarization curves presented in Section 4.4.

*Table 5.1. Parameters Used in the Finite Element Model.*

| Parameter    | Value  |        |
|--------------|--|--------|
| $\beta_{Al}$ | Passive                                      | -      |
|              | Active 1                                     | 0.26 V |
|              | Active 2                                     | 0.09 V |
| $k_{Al}$     | $2.32 \times 10^{-11}$ mol/m <sup>2</sup> /s |        |
| $E_{Al}$     | -1.6 V                                       |        |
| $k_{Fe}$     | $1.45 \times 10^{-6}$ mol/m <sup>2</sup> /s  |        |
| $E_{Fe}$     | -0.41 V                                      |        |
| $\beta_{Fe}$ | 0.154 V                                      |        |
| $D_{O_2}$    | $2.4 \times 10^{-9}$ m <sup>2</sup> /s       |        |
| $c_{O_2}$    | $2.6 \times 10^{-4}$ M                       |        |
| F            | 96,487 C/mol                                 |        |

Table 5.2 (Continued). Parameters Used in the Finite Element Model.

|                   |  |          |
|-------------------|--|----------|
| T                 | 298 K                                  |          |
| R                 | 8.134 J/mol/K                          |          |
| V <sub>m</sub>    | 0 V                                    |          |
| β <sub>O2al</sub> | 0.26 V                                 |          |
| k <sub>O2al</sub> | 4.2 x 10 <sup>-11</sup> m/s            |          |
| E <sub>O2al</sub> | 0.16 V                                 |          |
| k                 | Mild                                   | 0.01 S/m |
|                   | Aggressive                             | 0.1 S/m  |
| d                 | 100, 200, 500, 1000, 10000 μm          |          |
| l                 | 1 mm                                   |          |
| B <sub>O2f</sub>  | 0.26 V                                 |          |
| k <sub>O2f</sub>  | 7 x 10 <sup>-10</sup> m/s              |          |
| E <sub>O2f</sub>  | 0.16 V                                 |          |
| i <sub>pAl</sub>  | 7 x 10 <sup>-9</sup> A/cm <sup>2</sup> |          |

The corresponding current density vs. potential relationship based on the input parameters and Equations Equation 7 to Equation 16 for each reaction and metal combination are presented in Figure 5.2. This figure is provided to show that the observed experimental differences between the anodic and cathodic polarization curves obtained for each material are upheld in the simulations. In both cases the corrosion potential of aluminum is slightly less than that of steel, and importantly, oxygen reduction occurs at a higher rate on the steel surface than the aluminum surface. This however does not consider the change in oxygen reduction kinetics due to the presence of corrosion products which may enhance oxygen reduction.<sup>67</sup> Also not shown in the figure is the mass transfer limitation of the oxygen reduction which was set to a maximum current density of 10 μA/cm<sup>2</sup> for aluminum and 25 μA/cm<sup>2</sup> for steel. These values were estimated from the measured cathodic polarizations scans.

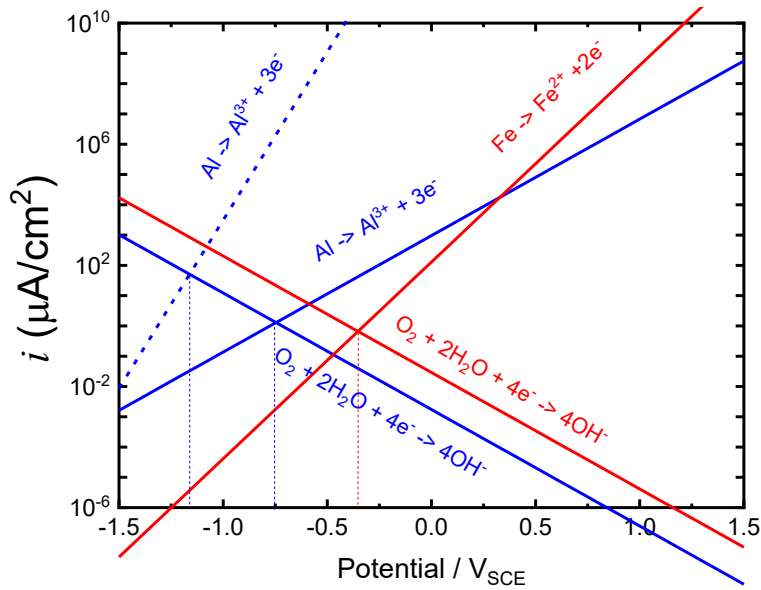


Figure 5.2. Polarization diagram of the reactions considered in the model according to the parameters listed in Table 5.1.

## 5.2. Simulation Results

In the initial stage of exposure when the aluminum is passive, little galvanic protection is afforded to the steel defect and the exposed steel corrodes at a rate dependent on the access to oxygen and the solution resistance between the defect site and the adjacent aluminum coating. As the space in the lock-seam decreases, the availability of oxygen decreases and therefore so does the corrosion rate. Figure 5.3 shows the defect corrosion current density as a function of position with the crevice height as a parameter for solution conductivities reflective of both mild Figure 5.3a, and aggressive Figure 5.3b conditions. The influence of solution conductivity decreases as the crevice height decreases since the resistance between the adjacent surface becomes controlled by the geometry of the crevice space. This would suggest that the looseness of the lock-seam has more influence on corrosion rate at defect locations than the conductivity of the solution.

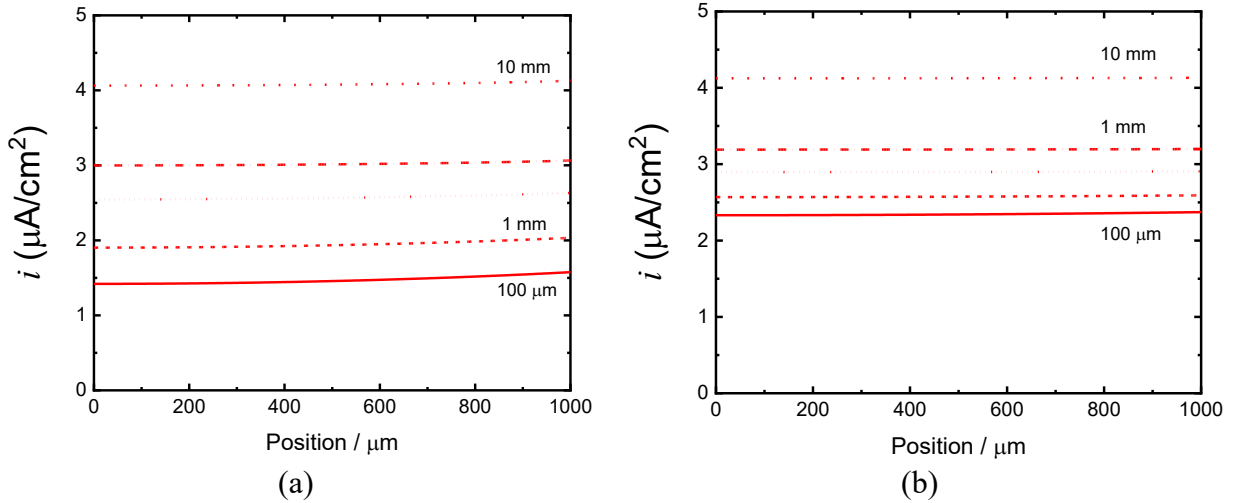


Figure 5.3. Steel corrosion current density as a function of position along defect surface with crevice gap width as a parameter for the passive condition: a) conductivity 0.01 S/m; b) conductivity = 0.1 S/m.

To show the influence of the crevice gap height on the cathodic kinetics that support the corrosion reactions, the oxygen reduction current density is expressed as a function of position along the aluminum boundary in Figure 5.4 for both mild and aggressive solution conductivities. The vertical red line reflects the location of the crevice boundary. In both cases, the presence of the crevice former results in a decrease in the magnitude of the oxygen reduction rates due to oxygen depletion within the crevice. Since oxygen reduction occurs more so external to the crevice, the pH may increase in this region and result in discoloration of the coating as was the case in most of the crevice exposure tests. An explanation is not presently available however regarding preferential coating discoloration within the crevice as was the case in 1 of the crevice specimens exposed to the aggressive solution.

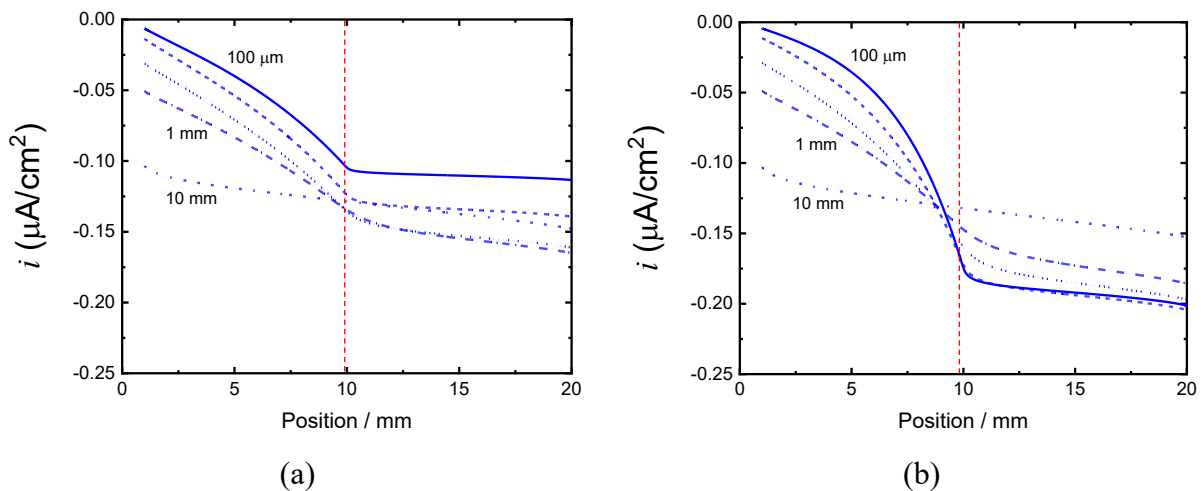


Figure 5.4. Oxygen reduction current density on aluminized surface as a function of position with crevice gap width as a parameter for the passive condition: a) conductivity 0.01 S/m; b) conductivity = 0.1 S/m.

Now the two actively corroding scenarios are considered. While it was not apparent that a state of aluminized coating corrosion was reached for the crevice cells, there was clear indication of this in the lock-seam immersion test as well as previous investigations. The crevice cells may not have been immersed long enough to reach this stage. In the active 1 case, the aluminum is assumed to corrode at a minimal rate that may reflect surface averaged kinetics of pitting corrosion. Figure 5.5a and Figure 5.5b show the anodic current density as a function of position along the steel and aluminum boundaries respectively considering the aggressive condition. Like the passive conditions, the aluminum only provides a minimal amount of protection to the defect and the corrosion rate is primarily controlled by the crevice height. However, the level of protection afforded to a defect location will depend on the kinetic parameters of the aluminum corrosion reaction.

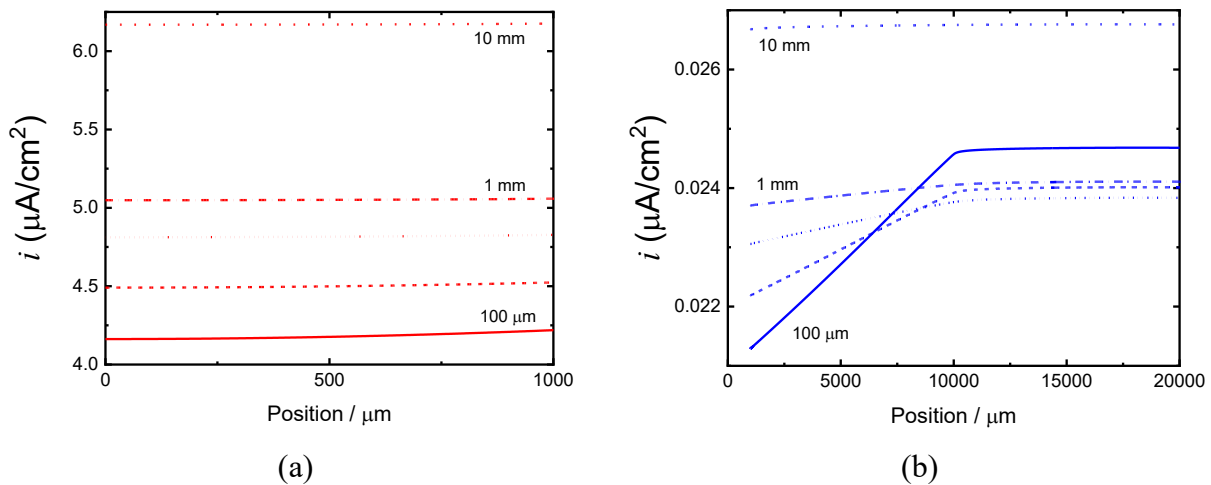


Figure 5.5. Anodic current density as a function of position with crevice gap width as a parameter for the active 1 condition with aggressive conductivity: a) steel; b) aluminum.

The active 2 condition assumes a lower value of the Tafel slope resulting in elevated values of the anodic current density and a lower corrosion potential which may more closely reflect aluminum that is able to corrode uniformly. Figure 5.6a shows the corrosion current density for both the steel and aluminum as a function of position with the crevice height as a parameter. Under such conditions, the aluminum corrodes at a rate of an order of magnitude greater than the active 1 condition and the steel corrodes at a rate of an order of magnitude less. Also, similar to the previous conditions, as the height of the crevice decreases, the corrosion rate of the defect decreases as well. The aluminum corrosion rate within the crevice is less than that of the aluminum external to the crevice again due to the availability of oxygen. Despite this, the steel defect is still afforded similar levels of protection.



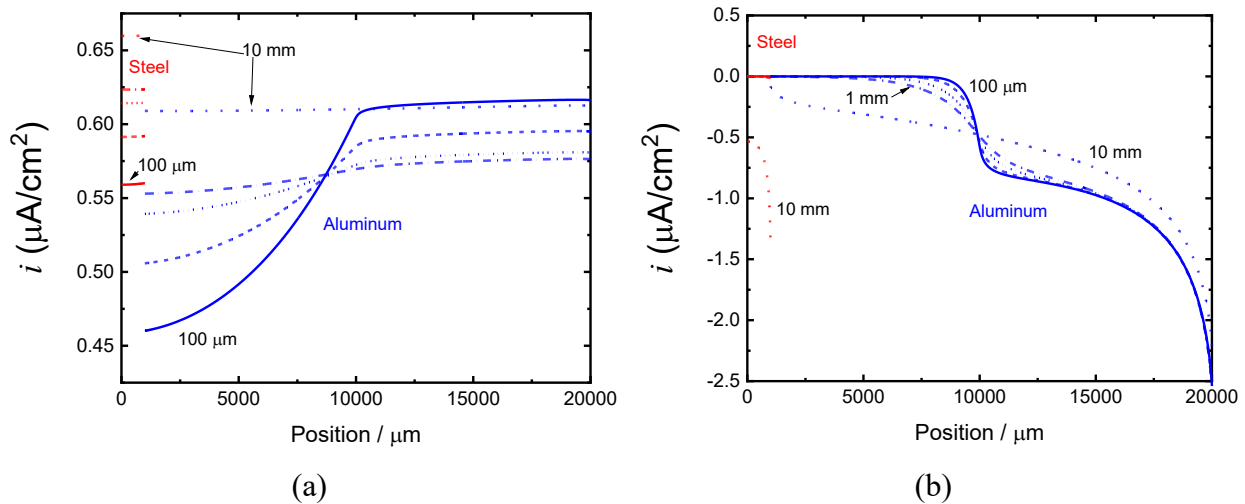


Figure 5.6. Current density as a function of position with crevice gap width as a parameter for the active 2 conditions with aggressive solution: a) anodic; b) cathodic.

### 5.3. Summary and Discussion

From the simulation results and under the assumptions imposed, defects within the lock-seam are likely to corrode at a slower rate than defects present external to the lock-seam of similar size. Whether the geometry of the lock-seam either decreases or extends the time to aluminum activation or promotes a more corrosive environment may be answered with more sophisticated models considering ionic transport and corrosion product hydrolysis and precipitation.

Such a model has been described by Dolgikh et al. for aluminized steel containing different amounts of zinc or magnesium considering fully immersed conditions without confinement<sup>68</sup>. The simulations were performed considering a cut edge geometry and an ~10,000 ppm NaCl solution. Under these conditions it is assumed that the aluminum actively corrodes and provides some protection to the steel. The result is a decrease in pH near the actively corroding region and an increase in pH at adjacent regions.

However, based on our exposure results in solutions more typical of natural waters, there was no indication of a substantial enough drop in pH within the crevice to accelerate corrosion of the aluminum and in most cases cathodic activity resulting in a rise in pH and discoloration of the aluminized coating occurred outside of the crevice which is in agreement with the simulation results. If such conditions developed after longer exposure times however it may be possible for the aluminum corrosion products to plug the lock-seam opening and therefore prevent any further corrosion damage.

## CHAPTER 6. POTENTIAL IMPLICATIONS TO SERVICE LIFE

Based on the current and previous investigations including laboratory experimental results and field sample analysis, a process model is proposed to describe corrosion propagation at coating deficiencies of moderate size (in the range of 1 mm or greater) of aluminized steel pipe. The model is used to suggest whether defects present in the lock-seam may reduce service life more so than defects present on the internal pipe wall but external to the lock-seam.

### 6.1. Description of Model

A schematic of the proposed corrosion damage propagation model considered defected aluminized steel exposed to natural waters is shown in Figure 6.1. A similar model was proposed by Akhoondan (2012).<sup>4</sup> For small defects (micrometric scale), the steel corrosion products can plug the defect and limit oxygen diffusion and therefore limit the corrosion rate.<sup>6,69</sup> Therefore, this discussion is limited to defect sizes that may result in premature corrosion damage. The role of corrosion products is not emphasized in the schematic but will have an influence on corrosion rate and propagation. It is assumed that the materials are constantly immersed.

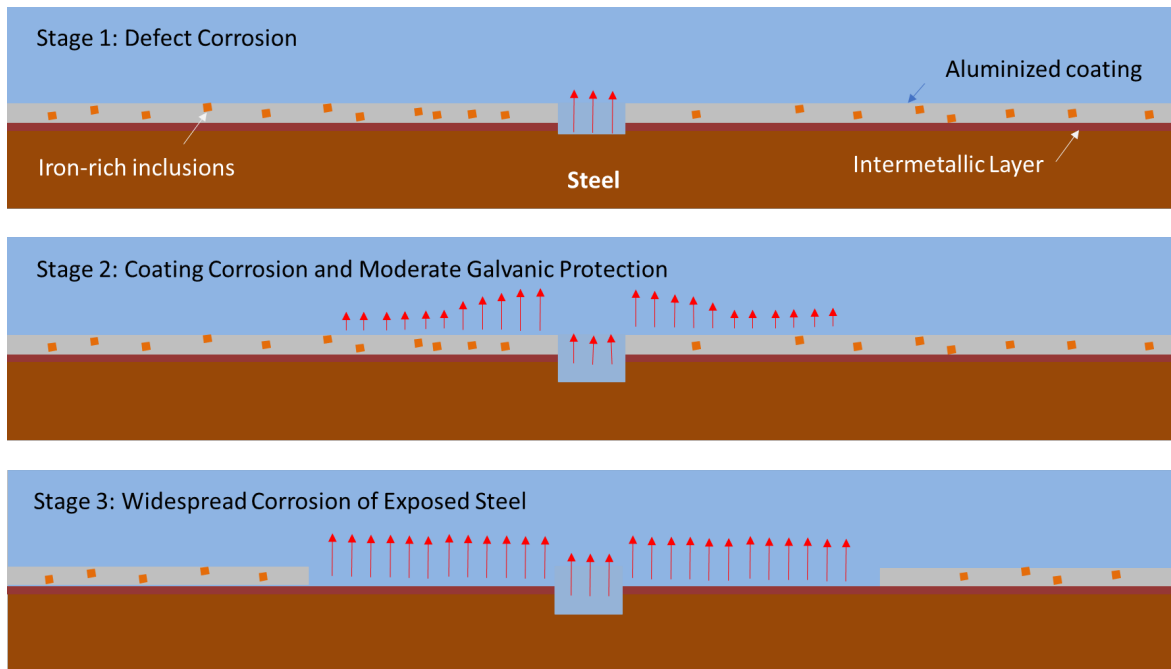


Figure 6.1. Corrosion damage propagation model schematic for defected aluminized steel.

#### Stage 1: Defect Corrosion

There is enough evidence to conclude that in the initial stage of exposure of defected aluminized steel to natural water, the exposed steel corrodes at a substantial rate with little protection provided by the passive aluminum coating. As the steel corrodes and corrosion products develop, the corrosion rate will be limited by the rate of oxygen diffusion across the product layer. However, if the corrosion products do not precipitate on the defect surface, the corrosion rate may only be kinetically limited.

The end of stage 1 is bound by the initiation of widespread corrosion of the aluminum coating, and therefore, its duration depends on the mechanisms promoting initiation. In a previous study, it was proposed that the cause of corrosion of the aluminum could be the local alkalization due to interaction of the aluminum with iron-rich inclusions. If this is truly the case, the time to corrosion initiation of the aluminum coating may be delayed in confined regions due to the limited availability of oxygen, therefore extending the duration of stage 1. However, while the duration of stage 1 may be extended in confined regions, the corrosion rate of the exposed steel will also be limited due to oxygen depletion in the confined space. Such a scenario agrees with the experimental results showing preferential corrosion of the aluminum coating external to confined regions but also limited corrosion damage within the lock-seam.

#### Stage 2: Aluminum depassivation and moderate galvanic protection

After a certain initial exposure period, the aluminum coating begins to corrode and can provide more protection to exposed steel. During this period, the steel still corrodes but at a much lower rate than in stage 1. Based on our finite element simulations, the depletion of oxygen within a confined region will limit the corrosion rate of the exposed steel and the aluminum coating, indicating that the duration of stage 2 is greater for the region within the lock-seam than an unconfined location.

The end of stage 2 is reached once the aluminum coating has been completely consumed thus exposing large areas of steel. It is not clear due to the time constraints of this work whether such a condition is feasible within a confined space such as the lock-seam. Upon analysis of the immersed galvanized steel lock-seams, it was clear that corrosion of the zinc coating deposited at the mouth of the lock-seams and prevent any further corrosion within it. It may be possible that a similar protection mechanism could occur for aluminized steel. Specifically, the corrosion of the aluminum within the lock-seam could result in aluminum corrosion products that plug the lock-seam and prevent further corrosion. One experimental observation that would support this speculation is the somewhat uniform presence of aluminum corrosion products on the surface of the exposed lock-seam sections, indicating corrosion product deposition is possible. Whether enough corrosion products could be produced to plug the confined region would depend on the looseness of the lock-seam. For this reason, it is recommended that lock-seams are tightly formed.

#### Stage 3: Widespread corrosion of exposed steel

Once corrosion of the aluminum coating has resulted in its complete consumption, bare steel is exposed and will corrode at a rate dependent on the composition of the water it is in contact with. Based on the discussion of stage 2, it is not expected that such a scenario will result from corrosion within the lock-seam, but this cannot be completely ruled out.

### 6.2. Summary

Based on the results presented in this work and the proposed corrosion propagation model, it is expected that defects within the lock-seam would not result in any more reduction in service life than that would result from corrosion at defects external to the lock-seam. Additionally, there was not enough evidence to suggest that defects generated within the lock-seam would cause any reduction in service life. This is based on there being little to no direct field exposure evidence of

a lock-seam failure due to premature corrosion. However, in discussions with the project manager of this project, it was revealed that in many cases the corrosion damage has been so severe that it was impossible to determine where it initiated. According to our results which consider natural water containing chlorides at neutral pH without scaling capabilities, it is more likely for such widespread damage to have initiated at a defect outside the confined region of the lock-seam. Adverse conditions promoting a more corrosive environment, such as acidic or alkaline solutions potentially due to microbial activity, could produce different results.

## CHAPTER 7. CONCLUSIONS

In this work, the corrosion performance of aluminized and galvanized steel pipe lock-seams exposed to simulated natural water conditions was assessed. The objective was to determine whether defects that are generated within the lock-seams during the fabrication process cause premature corrosion that would reduce service life. The experimental work comprised exposure testing, crevice experiments, electrochemical characterization, and finite element simulations. Based on the results, the following conclusions may be made:

- Defects in the coating of aluminized steel are preferential initiation sites for corrosion while zinc coatings can prevent corrosion of exposed steel considering defects of the typical size that may result from the manufacturing process.
- The defects present within the lock-seam of aluminized steel may corrode at a slower rate than those present external to the lock-seam due to the limited oxygen availability.
- Coating deficiencies generated within the lock-seams of aluminized steel are not expected to influence service life however coating defects external to the lock-seam but on the internal wall of the pipe may.

These conclusions are based only on the influence of chlorides as a contributor to corrosive conditions as this work did not consider the influence of scaling components or microbial-induced corrosion. Scaling precipitates were previously shown to help inhibit corrosion and therefore were not considered in this work. Further research should be conducted to formulate a service life model based on both corrosive ions and scaling or inhibitive components, possibly considering a corrosivity index that can be used to estimate corrosion rates on pipes with and without deficiencies. Such indices have been developed for aluminum<sup>70</sup> and aluminized steel corrosion in natural waters but neither directly considers the individual contributions to corrosion of both scaling precipitates and corrosive species.

## REFERENCES

- (1) AASHTO. AASHTO 36-16: Standard Specification for Corrugated Steel Pipe, Metallic-Coated, for Sewers and Drains. American Association of State and Highway Transportation Officials, 2016, pp 1–22.
- (2) AASHTO. AASHTO M274-87: Standard Specification for Steel Sheet, Aluminum-Coated (Type 2), for Corrugated Steel Pipe. American Association of State Highway and Transportation Officials, 2017.
- (3) Anastasopoulos, P. C.; Mannering, F. L. The Effect of Speed Limits on Drivers' Choice of Speed: A Random Parameters Seemingly Unrelated Equations Approach. *Anal. Methods Accid. Res.* **2016**, *10*, 1–11. <https://doi.org/10.1016/j.amar.2016.03.001>.
- (4) Akhoondan, M. Corrosion Evaluation and Durability Estimation of Aluminized Steel Drainage Pipes, University of South Florida, Tampa, Florida, 2012.
- (5) Pruncu, C. I.; Azari, Z.; Casavola, C.; Pappalettere, C. Characterization and Prediction of Cracks in Coated Materials: Direction and Length of Crack Propagation in Bimaterials. *Int. Sch. Res. Not.* **2015**, *2015*, 594147. <https://doi.org/10.1155/2015/594147>.
- (6) Caseres, L. Electrochemical Behavior of Aluminized Steel Type 2 in Scale-Forming Waters, University of South Florida, Tampa, Florida, 2007.
- (7) Sagüés, A. A.; Poor, N. D.; Cáseres, L.; Akhoondan, M. *Final Report: Development of A Rational Method for Predicting Corrosion Rates of Metals In Soils and Waters*. Florida Department of Transportation, Tallahassee, Florida, 2009.
- (8) Alvarez-Pampliega, A.; Lamaka, S. V. V.; Taryba, M. G. G.; Madani, M.; De Strycker, J.; Tourwé, E.; Ferreira, M. G. S. G. S.; Terryn, H. Cut-Edge Corrosion Study on Painted Aluminum Rich Metallic Coated Steel by Scanning Vibrating Electrode and Micro-Potentiometric Techniques. *Electrochim. Acta* **2012**, *61*, 107–117. <https://doi.org/10.1016/j.electacta.2011.11.110>.
- (9) Simmons, R.; McCullough, T. *Aluminized Pipe Evaluation*; Florida Department of Transportation, Tallahassee, Florida, 2015.
- (10) De Graeve, I.; Schoukens, I.; Lanzutti, A.; Andreatta, F.; Alvarez-Pampliega, A.; De Strycker, J.; Fedrizzi, L.; Terryn, H. Mechanism of Corrosion Protection of Hot-Dip Aluminium-Silicon Coatings on Steel Studied by Electrochemical Depth Profiling. *Corros. Sci.* **2013**, *76*, 325–336. <https://doi.org/10.1016/j.corsci.2013.07.005>.
- (11) Awan, G. H.; ul Hasan, F. The Morphology of Coating/Substrate Interface in Hot-Dip-Aluminized Steels. *Mater. Sci. Eng. A* **2008**, *472* (1–2), 157–165. <https://doi.org/10.1016/j.msea.2007.03.013>.
- (12) ASTM Committee A05. ASTM A929/A 929M: Standard Specification for Steel Sheet, Metallic-Coated by the Hot-Dip Process for Corrugated Steel Pipe. ASTM International,

- Philadelphia, Pa, **2013**, 02, 3–6. <https://doi.org/10.1520/A0463>.
- (13) Florida Department of Transportation. *State of Florida Department of Transportation Drainage Handbook Temporary Drainage Design Office of Design*, Drainage Section; Florida Department of Transportation, Tallahassee, Florida, 2019.
  - (14) Romie, K. *Water Chemistry of Lakes in the Southwest Florida Water Management District*; Southwest Florida Water Management District, Brooksville, Florida, 2000.
  - (15) Cáseres, L. J.; Sagüés, A. A. Corrosion of Aluminized Steel in Scale-Forming Waters. In *NACE International*; NACE International: Houston, Texas, 2005; pp 1–13.
  - (16) Akhoondan, M.; Sagüés, A. A. *Corrosion of Spiral Rib Aluminized Pipe*; Florida Department of Transportation, Tallahassee, Florida, 2012.
  - (17) Ault, P.; Ellor, J. A. *Durability Analysis of Aluminized Type 2 Corrugated Metal Pipe*; Federal Highway Administration, McLean, Virginia, 2000.
  - (18) California Department of Transportation. *Highway Design Manual*; California Department of Transportation, Sacramento, California, 2014.
  - (19) Bednar, L. Durability of Plain Galvanized Steel Drainage Pipe in South America: Criteria for Selection. *Transp. Res. Rec.* **1989**, 80–87.
  - (20) Florida Department of Transportation. *State of Florida Department of Transportation Drainage Manual Office of Design, Drainage Section*; Florida Department of Transportation, Tallahassee, Florida, 2019.
  - (21) Zhang, X. G. Galvanic Corrosion of Zinc and Its Alloys. *J. Electrochem. Soc.* **1996**, 143 (4), 1472. <https://doi.org/10.1149/1.1836662>.
  - (22) Vera, R.; Guerrero, F.; Delgado, D.; Araya, R. Atmospheric Corrosion of Galvanized Steel and Precipitation Runoff from Zinc in a Marine Environment. *J. Braz. Chem. Soc.* **2013**, 24 (3), 449–458. <https://doi.org/10.5935/0103-5053.20130060>.
  - (23) El-Mahdy, G. A.; Nishikata, A.; Tsuru, T. Electrochemical Corrosion Monitoring of Galvanized Steel under Cyclic Wet–Dry Conditions. *Corros. Sci.* **2000**, 42 (1), 183–194. [https://doi.org/10.1016/S0010-938X\(99\)00057-8](https://doi.org/10.1016/S0010-938X(99)00057-8).
  - (24) Ilhan-Sungur, E.; Cansever, N.; Cotuk, A. Microbial Corrosion of Galvanized Steel by a Freshwater Strain of Sulphate Reducing Bacteria (*Desulfovibrio* Sp.). *Corros. Sci.* **2007**, 49 (3), 1097–1109. <https://doi.org/10.1016/j.corsci.2006.05.050>.
  - (25) Padilla, V.; Alfantazi, A. Corrosion Film Breakdown of Galvanized Steel in Sulphate–Chloride Solutions. *Constr. Build. Mater.* **2014**, 66, 447–457. <https://doi.org/10.1016/J.CONBUILDMAT.2014.05.053>.
  - (26) Persson, D.; Thierry, D.; Karlsson, O. Corrosion and Corrosion Products of Hot Dipped

Galvanized Steel During Long-term Atmospheric Exposure at Different Sites World-Wide. *Corros. Sci.* **2017**, *126*, 152–165. <https://doi.org/10.1016/J.CORSCI.2017.06.025>.

- (27) Chen, Y. Y.; Chung, S. C.; Shih, H. C. Studies on The Initial Stages of Zinc Atmospheric Corrosion In The Presence of Chloride. *Corros. Sci.* **2006**, *48* (11), 3547–3564. <https://doi.org/10.1016/J.CORSCI.2005.12.007>.
- (28) Qu, Q.; Yan, C.; Wan, Y.; Cao, C. Effects of NaCl and SO<sub>2</sub> on the Initial Atmospheric Corrosion of Zinc. *Corros. Sci.* **2002**, *44* (12), 2789–2803. [https://doi.org/10.1016/S0010-938X\(02\)00076-8](https://doi.org/10.1016/S0010-938X(02)00076-8).
- (29) Almeida, E.; Morcillo, M.; Rosales, & B. Atmospheric Corrosion of Zinc Part 2: Marine Atmospheres. *Br. Corros. J.* **2000**, *35* (4), 289–296. <https://doi.org/10.1179/000705900101501362>.
- (30) Ogle, K.; Morel, S.; Jacquet, D. Observation of Self-Healing Functions on the Cut Edge of Galvanized Steel Using SVET and PH Microscopy. *J. Electrochem. Soc.* **2006**, *153*, 1–5. <https://doi.org/10.1149/1.2126577>.
- (31) Graedel, T. E. Corrosion Mechanisms for Aluminum Exposed to the Atmosphere. *J. Electrochem. Soc.* **1989**, *136* (4), 204–212. <https://doi.org/10.1149/1.2221162>.
- (32) Graedel, T. E. Corrosion Mechanisms for Zinc Exposed to the Atmosphere. *J. Electrochem. Soc.* **1989**, *136* (4), 193–203.
- (33) Wang, L.; Liu, G.; Zou, L.; Xue, D. Phase Evolution from Rod-like ZnO to Plate-like Zinc Hydroxysulfate during Electrochemical Deposition. *J. Alloys Compd.* **2010**, *493* (1–2), 471–475. <https://doi.org/10.1016/J.JALLCOM.2009.12.129>.
- (34) Melidis, P.; Sanozidou, M.; Mandusa, A.; Ouzounis, K. Corrosion Control by Using Indirect Methods. *Desalination* **2007**, *213* (1–3), 152–158. <https://doi.org/10.1016/J.DESAL.2006.03.606>.
- (35) Boersma, A.; Vercauteren, F.; Fischer, H.; Pizzocolo, F. Scaling Assessment, Inhibition and Monitoring of Geothermal Wells. In *43rd Workshop on Geothermal Reservoir Engineering*; Stanford University, Stanford, California, 2018.
- (36) Tomashov, N. D. Development of the Electrochemical Theory of Metallic Corrosion. *Corrosion* **1964**, *20* (1), 7t–14t. <https://doi.org/10.5006/0010-9312-20.1.7t>.
- (37) Liu, Y.; Ooi, A.; Tada, E.; Nishikata, A. Electrochemical Monitoring of the Degradation of Galvanized Steel in Simulated Marine Atmosphere. *Corros. Sci.* **2019**, *147*, 273–282. <https://doi.org/10.1016/J.CORSCI.2018.11.013>.
- (38) Sun, H.; Liu, S.; Sun, L. *A Comparative Study on the Corrosion of Galvanized Steel under Simulated Rust Layer Solution with and without 3.5wt%NaCl*; *Int. J. Electrochem. Sci.*;



Belgrade, Serbia, 2013; Vol. 8.

- (39) Perez, N. *Electrochemistry and Corrosion Science*, 2nd ed.; Springer, Boston, Massachusetts, 2016. <https://doi.org/10.1007/b118420>.
- (40) Hamlaoui, Y.; Pedraza, F.; Tifouti, L. Corrosion Monitoring of Galvanised Coatings through Electrochemical Impedance Spectroscopy. *Corros. Sci.* **2008**, *50* (6), 1558–1566. <https://doi.org/10.1016/j.corsci.2008.02.010>.
- (41) Molinas, A.; Mommandi, A. *Development of New Corrosion /Abrasion Guidelines for Selection of Culvert Pipe Materials*; Colorado Department of Transportation, Denver, Colorado, 2009.
- (42) Fujita, S.; Mizuno, D. Corrosion and Corrosion Test Methods of Zinc Coated Steel Sheets on Automobiles. *Corros. Sci.* **2007**, *49* (1), 211–219. <https://doi.org/10.1016/J.CORSCI.2006.05.034>.
- (43) Siggelkow, I. Evaluation of Corrosion in Crevices Where Materials with Different Surface Coatings Are Combined, Uppsala University, Uppsala, Sweden, 2011.
- (44) Stewart, K. C. Intermediate Attack in Crevice Corrosion by Cathodic Focusing, University of Virginia, Charlottesville, Virginia, 1999.
- (45) Szklarska-Smialowska, Z. Pitting Corrosion of Aluminum. *Corros. Sci.* **1999**, *41* (9), 1743–1767. [https://doi.org/10.1016/S0010-938X\(99\)00012-8](https://doi.org/10.1016/S0010-938X(99)00012-8).
- (46) Foley, R. T.; Nguyen, T. H. The Chemical Nature of Aluminum Corrosion. *J. Electrochem. Soc.* **1982**, *129* (3), 464. <https://doi.org/10.1149/1.2123881>.
- (47) Panossian, Z.; Mariaca, L.; Morcillo, M.; Flores, S.; Rocha, J.; Peña, J. J.; Herrera, F.; Corvo, F.; Sanchez, M.; Rincon, O. T.; Pridybailo, G.; Simancas, J. Steel Cathodic Protection Afforded by Zinc, Aluminium and Zinc/Aluminium Alloy Coatings in The Atmosphere. *Surf. Coatings Technol.* **2005**, *190* (2–3), 244–248. <https://doi.org/10.1016/j.surfcoat.2004.04.023>.
- (48) Lemmens, B.; Gonzalez Garcia, Y.; Corlu, B.; De Strycker, J.; De Graeve, I.; Verbeken, K. Study of the Electrochemical Behaviour of Aluminized Steel. *Surf. Coatings Technol.* **2014**, *260*, 34–38. <https://doi.org/10.1016/J.SURFCOAT.2014.06.064>.
- (49) Lemmens, B.; Springer, H.; Peeters, M.; De Graeve, I.; De Strycker, J.; Raabe, D.; Verbeken, K. Deformation Induced Degradation of Hot-Dip Aluminized Steel. *Mater. Sci. Eng. A* **2018**, *710* (July 2017), 385–391. <https://doi.org/10.1016/j.msea.2017.10.094>.
- (50) Siitari, D. W.; Alkire, R. C. Initiation of Crevice Corrosion: I. Experimental Investigations on Aluminum and Iron. *J. Electrochem. Soc.*; **1982**, *129* (3), 481–487.
- (51) Allély, C.; Dosdat, L.; Clauzeau, O.; Ogle, K.; Volovitch, P. Anticorrosion Mechanisms of Aluminized Steel for Hot Stamping. *Surf. Coatings Technol.* **2014**, *238*, 188–196.

<https://doi.org/10.1016/J.SURFCOAT.2013.10.072>.

- (52) Jorcin, J.-B.; Blanc, C.; Pébère, N.; Tribollet, B.; Vivier, V. Galvanic Coupling Between Pure Copper and Pure Aluminum. *J. Electrochem. Soc.* **2008**, *155* (1), C46-C51. <https://doi.org/10.1149/1.2803506>.
- (53) Liu, C.; Kelly, R. G. A Review of the Application of Finite Element Method (FEM) to Localized Corrosion Modeling. *Corrosion*. National Assoc. of Corrosion Engineers International, 2019, pp 1285–1299. <https://doi.org/10.5006/3282>.
- (54) Cross, S. R.; Gollapudi, S.; Schuh, C. A. Validated Numerical Modeling of Galvanic Corrosion of Zinc and Aluminum Coatings. *Corros. Sci.* **2014**, *88*, 226–233. <https://doi.org/10.1016/J.CORSCI.2014.07.033>.
- (55) Lee, J. S.; Reed, M. L.; Kelly, R. G. Combining Rigorously Controlled Crevice Geometry and Computational Modeling for Study of Crevice Corrosion Scaling Factors. *J. of The Electrochem. Soc.* **2004**, *151* (7), B423-B433. <https://doi.org/10.1149/1.1753581>.
- (56) Alkire, R. C.; Siitari, D. Initiation of Crevice Corrosion II. Mathematical Model for Aluminum in Sodium Chloride Solutions. *J. Electrochem. Soc.*; *129* (3), 488-496. **1982**.
- (57) Hebert, K.; Alkire, R. Dissolved Metal Species Mechanism for Initiation of Crevice Corrosion of Aluminum: II . Mathematical Model. *J. Electrochem. Soc.* **1983**, *130* (5), 1007-1014.
- (58) Tang, N.-Y. Control of Silicon Reactivity in General Galvanizing. *J. Phase Equilibria Diffus.* **2008**, *29* (4), 337–344. <https://doi.org/10.1007/s11669-008-9321-0>.
- (59) Pistofidis, N.; Vourlias, G.; Konidaris, S.; Pavlidou, E.; Stergiou, A.; Stergioudis, G. Microstructure of Zinc Hot-Dip Galvanized Coatings Used for Corrosion Protection. *Mater. Lett.* **2006**, *60* (6), 786–789. <https://doi.org/10.1016/J.MATLET.2005.10.013>.
- (60) Bouché, K.; Barbier, F.; Coulet, A. Intermetallic Compound Layer Growth Between Solid Iron and Molten Aluminium. *Mater. Sci. Eng. A* **1998**, *249* (1–2), 167–175. [https://doi.org/10.1016/S0921-5093\(98\)00573-5](https://doi.org/10.1016/S0921-5093(98)00573-5).
- (61) Marder, A. R. The Metallurgy of Zinc-Coated Steel. *Prog. Mater. Sci.* **2000**, *45* (3), 191–271. [https://doi.org/10.1016/S0079-6425\(98\)00006-1](https://doi.org/10.1016/S0079-6425(98)00006-1).
- (62) Bicao, P.; Jianhua, W.; Xuping, S.; Zhi, L.; Fucheng, Y. Effects of Zinc Bath Temperature on the Coatings of Hot-Dip Galvanizing. *Surf. Coatings Technol.* **2008**, *202* (9), 1785–1788. <https://doi.org/10.1016/J.SURFCOAT.2007.07.044>.
- (63) Giorgi, M.-L.; Durighello, P.; Nicolle, R. Dissolution Kinetics of Iron in Liquid Zinc. *J. Mater. Sci.* **2004**, *39*(18), 5803-5808.
- (64) ASTM. ASTM A 924M - 09: Standard Specification for General Requirements for Steel Sheet , Metallic-Coated By. **2009**, *i* (July 1999), 1–12. <https://doi.org/10.1520/A0924>.

- (65) Shakelford, J. F. Chapter 6: Mechanical Behavior. In *Introduction to Materials Science for Engineers*; Pearson, 2005.
- (66) Watson, W.; Orazem, M. E. *EIS: Measurement Model Program*; ECSarXiv, 2020. <https://doi.org/10.1149/OSF.IO/KZE9X>.
- (67) Stratmann, M.; Müller, J. The Mechanism of the Oxygen Reduction on Rust-Covered Metal Substrates. *Corros. Sci.* **1994**, *36* (2), 327–359. [https://doi.org/10.1016/0010-938X\(94\)90161-9](https://doi.org/10.1016/0010-938X(94)90161-9).
- (68) Dolgikh, O.; Simillion, H.; Lamaka, S. V.; Bastos, A. C.; Xue, H. B.; Taryba, M. G.; Oliveira, A. R.; Allély, C.; Van Den Bossche, B.; Van Den Bergh, K.; De Strycker, J.; Deconinck, J. Corrosion Protection of Steel Cut-Edges by Hot-Dip Galvanized Al(Zn,Mg) Coatings in 1 Wt% NaCl: Part II. Numerical Simulations. *Mater. Corros.* **2018**, *70* (5), 780–792. <https://doi.org/10.1002/maco.201810210>.
- (69) AK Steel Corporation, Aluminized Steel Type 2 Product Features. *AK Steel Corporation*, West Chester, Ohio, 2013.
- (70) Pathak, B. R.; Godard, H. P. Equation for Predicting the Corrosivity of Natural Fresh Waters to Aluminium. *Nature*. Nature Publishing Group June 1, 1968, pp 893–894. <https://doi.org/10.1038/218893a0>.